UNIVERSITY OF CALIFORNIA SAN DIEGO

Illuminating opioid signaling with caged peptides and peptide sensors

A Dissertation submitted in partial satisfaction of the requirements
for the degree Doctor of Philosophy

in

Biology

by

Xinyi Jenny He

Committee in charge:

Professor Matthew Banghart, Chair
Professor Brenda Bloodgood
Professor Jeffry Isaacson
Professor Nick Spitzer
Professor Roger Sunahara

2022

The Dissertation of Xinyi Jenny He is approved, and it is acceptable in quality and form for publication on microfilm and electronically.

University of California San Diego

2022

DEDICATION

To Mom, Dad, and Frank – home is where ever you are.

TABLE OF CONTENTS

LIST OF FIGURES

LIST OF ABBREVIATIONS

4-AP	4-Aminopyridine
AC	Adenylyl cyclase
ACSF	Artificial cerebro-spinal fluid
AAV	Adeno-associated virus
ATP	Adenosine triphosphate
BC	Basket cell
cAMP	Cyclic adenosine monophosphate
CB1R	Cannabinoid receptor
CCK	Cholescytokinin
ChR2	Channelrhodopsin
CNiFER	Cell-based Neurotransmitter fluorescent engineered reporter
cpGRP	Circularly permuted green fluorescent protein
CSF	Cerebrospinal fluid
CYD8	CNB-Y-Dynorphin-8
*D**	Apparent diffusion coefficient
D1 MSN	Direct pathway medium spiny neuron
DA	Dopamine
DAMGO	[d-Ala^2, NMe-Phe^4, Gly-ol^5]enkephalin
DCV	Dense core vesicle
dF/F	Delta Fluorescence over baseline fluorescence
DOR	Delta opioid receptor

DREADD	Designer receptors exclusively activated by designer drugs
Dyn8	Dynorphin-8
eIPSC	Electrically-evoked IPSC
ELISA	Enzyme-linked immunoassay
FSK	Forskolin
GABA	γ-aminobutyric acid
GIRK	Inward rectifying potassium channel
GPCR	G protein-coupled receptor
GRAB	Genetically encoded GPCR-activation-based
GRP	Gastrin-releasing peptide
HCN	Hyperpolarization-activated cyclic nucleotide-gated
hMOR	human MOR
IPSC	Inhibitory Post Synaptic Potential
KO	Knockout
KOR	Kappa opioid receptor
Kv	Voltage-gated potassium channels
LC	Locus coeruleus
LE	[Leu^5]-enkephalin
LHRH	Luteinizing hormone-releasing hormone
LTD	Long term depression
MERF	Met-enkephalin-Arg-Phe
mIPSC	Miniature inhibitory post-synaptic currents
MNV-D8	MNV-Dynorphin-8

MOR	Mu opioid receptor
NLX	Naloxone
NOR	Nociceptin opioid receptor
oIPSC	Optically-evoked IPSC
OptoXRs	Light-activated chimeric GPCRs
PC	Pyramidal Cell
Penk	Proenkephalin
PI	Peptidase inhibitor
PKA	Protein Kinase A
PKC	Protein kinase C
PPR	Paired-pulse ratio
PV	Parvalbumin
ROI	Region of interest
SNAP-25	25 kDa synaptosome-associated protein
SNARE	N-ethylmaleimide-sensitive factor attachment protein receptor
SST	Somatostatin
VGCC/VSCC	Voltage-gated/sensitive calcium channel
VIP	Vasoactive-intestinal peptide
VTA	Ventral tegmental area

ACKNOWLEDGEMENTS

I'd like to thank my advisor Matthew Banghart for taking me in as his first graduate student, teaching me how to do patch-clamp electrophysiology, training me to think rigorously about science, and coaching me in presenting my science to the community. The amount that I've learned from Matt goes beyond this dissertation and will stay with me through my career.

Thank you to my committee members Brenda Bloodgood, Nick Spitzer, Jeff Isaacson, and Roger Sunahara for their valuable discussions and feedback. I am especially grateful to Brenda, who also served as my teaching mentor and helped me survive my first experience teaching as an instructor of record.

Thank you to the members of the Banghart lab, especially Giulia Livrizzi, Shannan McClain, Desiree Johnson, Susan Lubejko, and Caroline Johnson, for creating the most supportive and enjoyable environment to do science. I would not have made it without our coffee breaks, group chats, discussions about reality TV, and overall hype for each other's successes.

Thank you to my friends and cohort-mates, in particular Leslie Nanninga, Grace Gibbon, Alicia Romero, Kaito Kikuchi, and Bianca Barriga, for being there for the fun times as well as the hard times during graduate school. I will forever cherish the climbing trips, ceramics classes, and beach bonfires shared together.

And last but not least, thank you to my fiancé Damon Yeh for listening to my complaints over the years, tolerating when I'm always late for dinner, and bringing me joy outside of lab.

Chapter 2, in full, is a reprint of the material as it appears in He, X. J., Patel, J, Weiss, C, Ma, X., Bloodgood, B. L., Banghart, M. R. “Convergent, functionally independent signaling by mu and delta opioid receptors in hippocampal parvalbumin interneurons”. *Elife* **10**, e69746 (2021). The dissertation author was the primary investigator and author of this paper.

Chapter 3 contains unpublished material coauthored with Tian, Lin and Banghart, Matthew. The dissertation author was the primary investigator and author of this chapter.

VITA

2014	Bachelor of Arts in Neuroscience and Art, Pomona College
2014-2016	Postbaccalaureate Fellow, National Institutes of Health
2017-2020	Teaching Assistant, University of California San Diego
2021	Course Instructor, University of California San Diego
2022	Doctor of Philosophy in Biology, University of California San Diego

PUBLICATIONS

Ma X, Johnson DJ, **He XJ**, Layden AE, McClain SP, Yung JC, Banghart MR. "A caged DAMGO for selective photoactivation of endogenous mu opioid receptors *in vivo*". *Manuscript submitted.*

He XJ, Patel J, Weiss CE, Ma X, Bloodgood BL, and Banghart MR. "Convergent, functionally independent signaling by mu and delta opioid receptors in hippocampal parvalbumin interneurons". *Elife* **10**, e69746 (2021).

He XJ, and Banghart MR. "It's Lights out for Presynaptic Terminals." *Neuron,* vol. 109, no. 11, 2021, pp. 1755–1757., doi:10.1016/j.neuron.2021.05.015.

Banghart MR, **He XJ**, and Sabatini BL. "A Caged Enkephalin Optimized for Simultaneously Probing Mu and Delta Opioid Receptors". *ACS Chem Neurosci* **9,** 684–690 (2018).

Zhang Q, Li S, Wong HC, **He XJ**, Beirl A, Petralia RS, Wang Y, Kindt KS. "Synaptically silent sensory hair cells in zebrafish are recruited after damage". *Nat Commun* **9,** 1388 (2018).

Sheets L, **He XJ**, Olt J, Schreck M, Petralia RS, Wang Y, Zhang Q, Beirl A, Nicolson T, Marcotti W, Trapani JG, Kindt KS. "Enlargement of Ribbons in Zebrafish Hair Cells Increases Calcium Currents But Disrupts Afferent Spontaneous Activity and Timing of Stimulus Onset". *J. Neurosci.* **37,** 6299–6313 (2017).

Zhang Q, **He XJ**, Wong C, and Kindt KS. "Functional Calcium Imaging in Zebrafish Lateral-line Hair Cells." *Methods in Cell Biology* (2016).

FIELDS OF STUDY

Major Field: Neurobiology

Studies in Neurophysiology
Professor Matthew Banghart, University of California San Diego

ABSTRACT OF THE DISSERTATION

Illuminating opioid signaling with caged peptides and peptide sensors

by

Xinyi Jenny He

Doctor of Philosophy in Biology

University of California San Diego, 2022

Professor Matthew Banghart, Chair

Endogenous opioids are neuropeptides, which are a type of specialized neurotransmitter that is poorly understand compared to classical neurotransmitters. It is unknown the time scale of action of neuropeptides, the spread of the peptide, or how one peptide might interact with multiple receptors. Mu and delta opioid receptors (MORs and

DORs) are both present on hippocampal interneurons and both bind the opioid peptide enkephalin. It is debated whether or not these two functionally similar receptors interact when co-expressed in the same cells, which would have huge implications on drug design and development. Using electrophysiological assays with novel photoactivateable peptides, we found that DOR has faster onset kinetics and higher ligand potency to enkephalin than MOR, making it the dominant receptor. We found no evidence of functional interactions of MOR and DOR in assays for cross-desensitization and heteromer formation suggesting that the two receptors function independently even though they share signaling pathways. In a separate study, to ask about neuropeptide spread, we tested a novel genetically encoded fluorescent sensor, kLight, based on the kappa opioid receptor (KOR) to detect dynorphin, another opioid peptide. Using simultaneous dynorphin uncaging and imaging of kLight activation, we extracted the apparent diffusion coefficient of dynorphin in brain slices. This coefficient can be used to compare diffusion across multiple conditions and address the question of how far a neuropeptide spreads once it's released. These approaches leverage the latest tools to address the holes in our knowledge of opioid signaling and neuropeptide signaling more broadly.

CHAPTER 1. Introduction

Part I. Mu and delta opioid receptors of the hippocampus

Opioids and opioid receptors

Opioids are one of the most powerful classes of drugs and substances, whose use dates back well before modern science. There is evidence of opium use by the Sumerians in the third millennium B.C., although opioids came into prominence after opium was brought to China in the eighth century A.D., and then subsequently Europe, resulting in the Opium Wars of the 19th century (Brownstein, 1993). Today's opioid epidemic is a huge public health problem, with increasing deaths from overdose year to year. While this is an enormous issue that needs to be tackled from multiple angles, a better understanding of how opioids function in the mammalian brain can yield some insight.

Opioids, both natural and synthetic, act on the body by binding to certain receptors, known as opioid receptors. Opioid receptors are G protein-coupled receptors (GPCRs) which are seven-transmembrane proteins that when activated, trigger a downstream signaling cascade resulting in changes in cellular physiology. There are four subtypes of opioid receptors: mu, delta, kappa, and nociceptin opioid receptors (MOR, DOR, KOR, NOR). All four of these GPCRs couple to inhibitory G proteins $G\alpha_{i/o}$, making them generally inhibitory to the cell that they're present on. Although these receptors are functionally similar, they are differentially expressed throughout the nervous system (Kibaly et al., 2019) such that activation of each receptor subtype leads to a different behavioral consequence to the animal (Kieffer, 2009). Generally speaking – MOR, the target of morphine, produces euphoria which is why drugs targeting MOR are addictive. DOR has anxiolytic and antidepressant properties, and KOR produces feelings of dysphoria (**Figure 1.1**). Not as much is known about NOR, but I will be

focusing on MOR, DOR, and KOR in my dissertation. Importantly, activation of all of these receptors leads to the inhibition of pain – analgesia.

These opioid receptors do not only respond to exogenous drugs such as morphine. Rather, they were first evolved to sense endogenous opioids – opioid peptides that an animal's body naturally produces. One well known example is β-endorphin (named after morphine, "endo"-"morphine"), which preferentially activate MORs and are thought to be responsible for the "runners high" that an athlete experiences after physical activity (Boecker et al., 2008; Carr et al., 1981). Other peptides include the enkephalins, which activate MOR and DOR, and dynorphins, which activate KOR preferentially (**Figure 1.1**). While these peptides typically bind more strongly to one or two receptors, they have the capability of activating all opioid receptors at high enough concentrations (Toll et al., 1998).

Enkephalins, dynorphins, and β-endorphins fall under a class of signaling molecules known as neuropeptides. Neuropeptides are type of neurotransmitter, released by a presynaptic neuron and bind to receptors on a postsynaptic neuron. Unlike classical amino acid neurotransmitters, neuropeptides are synthesized at the cell body and prepackaged into dense core vesicles. More on the distinctions and puzzles of neuropeptide signaling will be discussed in Part II of this chapter. While the properties of classical neurotransmitters, like glutamate and γ-aminobutyric acid (GABA), have been well studied, the parameters of neuropeptide signaling are still unknown. There are many open questions about the interactions of neuropeptides like enkephalin, with endogenous MOR and DOR. This dissertation aims to address some of these questions on a cellular level using brain slice electrophysiology and photoactivatable peptides.

Opioid receptors in the hippocampus

Much of what the field has learned about opioid receptors was learned through experiments in the hippocampus. The hippocampus is one of the most studied areas of the brain, with an established role in learning and memory. It is highly organized, with defined streams of information flow and dedicated cell types that each have roles to play in this circuit computation. Such makes it an attractive system to study basic properties of neurotransmission and information processing.

This dissertation will focus on a microcircuit in the CA1 region of the hippocampus where opioid receptors are expressed, and their functions are thought to be understood. In CA1, MOR and DOR are primarily expressed on parvalbumin (PV) basket cells (Stumm et al., 2004). PV basket cells are inhibitory interneurons that target the perisomatic region of pyramidal cells to inhibit pyramidal cell firing (Pelkey et al., 2017). Due to their firing properties, PV basket cells are often also referred to as Fast Spiking basket cells to differentiate them from Regular Spiking basket cells, also known as cholecystokinin (CCK) basket cells (Glickfeld and Scanziani, 2006). These cells are differentially modulated, with PV cells being inhibited by MOR agonists while CCK cells are inhibited by cannabinoid receptor (CB1R) agonists (Figure 1.2) (Freund and Katona, 2007; Glickfeld et al., 2008)

While MOR's function on PV basket cells is well established, the role of DORs is less clear. In the PV cell body, MORs open a G-protein coupled inward rectifying potassium channel (GIRK) to hyperpolarize the cell (Wimpey and Chavkin, 1991). Presynaptically, opioid receptors are poised to block release of GABA, an inhibitory neurotransmitter. While both MOR and DOR agonists inhibit spontaneous GABA release (Lupica, 1995), only MOR agonists have previously been found to also block evoked release in CA1 (Capogna et al., 1993; Lupica and Dunwiddie,

1991). Other studies have suggested anatomical separation between interneurons that express MOR and DOR (Svoboda et al., 1999), implying a functional difference between cells expressing the two receptors.

Despite these data that DOR may play a smaller role in the CA1 microcircuit, immunohistochemical evidence does show that it is highly expressed in PV cells in particular (Erbs et al., 2012; Stumm et al., 2004). A more recent study in mice established a role for DORs for causing long-term depression at PV synapses in CA2, and transient suppression in CA1 (Piskorowski and Chevaleyre, 2013). Because enkephalin, an opioid neuropeptide found in the hippocampus, activates both MOR and DOR, it is critical to understand the actions of both MOR and DOR to appreciate the effect of endogenous opioid signaling in the hippocampus.

Mechanisms of opioid signaling across subcellular compartments

Activation of opioid receptors leads to a myriad of physiological changes in the cell that can depend on the subcellular localization of the receptor. Mechanisms of signaling at the somato-dendritic compartment have been relatively well studied. As with all GPCRs, ligand binding to opioid receptor causes the Gα and Gβγ subunits to separate and act on their respective effector proteins. At the somato-dentritic compartment, Gβγ causes the opening of GIRKs, which causes hyperpolarization of the cell (Torrecilla et al., 2002; Wimpey and Chavkin, 1991). As with other $G_{i/o}$ coupled receptors, the Gα subunit causes inhibition of cyclic adenosine monophosphate (cAMP) production via adenylyl cyclase (AC) and downregulation of protein kinase A (PKA) (Minneman and Iversen, 1976). In addition to GIRKs, this cAMP pathway also leads to the opening of voltage-gated potassium channels (K_v) (Wimpey and Chavkin, 1992) and closing of hyperpolarization-activated cyclic nucleotide-gated (HCN) channels (Ingram and

Williams, 1994; Svoboda and Lupica, 1998), both of which also lead to net hyperpolarization of the cell.

The mechanisms of opioid receptors at the presynaptic terminal to suppress neurotransmitter release have not yet been demonstrated. It is presumed that, like other $G_{i/o}$ coupled receptors, opioid receptors act via Gβγ to inhibit voltage-gated calcium channels (VGCCs) to suppress vesicle release (Brody and Yue, 2000; Waard et al., 1997). However, studies showing that opioid agonists suppress miniature inhibitory post-synaptic currents (mIPSCs) suggest that there could be a mechanism downstream of VGCCs, since inhibition of VGCCs does not affect mIPSCs (Capogna et al., 1993; Scanziani et al., 1992). Another mechanism that has been established for inhibitory serotonin receptors at the presynaptic terminal involves Gβγ directly inhibiting release machinery by binding to the C-terminus of the 25 kDa synaptosome-associated protein (SNAP-25) (Gerachshenko et al., 2005). SNAP-25 is a critical component of the soluble N-ethylmaleimide-sensitive factor attachment protein receptor (SNARE) complex which is needed for vesicle release. These two Gβγ pathways are not mutually exclusive, as SNARE inhibition is also calcium dependent (Yoon et al., 2007) and some receptors have the capability to switch pathways depending on the microarchitecture of the primed vesicle complex (Hamid et al., 2014).

These putative mechanisms for opioid receptors in these two subcellular compartments are laid out in **Figure 1.3**. In Chapter 2, we set out to address the question of whether or not MOR and DOR utilize the same mechanisms within the somato-dendritic compartment and the presynaptic terminal.

The debate on functional interactions

The presence of both MOR and DOR in hippocampal PV cells opens the possibility that they could functionally interact. This means that engaging both receptors at the same time might cause enhancement or occlusion of signaling, at any point in their biochemical pathway. In the last 15 years, much attention has been paid to a putative interaction between MOR and DOR in the formation of heteromers (Cahill and Ong, 2018; Fujita et al., 2015; Gomes et al., 2013). Heteromers are signaling complexes made up of multiple receptors, that have a signaling profile distinct from the individual receptors. As opioid abuse is a public health emergency, the promise of a MOR/DOR heteromer with therapeutic potential has huge implications on drug design and discovery.

Some of the first evidence of MOR/DOR interaction indicative of a heteromer came from morphine analgesia assays. Repeated morphine administration is known to cause analgesic tolerance in rodents and in humans, presumably dependent on MOR desensitization (Bohn et al., 2000; Williams et al., 2013). Somewhat surprisingly, in early evidence of heteromers, DOR antagonists naltrindole and TIPP-Psi were able to attenuate the development of morphine tolerance (Fundytus et al., 1995), implying a role for DOR in this MOR-dependent pathway. Consistent with that data, TIPP-Psi was also found to potentiate MOR activity both in an *in vitro* cAMP assay as well as an *in vivo* analgesia assay (Gomes et al., 2004). More direct evidence came from the development of antibodies that specifically recognize the MOR/DOR heteromer to show its presence in multiple brain areas, and upregulation of the heteromer following chronic morphine administration (Gupta et al., 2010). Development of MOR-mcherry and DOR-eGFP knock-in mice allowed visualization of co-expression on a circuit and cellular level to identify areas of the brain that express both receptors and thus have the potential for heteromer formation

(Erbs et al., 2015). One of these areas was the hippocampus, and indeed co-immunoprecipitation of hippocampus tissue detected close proximity of MOR and DOR suggesting the formation of the heteromer.

Despite these data supporting the existence of a MOR/DOR heteromer, the functional relevance of the heteromer in native tissue is still contested. Behavioral studies that rely on DOR blockade can also inhibit learning and memory because DOR has been found to be necessary for hippocampal learning (Merrer et al., 2013). MOR/DOR specific antibodies may actually stabilize the conformation of the heteromer, overestimating its presence in native tissue (Spangler et al., 2019). Genetic knock-in strategies may also not be reflective of trafficking patterns of the endogenous receptors. There is some physiology data in the ventral tegmental area (VTA) showing augmented MOR responses in TIPP-Psi and augmented DOR responses in CTAP, suggesting the presence of heteromers (Margolis et al., 2017). However, this data is disputable as a separate study shows that MORs are not found in these neurons (Galaj et al., 2020). Another group found functional synergism between MOR and DOR, but no evidence of heteromers after chronic morphine treatment (Zhang and Pan, 2010). Lastly, MOR and DOR were found to traffic separately, with MOR surface expression unaffected by DOR activation and internalization (Wang et al., 2018). Notably, the same group found that a heteromer specific agonist CYM51010 activated GIRK currents in DOR knockout mice, questioning the specificity of heteromer targeted pharmacology.

In total, the substantial body of work on MOR/DOR heteromers show that they can exist, at least in exogenously expressed receptor systems and using probes thought to be specific for the MOR/DOR heteromer. However, unequivocal evidence for the presence and functional relevance of the MOR/DOR heteromer using native receptors on a single cell level, is yet to be

achieved. The PV basket cells in the hippocampus provide an ideal system to study potential functional interactions of all types between endogenously expressed MOR and DOR, and moreover to determine if the presence of the two receptors alone is enough to lead to the formation of a heteromer.

The current study aims to address some of the open questions outlined above. We used PV interneurons of the hippocampus to study the function of presynaptic and somato-dendritic MOR and DOR. Using novel photoactivable enkephalins, we developed sensitive assays for ligand potency and receptor signaling kinetics for MOR and DOR. These assays revealed a dominant role for DOR in the enkephalin response at this cell type, challenging the presumptions of opioid signaling in the hippocampus to date. Lastly, we found no evidence of functional interactions in a test for cross-desensitization and in a test for MOR/DOR heteromers, implying that co-expression of the two receptors is not sufficient for heteromer formation.

Part II. The black box of neuropeptide signaling

Neuropeptides as a specialized type of neurotransmitter

Neuropeptides are neurotransmitters in that they are synthesized and released from a presynaptic neuron, and then bind to receptors on postsynaptic neurons to produce a postsynaptic response. However, while neurotransmitter signaling has been very well characterized for classical amino acid and amine transmitters, there are still vast unknowns about neuropeptide signaling. Neuropeptides are made up of small chains of amino acids, and are therefore are much larger than amino acid and amine transmitters. While classical neurotransmitters are synthesized and stored at the presynaptic terminal in synaptic vesicles, neuropeptides are generally

synthesized in the cell body in the form of precursor peptides. These precursors are packaged into dense core vesicles (DCV) and must be transported long distances to their release sites. Dense core vesicles are much larger than synaptic vesicles (80-200 nm compared to 30-40 nm), and are named because they have a characteristic electron dense core that appears dark using electron microscopy (Edwards, 1998). While inside DCVs, the precursor peptides are processed by enzymes to their mature forms, of which there can be multiple within one vesicle, and then are ready to be released.

Once released, there are yet more distinctions between classical neurotransmission and neuropeptide transmission. Classical neurotransmission is generally fast – once the neurotransmitter is released, it travels ultra short distances (nanometers) across the synaptic cleft and to binds to its receptor, which often times are ion channels that are fast to open and close (milliseconds). After release, the neurotransmitter is quickly reuptaken to the presynaptic terminal by transporter proteins, terminating the signal and enabling the neurotransmitter to be repackaged and recycled quickly. In contrast, neuropeptides are thought to travel by *volume transmission*, long distance signaling within the brain (of at least micrometers) mediated by diffusion (van den Pol, 2012). The postsynaptic receptor for neuropeptides are GPCRs, which take longer to activate and trigger a signaling cascade that can be long lasting (seconds and greater). Once released, neuropeptides are slowly degraded by peptidases, therefore replenishment of the neuropeptide requires protein synthesis at the cell body and trafficking of DCVs. These differences between fast amino acid transmission and neuropeptide transmission are summarized in **Figure 1.4**.

Early evidence of neuropeptide release came from work done in the sympathetic ganglia of bullfrog, where a peptide resembling luteinizing hormone-releasing hormone (LHRH) was

found to elicit a slow post synaptic potential using a prolonged stimulus of 10 hz for 10 sec (Jan and Jan, 1982). This pointed to the idea that neuropeptide release is driven by prolonged high frequency stimuli, as opposed to neurotransmitters which can be driven by single action potentials. While this is a straightforward model, multiple groups have found it difficult to drive and detect release despite stimulating cells that are known to express neuropeptide (personal correspondences). For example, high frequency optogenetic stimulation of direct pathway medium spiny neurons (D1 MSNs) failed to evoke detectable dynorphin release, even though these neurons are known to synthesize dynorphin and GABA (Edwards et al., 2017). This raises the possibility that neuropeptide secretion may be under differential control of release – depending on the peptide, neuron class, brain region, etc – and that high frequency stimuli may not be enough to drive release under all conditions.

Other than electrical signals, what other forms of signals might modulate neuropeptide release? One possibility is intracellular second messengers, such as nucleotides, kinases, phosphatases, and other small molecules. In *Drosophila*, cAMP signaling was found to evoke release of a tagged, synthetic neuropeptide independent of extracellular Ca^{2+} (Shakiryanova et al., 2011). Protein kinase C (PKC) was found to regulate DCV release from neurons in *C elegans*, with PKC mutants to have reduced release of a YFP tagged FMRF amide-related peptide (Sieburth et al., 2007). These studies were performed on simpler model organisms because of their ease of access and tractability. Whether or not the findings apply to mammalian neurons is still to be determined. Both these studies also utilized a tagging approach to quantify DCV release, which may itself perturb DCV function.

That being said, there are numerous examples of neuropeptide release in the rodent brain found in literature which can inform further studies, with the caveat that the same rules may not

apply across all neuropeptide systems. Optogenetic stimulation of dynorphin-containing cells in a brain slice at 10 Hz for 15 min causes secretion of Dynorphin-A that is measurable though enzyme-linked immunoassay (ELISA) (Al-Hasani et al., 2015). 50 hz optogenetic stimulation of D1 MSNs drives release of substance P as measured using ELISA and electrophysiology (Francis et al., 2019). Despite this, electrophysiological evidence of opioid peptide release has been more limited. Endogenously released opioids caused long term depression (LTD) of excitatory inputs in the dorsal striatum which was only revealed with bath application of peptidase inhibitors (Atwood et al., 2014). In the amygdala, opioid release was also potentiated with the addition of peptidase inhibitors (Winters et al., 2017). And in the ventral striatum, the effects of Met-enkephalin-Arg-Phe (MERF) was revealed with the peptidase inhibitor captopril (Trieu et al., 2022). These studies suggest that the effects of endogenously released opioid peptides are subtle and challenging to measure using typical assays, but may be enhanced with the application of peptidase inhibitors.

Questions of neuropeptide release

The difficulty of studying neuropeptide release means that there is a trove of open questions related to neuropeptide signaling and release. Many of the principles that are taken for granted for neurotransmission do not necessarily apply to neuropeptides. For example, while classical neurotransmitters are released at synapses, the sites of neuropeptide release are unknown. Electron microscopy shows that DCVs are capable of being released at the cell body and dendrites as well as in axons (Morris and Pow, 1991). The location of neuropeptide release may also be differentially regulated, such as dendritic and axonal release being under the control

of different calcium channels (Simmons et al., 1995), and so may determine the function of the neuropeptide.

Another question is what are the contents of a DCV that are released during exocytosis? DCVs contain precursor peptides which are cleaved to mature peptides by enzymes inside the vesicle. However, one precursor peptide can give rise to multiple neuropeptides and multiple forms of a single neuropeptide. For example, proenkephalin is cleaved to multiple copies of met-enkephalin, leu-enkephalin, and other peptides (Fricker et al., 2020). Prodynorphin also gives rise to leu-enkephalin and dynorphins of various lengths, dynorphin A and dynorphin B. There has previously been evidence of neurons expressing more than one neuropeptide, but we now know that the vast majority of cortical neurons express several neuropeptides (Smith et al., 2019). Are different peptides present in the same DCVs and is their release differentially modulated? Dynorphin and orexin have been found to be present within the same DCVs in the hypothalamus (Muschamp et al., 2014). D1 MSNs in the striatum are known to express both dynorphin and substance P (Bockstaele et al., 1995), yet stimuli that drive substance P release are insufficient to drive and detect dynorphin release (unpublished data from the Banghart lab).

These questions are still far from being answered, but we will attempt to address another fundamental question in Chapter 3 – how far do neuropeptides travel when released? In some areas of the brain, there are mismatches between expression of peptides and their receptor, raising the possibility that a peptide may have to travel large distances to reach its cognate receptor (Herkenham, 1987). Due to the long half-life of peptides and the exquisite sensitivity of GPCR receptors to neuropeptides (Ludwig and Leng, 2006), diffusion of neuropeptide may still be able to signal large distances away from the release site. If the volume transmission

hypothesis is true, then how far can a neuropeptide diffuse and still produce meaningful signaling?

Novel tools to study neuropeptide signaling

As discussed above, neuropeptide signaling has historically been challenging to study because it is difficult to drive release and difficult to measure it. Stimulating electrodes are nonspecific and cause the release of many substances in addition to the neuropeptide under study. The conditions driving release are also unclear and high frequency electrical stimulus alone is often not enough to drive measurable peptide release. On the measurement side, neuropeptides act on a slow time scale, often eliciting subtle physiological changes in the postsynaptic cell, or changes that we don't yet understand and know how to quantify. This means traditional electrophysiology assays may be insufficient to detect peptide release, at least until we can define the conditions more precisely. However, recent years have seen a remarkable growth in neuroscience technology and we now have tools that can be leveraged to overcome some of these limitations and answer questions about neuropeptide signaling.

One of the most significant advances in the field of neuroscience in the last 15 years is that of optogenetics, giving scientists the ability to activate neurons in brain circuits with light (Boyden et al., 2005). Even better is the ability to selectively drive certain classes of neurons with cell-type specific animal lines, allowing researchers to target cells that express certain neuropeptides. This has been used to drive substance P and dynorphin, as examples (Al-Hasani et al., 2018; Francis et al., 2019). While there are still other substances released with optogenetic stimuli, the possibilities are limited by the cell class. In the case that channelrhodopsin (ChR2) stimulation is not enough to drive release, there are also chemogenetic tools to selectively

activate intracellular signaling pathways in a cell-specific manner. Designer receptors exclusively activated by designer drugs (DREADDs), such as hM3Dq, hM4Di, and Gs-DREADD, allow activation of GPCR pathways and secondary messengers in the cell (Roth, 2016). This can lead to increased cAMP signaling, for example, which may facilitate neuropeptide release (Shakiryanova et al., 2011). In addition, there are also light-activated chimeric GPCRs (OptoXRs) which allow for spatiotemporal specificity in GPCR activation (Tichy et al., 2019). Utilization of these tools or a combination of these tools gives researchers the opportunity to drive neuropeptide release in a cell-type specific and input specific way.

In the absence of robust endogenous neuropeptide release, another recent tool is the development of photoactivatable peptides which can mimic peptide release and also be used to probe the function of a peptide in its natural circuit. The caging of classical neurotransmitters has been utilized as a tool for many years, with caged glutamate being the most prominent example (Callaway and Katz, 1993). Opioid peptides can be caged in a similar way, with a caging group attached in a position that attenuates activity at opioid receptors, until exposure to light frees the peptide and renders it active (Banghart and Sabatini, 2012). This strategy has proved effective for dynorphin-8, leu-enkephalin (Banghart et al., 2018), and even opioid receptor antagonist naloxone (Banghart et al., 2013). Unlike other methods of applying neuropeptides such as bath perfusion or pressure injection, pre-equilibration and photoactivation of caged peptide occurs within microseconds and can be tightly controlled in terms of concentration, timing, and space. This makes it an ideal tool to study how a circuit responds to neuropeptide signaling.

Another major advance that will revolutionize the way we study neuropeptide signaling is the development of genetically encoded fluorescent sensors. Past methods of detecting neuropeptide release have relied on electrophysiology (low throughput, subject to noise) or

microdialysis (slow, no spatiotemporal resolution). Development of genetically encoded calcium sensors have greatly facilitated the study of neural activity both in brain slice and *in vivo*. Sensors for neurotransmitters are still in their early phases, but have already been widely implemented, especially for dopamine (Patriarchi et al., 2018; Sun et al., 2018). As these sensors are based on attaching a circularly permuted green fluorescent protein (cpGFP) on the GPCR of interest, they can theoretically be designed for any GPCR. The work by two groups on the dopamine sensors have already led to development of other sensors. In addition to the genetically encoded GPCR-activation-based (GRAB) dopamine (DA) sensor, GRAB sensors for adenosine triphosphate (ATP) (Wu et al., 2021), norepinephrine (Feng et al., 2019), and most recently oxytocin (Qian et al., 2022) have been developed by Yulong Li's group. Lin Tian's group, responsible for dLight, have created sensors for serotonin (Dong et al., 2021) and gastrin-releasing peptide (GRP) (Melzer et al., 2021). They are also working on creating sensors based on the opioid receptors, MOR, DOR, and KOR, to detect opioid peptides. Our lab has been working in collaboration with their group to characterize these sensors and validate their use in brain slice and *in vivo*.

To that end, I will be focusing on a specific sensor, kLight, used to detect dynorphin. In Chapter 3 I'll describe the characterization of multiple variants of kLight to determine the optimal variant. Coupling kLight with photoactivation of caged dynorphin, we can evoke photorelease of dynorphin and image subsequent activation of kLight. We then used spatially restricted uncaging to determine an apparent diffusion coefficient of dynorphin which can be used to answer the question of how far a neuropeptide travels once it's released. The utilization of these tools, both separately and together, will greatly expand our knowledge of neuropeptide signaling.

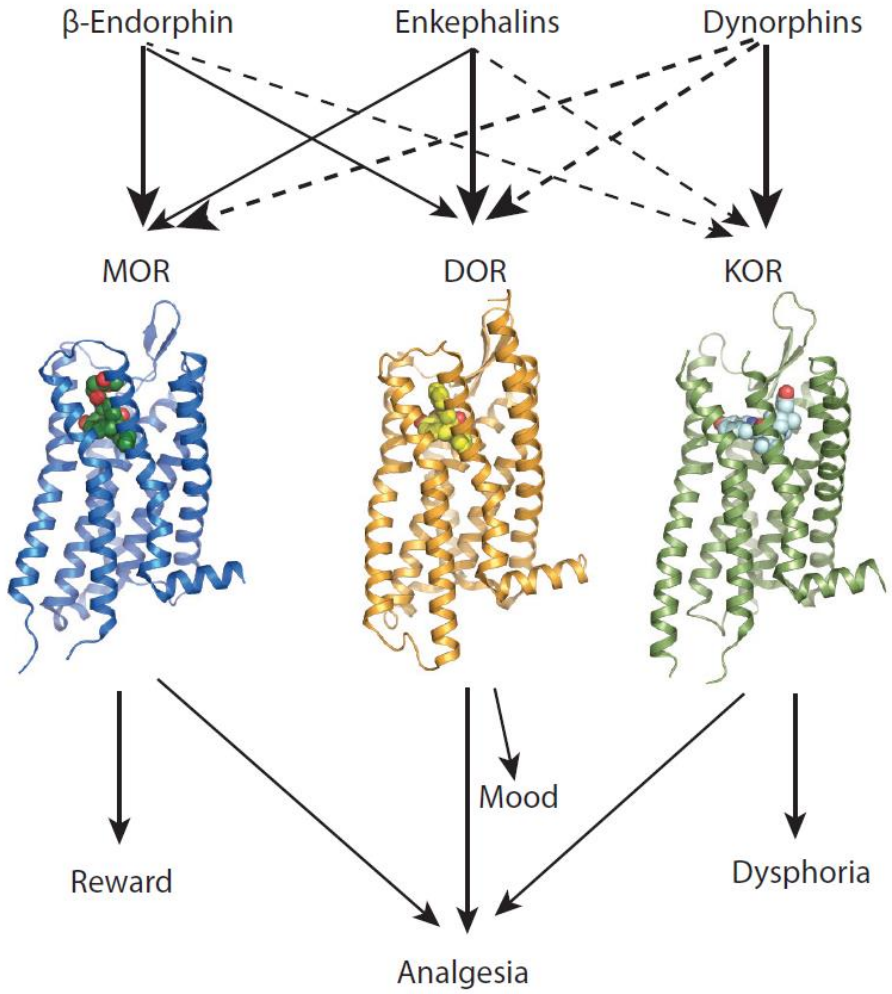

Figure 1.1. The interaction between endogenous opioid peptides, receptors, and behavioral outcomes.
The affinity of the peptide to each receptor is indicated by the strength of the arrow. For example, β-Endorphin binds to MOR most strongly, followed by DOR, then KOR. All three receptors produce analgesia, but each receptor also produces other behavioral consequences depending on the brain circuits of the receptor. Generally speaking, MOR is rewarding, DOR leads to decreases in anxiety, and KOR produces dysphoria. This figure was adapted from Corder et al., 2018 and Kiefer, 2009.

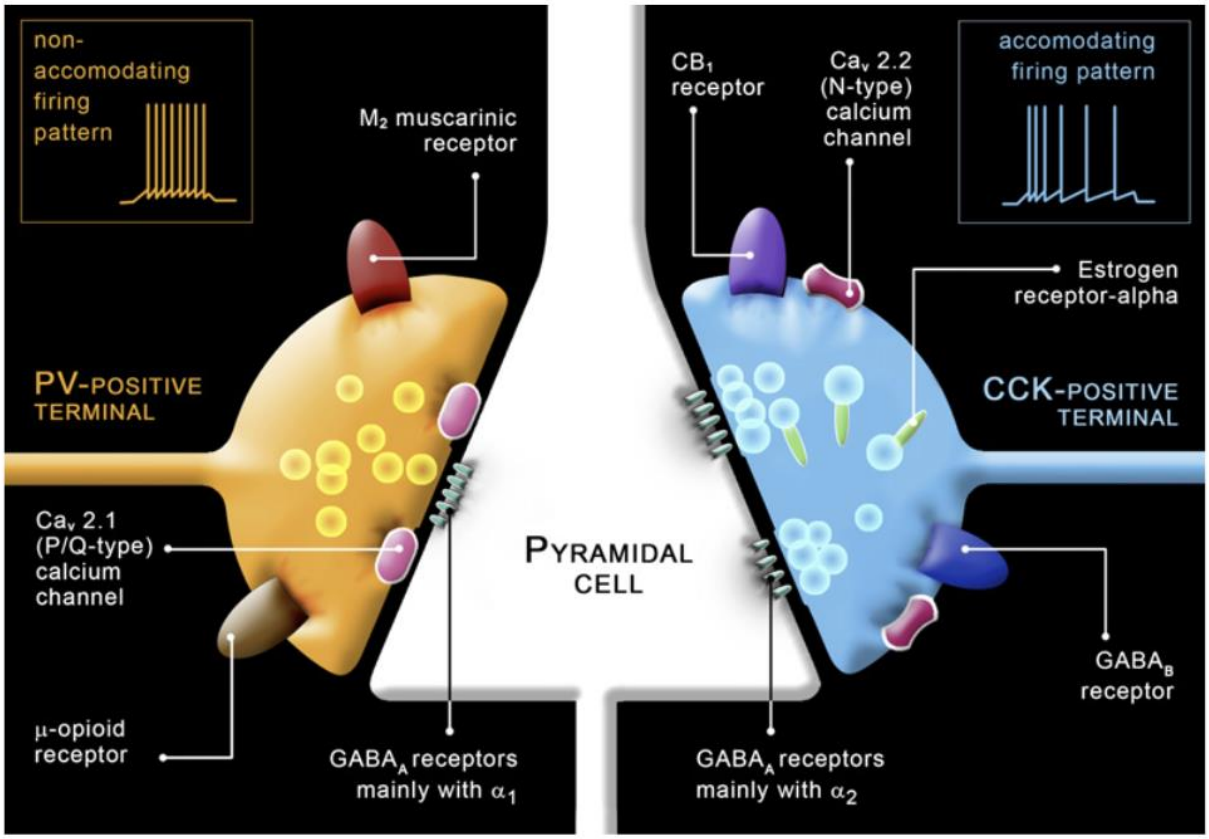

Figure 1.2. Basket cell synapses onto pyramidal cells in the hippocampus.
There are two types of basket cells that form perisomatic synapses onto pyramidal cells, PV basket cells and CCK basket cells. They are differentiated by the firing patterns, calcium channel types, and distinct receptors. CCK basket cells are known to express CB1 receptors while PV basket cells are known to express MORs (Glickfeld et al., 2008). Notably, any mention of the role of DOR is missing from this figure and from several papers describing this synapse. This figure is reprinted with permission from Freund and Katona, 2007.

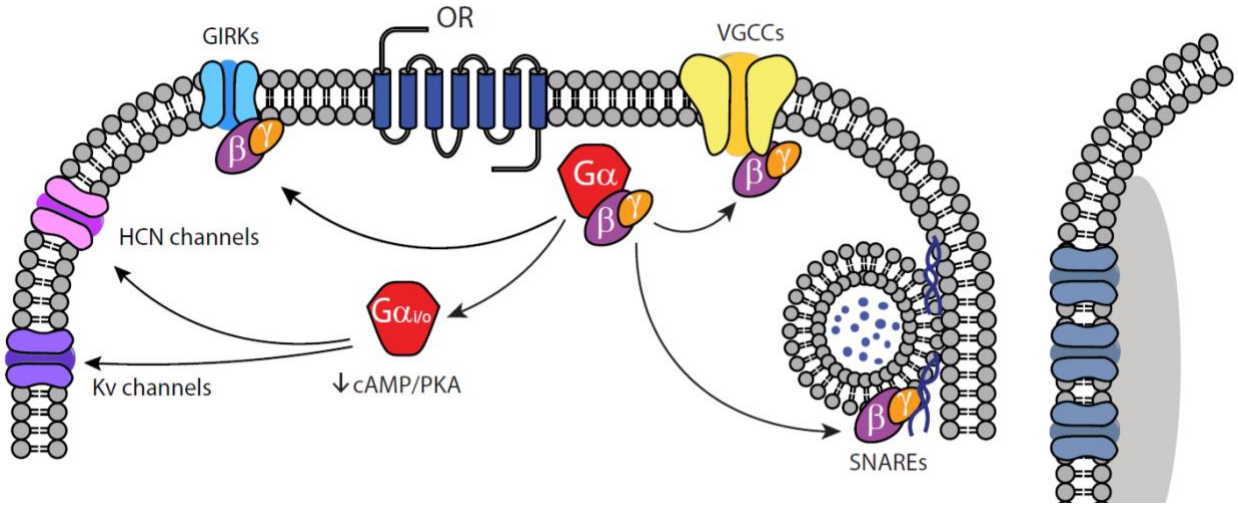

Figure 1.3. Putative mechanisms of opioid receptor signaling at the somato-dendritic and presynaptic compartments.
At the somato-dendritic compartment, opioid receptors open GIRKs to hyperpolarize the cell (Torrecilla et al., 2002; Wimpey and Chavkin, 1991). They also inhibit cAMP production which leads to opening of voltage-gated potassium channels (K_v) and closing of HCN channels (Ingram and Williams, 1994; Wimpey and Chavkin, 1992). At the presynaptic terminal, opioid receptors are likely to act through voltage caged calcium channels (VGCCs) or SNARE machinery, as have been shown for other $G_{i/o}$ coupled receptors (Brody and Yue, 2000; Gerachshenko et al., 2005).

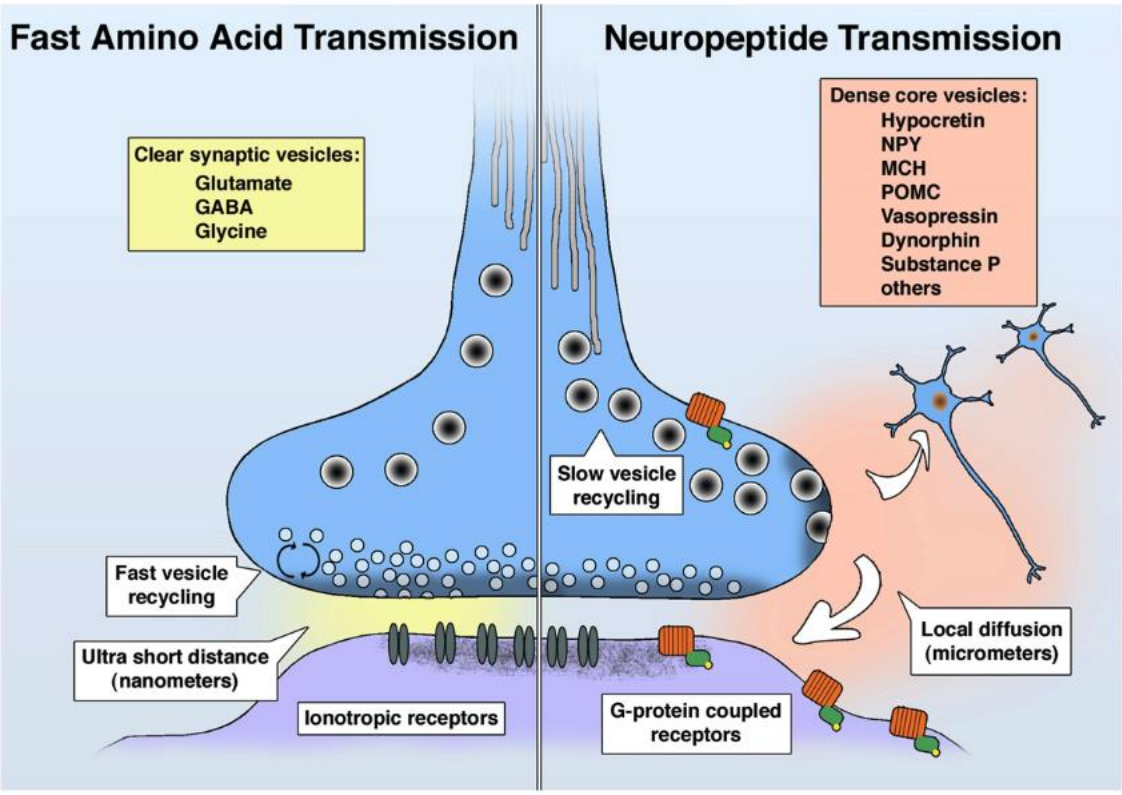

Figure 1.4. Comparison of classical neurotransmission with neuropeptide transmission. Classical neurotransmitters including glutamate and GABA are stored in clear synaptic vesicles and released at a synaptic cleft. They travel ultrashort distances, often to ionotropic receptors, and are quickly recycled leading to spatio-temporal specificity in signaling. On the other hand, neuropeptides are stored in dense core vesicles. While it is unknown where the release sites are, once released, neuropeptides diffuse to their post-synaptic targets which are GPCRs. Combined with this, lack of clearance and slow recycling leads to slow, prolonged responses. This figure is reprinted with permission from van den Pol, 2012.

References

Abraham, A.D., Casello, S.M., Schattauer, S.S., Wong, B.A., Mizuno, G.O., Mahe, K., Tian, L., Land, B.B., and Chavkin, C. (2021). Release of endogenous dynorphin opioids in the prefrontal cortex disrupts cognition. Neuropsychopharmacol *46*, 2330–2339.

Airan, R.D., Thompson, K.R., Fenno, L.E., Bernstein, H., and Deisseroth, K. (2009). Temporally precise in vivo control of intracellular signalling. Nature *458*, 1025–1029.

Al-Hasani, R., McCall, J.G., Shin, G., Gomez, A.M., Schmitz, G.P., Bernardi, J.M., Pyo, C.-O., Park, S.I., Marcinkiewcz, C.M., Crowley, N.A., et al. (2015). Distinct Subpopulations of Nucleus Accumbens Dynorphin Neurons Drive Aversion and Reward. Neuron *87*, 1063–1077.

Al-Hasani, R., Wong, J.-M.T., Mabrouk, O.S., McCall, J.G., Schmitz, G.P., Porter-Stransky, K.A., Aragona, B.J., Kennedy, R.T., and Bruchas, M.R. (2018). In vivo detection of optically-evoked opioid peptide release. ELife *7*, e36520.

Atwood, B.K., Kupferschmidt, D.A., and Lovinger, D.M. (2014). Opioids induce dissociable forms of long-term depression of excitatory inputs to the dorsal striatum. Nature Neuroscience *17*, 540–548.

Banghart, M.R., and Sabatini, B.L. (2012). Photoactivatable neuropeptides for spatiotemporally precise delivery of opioids in neural tissue. Neuron *73*, 249–259.

Banghart, M.R., Williams, J.T., Shah, R.C., Lavis, L.D., and Sabatini, B.L. (2013). Caged Naloxone Reveals Opioid Signaling Deactivation Kinetics. Molecular Pharmacology *84*, 687–695.

Banghart, M.R., He, X.J., and Sabatini, B.L. (2018). A Caged Enkephalin Optimized for Simultaneously Probing Mu and Delta Opioid Receptors. ACS Chemical Neuroscience *9*, 684–690.

Barreca, T., Siani, C., Franceschini, R., Francaviglia, N., Messina, V., Perria, C., and Rolandi, E. (1986). Diurnal beta-endorphin changes in human cerebrospinal fluid. Life Sci *38*, 2263–2267.

Bing, G., Wilson, B., Hudson, P., Jin, L., Feng, Z., Zhang, W., Bing, R., and Hong, J.-S. (1997). A single dose of kainic acid elevates the levels of enkephalins and activator protein-1 transcription factors in the hippocampus for up to 1 year. Proceedings of the National Academy of Sciences *94*, 9422–9427.

Blasco-Ibáñez, J., Martínez-Guijarro, F., and Freund, T. (1998). Enkephalin-containing interneurons are specialized to innervate other interneurons in the hippocampal CA1 region of the rat and guinea-pig. European Journal of Neuroscience *10*, 1784–1795.

Bloodgood, B.L., Sharma, N., Browne, H.A., Trepman, A.Z., and Greenberg, M.E. (2013). The activity-dependent transcription factor NPAS4 regulates domain-specific inhibition. Nature *503*, 121–125.

Bockstaele, E.J. van, Gracy, K.N., and Pickel, V.M. (1995). Dynorphin-immunoreactive neurons in the rat nucleus accumbens: Ultrastructure and synaptic input from terminals containing substance P and/or dynorphin. J Comp Neurol *351*, 117–133.

Boecker, H., Sprenger, T., Spilker, M.E., Henriksen, G., Koppenhoefer, M., Wagner, K.J., Valet, M., Berthele, A., and Tolle, T.R. (2008). The Runner's High: Opioidergic Mechanisms in the Human Brain. Cereb Cortex *18*, 2523–2531.

Bohn, L.M., Gainetdinov, R.R., Lin, F.-T., Lefkowitz, R.J., and Caron, M.G. (2000). μ-Opioid receptor desensitization by β-arrestin-2 determines morphine tolerance but not dependence. Nature *408*, 720.

Boyden, E.S., Zhang, F., Bamberg, E., Nagel, G., and Deisseroth, K. (2005). Millisecond-timescale, genetically targeted optical control of neural activity. Nat Neurosci *8*, 1263–1268.

Brigidi, G.S., Hayes, M.G.B., Santos, N.P.D., Hartzell, A.L., Texari, L., Lin, P.-A., Bartlett, A., Ecker, J.R., Benner, C., Heinz, S., et al. (2019). Genomic Decoding of Neuronal Depolarization by Stimulus-Specific NPAS4 Heterodimers. Cell *179*, 373-391.e27.

Brody, D., and Yue, D. (2000). Relief of G-protein inhibition of calcium channels and short-term synaptic facilitation in cultured hippocampal neurons. The Journal of Neuroscience : The Official Journal of the Society for Neuroscience *20*, 889–898.

Brownstein, M.J. (1993). A brief history of opiates, opioid peptides, and opioid receptors. Proc National Acad Sci *90*, 5391–5393.

Cahill, C.M., and Ong, E. (2018). Delta Opioid Receptor Pharmacology and Therapeutic Applications. Handbook of Experimental Pharmacology *247*, 115–127.

Cahill, C.M., McClellan, K.A., Morinville, A., Hoffert, C., Hubatsch, D., O'Donnell, D., and Beaudet, A. (2001a). Immunohistochemical distribution of delta opioid receptors in the rat central nervous system: Evidence for somatodendritic labeling and antigen-specific cellular compartmentalization. J Comp Neurol *440*, 65–84.

Cahill, C.M., Morinville, A., Lee, M.-C., Vincent, J.-P., Collier, B., and Beaudet, A. (2001b). Prolonged Morphine Treatment Targets δ Opioid Receptors to Neuronal Plasma Membranes and Enhances δ-Mediated Antinociception. J Neurosci *21*, 7598–7607.

Cahill, C.M., Holdridge, S.V., and Morinville, A. (2007). Trafficking of δ-opioid receptors and other G-protein-coupled receptors: implications for pain and analgesia. Trends Pharmacol Sci *28*, 23–31.

Callaway, E.M., and Katz, L.C. (1993). Photostimulation using caged glutamate reveals functional circuitry in living brain slices. Proc National Acad Sci *90*, 7661–7665.

Capogna, M., Gähwiler, B.H., and Thompson, S.M. (1993). Mechanism of mu-opioid receptor-mediated presynaptic inhibition in the rat hippocampus in vitro. The Journal of Physiology *470*, 539–558.

Carr, D.B., Bullen, B.A., Skrinar, G.S., Arnold, M.A., Rosenblatt, M., Beitins, I.Z., Martin, J.B., and McArthur, J.W. (1981). Physical Conditioning Facilitates the Exercise-Induced Secretion of Beta-Endorphin and Beta-Lipotropin in Women. New Engl J Medicine *305*, 560–563.

Commons, K.G., Beck, S.G., Rudoy, C., and Bockstaele, E.J.V. (2001). Anatomical evidence for presynaptic modulation by the delta opioid receptor in the ventrolateral periaqueductal gray of the rat. J Comp Neurol *430*, 200–208.

Dalayeun, J.F., Norès, J.M., and Bergal, S. (1993). Physiology of β-endorphins. A close-up view and a review of the literature. Biomed Pharmacother *47*, 311–320.

Dong, C., Ly, C., Dunlap, L.E., Vargas, M.V., Sun, J., Hwang, I.-W., Azinfar, A., Oh, W.C., Wetsel, W.C., Olson, D.E., et al. (2021). Psychedelic-inspired drug discovery using an engineered biosensor. Cell *184*, 2779-2792.e18.

Drake, C., Terman, G., Simmons, M., Milner, T., Kunkel, D., Schwartzkroin, P., and Chavkin, C. (1994). Dynorphin opioids present in dentate granule cells may function as retrograde inhibitory neurotransmitters. J Neurosci *14*, 3736–3750.

Edwards, R.H. (1998). Neurotransmitter release: Variations on a theme. Curr Biol *8*, R883–R885.

Edwards, N.J., Tejeda, H.A., Pignatelli, M., Zhang, S., McDevitt, R.A., Wu, J., Bass, C.E., Bettler, B., Morales, M., and Bonci, A. (2017). Circuit specificity in the inhibitory architecture of the VTA regulates cocaine-induced behavior. Nature Neuroscience *20*, nn.4482.

Erbs, E., Faget, L., Scherrer, G., Kessler, P., Hentsch, D., Vonesch, J.-L., Matifas, A., Kieffer, B.L., and Massotte, D. (2012). Distribution of delta opioid receptor-expressing neurons in the mouse hippocampus. Neuroscience *221*, 203–213.

Erbs, E., Faget, L., Scherrer, G., Matifas, A., Filliol, D., Vonesch, J.-L., Koch, M., Kessler, P., Hentsch, D., Birling, M.-C., et al. (2015). A mu–delta opioid receptor brain atlas reveals neuronal co-occurrence in subcortical networks. Brain Struct Funct *220*, 677–702.

Faget, L., Erbs, E., Merrer, J.L., Scherrer, G., Matifas, A., Benturquia, N., Noble, F., Decossas, M., Koch, M., Kessler, P., et al. (2012). In Vivo Visualization of Delta Opioid Receptors upon Physiological Activation Uncovers a Distinct Internalization Profile. The Journal of Neuroscience *32*, 7301–7310.

Feng, J., Zhang, C., Lischinsky, J.E., Jing, M., Zhou, J., Wang, H., Zhang, Y., Dong, A., Wu, Z., Wu, H., et al. (2019). A Genetically Encoded Fluorescent Sensor for Rapid and Specific In Vivo Detection of Norepinephrine. Neuron *102*, 745-761.e8.

Francis, T.C., Yano, H., Demarest, T.G., Shen, H., and Bonci, A. (2019). High-Frequency Activation of Nucleus Accumbens D1-MSNs Drives Excitatory Potentiation on D2-MSNs. Neuron.

Freund, T.F., and Katona, I. (2007). Perisomatic Inhibition. Neuron *56*, 33–42.

Fricker, L.D., Margolis, E., Gomes, I., and Devi, L.A. (2020). Five decades of research on opioid peptides: Current knowledge and unanswered questions. Mol Pharmacol *98*, mol.120.119388.

Fuentealba, P., Tomioka, R., Dalezios, Y., Márton, L.F., Studer, M., Rockland, K., Klausberger, T., and Somogyi, P. (2008). Rhythmically Active Enkephalin-Expressing GABAergic Cells in the CA1 Area of the Hippocampus Project to the Subiculum and Preferentially Innervate Interneurons. The Journal of Neuroscience *28*, 10017–10022.

Fujita, W., Gomes, I., and Devi, L.A. (2015). Heteromers of μ-δ opioid receptors: new pharmacology and novel therapeutic possibilities. Brit J Pharmacol *172*, 375–387.

Fundytus, M.E., Schiller, P.W., Shapiro, M., Weltrowska, G., and Coderre, T.J. (1995). Attenuation of morphine tolerance and dependence with the highly selective δ-opioid receptor antagonist TIPP[ψ]. Eur J Pharmacol *286*, 105–108.

Galaj, E., Han, X., Shen, H., Jordan, C.J., He, Y., Humburg, B., Bi, G.-H., and Xi, Z.-X. (2020). Dissecting the Role of GABA Neurons in the VTA versus SNr in Opioid Reward. J Neurosci *40*, 8853–8869.

Gall, C. (1988). Seizures induce dramatic and distinctly different changes in enkephalin, dynorphin, and CCK immunoreactivities in mouse hippocampal mossy fibers. J Neurosci *8*, 1852–1862.

Gall, C., Brecha, N., Karten, H.J., and Chang, K. (1981). Localization of enkephalin-like immunoreactivity to identified axonal and neuronal populations of the rat hippocampus. J Comp Neurol *198*, 335–350.

Gerachshenko, T., Blackmer, T., Yoon, E.-J., Bartleson, C., Hamm, H.E., and Alford, S. (2005). Gβγ acts at the C terminus of SNAP-25 to mediate presynaptic inhibition. Nature Neuroscience *8*, nn1439.

Gerfen, C.R. (1992). The neostriatal mosaic: multiple levels of compartmental organization. Trends in Neurosciences *15*, 133–139.

Glickfeld, L.L., and Scanziani, M. (2006). Distinct timing in the activity of cannabinoid-sensitive and cannabinoid-insensitive basket cells. Nature Neuroscience *9*, 807–815.

Glickfeld, L.L., Atallah, B.V., and Scanziani, M. (2008). Complementary Modulation of Somatic Inhibition by Opioids and Cannabinoids. The Journal of Neuroscience *28*, 1824–1832.

Gomes, I., Gupta, A., Filipovska, J., Szeto, H.H., Pintar, J.E., and Devi, L.A. (2004). A role for heterodimerization of μ and δ opiate receptors in enhancing morphine analgesia. P Natl Acad Sci Usa *101*, 5135–5139.

Gomes, I., Ayoub, M.A., Fujita, W., Jaeger, W.C., Pfleger, K.D.G., and Devi, L.A. (2013). G Protein–Coupled Receptor Heteromers. Annu Rev Pharmacol *56*, 1–23.

Gupta, A., Mulder, J., Gomes, I., Rozenfeld, R., Bushlin, I., Ong, E., Lim, M., Maillet, E., Junek, M., Cahill, C.M., et al. (2010). Increased Abundance of Opioid Receptor Heteromers After Chronic Morphine Administration. Sci. Signal. *3*, ra54–ra54.

Hamid, E., Church, E., Wells, C.A., Zurawski, Z., Hamm, H.E., and Alford, S. (2014). Modulation of Neurotransmission by GPCRs Is Dependent upon the Microarchitecture of the Primed Vesicle Complex. The Journal of Neuroscience *34*, 260–274.

Hartzell, A.L., Martyniuk, K.M., Brigidi, G.S., Heinz, D., Djaja, N.A., Payne, A., and Bloodgood, B.L. (2018). Npas4 recruits CCK basket cell synapses and enhances cannabinoid-sensitive inhibition in the mouse hippocampus. ELife *7*.

Herkenham, M. (1987). Mismatches between neurotransmitter and receptor localizations in brain: observations and implications. Neuroscience *23*, 1–38.

Ingram, S.L., and Williams, J.T. (1994). Opioid inhibition of Ih via adenylyl cyclase. Neuron *13*, 179–186.

Jan, L.Y., and Jan, Y.N. (1982). Peptidergic transmission in sympathetic ganglia of the frog. J Physiology *327*, 219–246.

Jullié, D., Stoeber, M., Sibarita, J.-B., Zieger, H.L., Bartol, T.M., Arttamangkul, S., Sejnowski, T.J., Hosy, E., and Zastrow, M. von (2019). A Discrete Presynaptic Vesicle Cycle for Neuromodulator Receptors. Neuron *105*, 663-677.e8.

Kanamatsu, T., Obie, J., Grimes, L., McGinty, J., Yoshikawa, K., Sabol, S., and Hong, J. (1986). Kainic acid alters the metabolism of Met5-enkephalin and the level of dynorphin A in the rat hippocampus. J Neurosci *6*, 3094–3102.

Kibaly, C., Xu, C., Cahill, C.M., Evans, C.J., and Law, P.-Y.Y. (2019). Non-nociceptive roles of opioids in the CNS: opioids' effects on neurogenesis, learning, memory and affect. Nature Reviews. Neuroscience *20*, 5–18.

Kieffer, B.L. (2009). Opioid Peptides and Receptors. In Encyclopedia of Neuroscience, pp. 235–240.

Leroy, F., Solis, C.A. de, Boyle, L.M., Bock, T., Lofaro, O.M., Buss, E.W., Asok, A., Kandel, E.R., and Siegelbaum, S.A. (2021). Enkephalin release from VIP interneurons in the hippocampal CA2/3a region mediates heterosynaptic plasticity and social memory. Mol Psychiatr 1–22.

Lonart, G., Schoch, S., Kaeser, P.S., Larkin, C.J., Südhof, T.C., and Linden, D.J. (2003). Phosphorylation of RIM1alpha by PKA triggers presynaptic long-term potentiation at cerebellar parallel fiber synapses. Cell *115*, 49–60.

Ludwig, M., and Leng, G. (2006). Dendritic peptide release and peptide-dependent behaviours. Nat Rev Neurosci *7*, 126–136.

Lupica, C.R. (1995). Delta and mu enkephalins inhibit spontaneous GABA-mediated IPSCs via a cyclic AMP-independent mechanism in the rat hippocampus. The Journal of Neuroscience : The Official Journal of the Society for Neuroscience *15*, 737–749.

Lupica, C.R., and Dunwiddie, T.V. (1991). Differential effects of mu- and delta-receptor selective opioid agonists on feedforward and feedback GABAergic inhibition in hippocampal brain slices. Synapse *8*, 237–248.

Margolis, E.B., Fujita, W., Devi, L.A., and Fields, H.L. (2017). Two delta opioid receptor subtypes are functional in single ventral tegmental area neurons, and can interact with the mu opioid receptor. Neuropharmacology *123*, 420–432.

Melzer, S., Newmark, E.R., Mizuno, G.O., Hyun, M., Philson, A.C., Quiroli, E., Righetti, B., Gregory, M.R., Huang, K.W., Levasseur, J., et al. (2021). Bombesin-like peptide recruits disinhibitory cortical circuits and enhances fear memories. Cell.

Merrer, J.L., Rezai, X., Scherrer, G., Becker, J.A.J., and Kieffer, B.L. (2013). Impaired Hippocampus-Dependent and Facilitated Striatum-Dependent Behaviors in Mice Lacking the Delta Opioid Receptor. Neuropsychopharmacology *38*, npp20131.

Minneman, K.P., and Iversen, L.L. (1976). Enkephalin and opiate narcotics increase cyclic GMP accumulation in slices of rat neostriatum. Nature *262*, 313–314.

Morris, J.F., and Pow, D.V. (1991). Widespread release of peptides in the central nervous system: Quantitation of tannic acid-captured exocytoses. Anatomical Rec *231*, 437–445.

Muschamp, J.W., Hollander, J.A., Thompson, J.L., Voren, G., Hassinger, L.C., Onvani, S., Kamenecka, T.M., Borgland, S.L., Kenny, P.J., and Carlezon, W.A. (2014). Hypocretin (orexin) facilitates reward by attenuating the antireward effects of its cotransmitter dynorphin in ventral tegmental area. Proc National Acad Sci *111*, E1648–E1655.

Nicholson, C., and Tao, L. (1993). Hindered diffusion of high molecular weight compounds in brain extracellular microenvironment measured with integrative optical imaging. Biophys J *65*, 2277–2290.

Park, D., and Dunlap, K. (1998). Dynamic Regulation of Calcium Influx by G-Proteins, Action Potential Waveform, and Neuronal Firing Frequency. J Neurosci *18*, 6757–6766.

Patriarchi, T., Cho, J.R., Merten, K., Howe, M.W., Marley, A., Xiong, W.-H.H., Folk, R.W., Broussard, G.J., Liang, R., Jang, M.J., et al. (2018). Ultrafast neuronal imaging of dopamine dynamics with designed genetically encoded sensors. Science (New York, N.Y.) *360*.

Pelkey, K.A., Chittajallu, R., Craig, M.T., Tricoire, L., Wester, J.C., and McBain, C.J. (2017). Hippocampal GABAergic Inhibitory Interneurons. Physiol Rev *97*, 1619–1747.

Persoon, C.M., Hoogstraaten, R.I., Nassal, J.P., Weering, J.R.T. van, Kaeser, P.S., Toonen, R.F., and Verhage, M. (2019). The RAB3-RIM Pathway Is Essential for the Release of Neuromodulators. Neuron.

Piskorowski, R.A., and Chevaleyre, V. (2013). Delta-Opioid Receptors Mediate Unique Plasticity onto Parvalbumin-Expressing Interneurons in Area CA2 of the Hippocampus. The Journal of Neuroscience *33*, 14567–14578.

Puehler, W., Zöllner, C., Brack, A., Shaqura, M.A., Krause, H., Schäfer, M., and Stein, C. (2004). Rapid upregulation of μ opioid receptor mrna in dorsal root ganglia in response to peripheral inflammation depends on neuronal conduction. Neuroscience *129*, 473–479.

Qian, T., Wang, H., Wang, P., Geng, L., Mei, L., Osakada, T., Tang, Y., Kania, A., Grinevich, V., Stoop, R., et al. (2022). Compartmental Neuropeptide Release Measured Using a New Oxytocin Sensor. Biorxiv 2022.02.10.480016.

Reiner, A. (1988). Handbook of Chemical Neuroanatomy. Volume 4: GABA and Neuropeptides in the CNS, Part I . A. Björklund , T. Hökfelt. Q Rev Biology *63*, 244–245.

Roth, B.L. (2016). DREADDs for Neuroscientists. Neuron *89*, 683–694.

Scanziani, M., Capogna, M., Gähwiler, B.H., and Thompson, S.M. (1992). Presynaptic inhibition of miniature excitatory synaptic currents by baclofen and adenosine in the hippocampus. Neuron *9*, 919–927.

Schoffelmeer, A.N., Warden, G., Hogenboom, F., and Mulder, A.H. (1991). Beta-endorphin: a highly selective endogenous opioid agonist for presynaptic mu opioid receptors. J Pharmacol Exp Ther *258*, 237–242.

Shakiryanova, D., Zettel, G.M., Gu, T., Hewes, R.S., and Levitan, E.S. (2011). Synaptic neuropeptide release induced by octopamine without Ca2+ entry into the nerve terminal. Proceedings of the National Academy of Sciences *108*, 4477–4481.

Shirayama, Y., Ishida, H., Iwata, M., Hazama, G., Kawahara, R., and Duman, R.S. (2004). Stress increases dynorphin immunoreactivity in limbic brain regions and dynorphin antagonism produces antidepressant-like effects. J Neurochem *90*, 1258–1268.

Sieburth, D., Madison, J.M., and Kaplan, J.M. (2007). PKC-1 regulates secretion of neuropeptides. Nature Neuroscience *10*, 49–57.

Simmons, M.L., Terman, G.W., Gibbs, S.M., and Chavkin, C. (1995). L-type calcium channels mediate dynorphin neuropeptide release from dendrites but not axons of hippocampal granule cells. Neuron *14*, 1265–1272.

Smith, S.J., Sümbül, U., Graybuck, L.T., Collman, F., Seshamani, S., Gala, R., Gliko, O., Elabbady, L., Miller, J.A., Bakken, T.E., et al. (2019). Single-cell transcriptomic evidence for dense intracortical neuropeptide networks. Elife *8*, e47889.

Soler-Llavina, G.J., and Sabatini, B.L. (2006). Synapse-specific plasticity and compartmentalized signaling in cerebellar stellate cells. Nat Neurosci *9*, 798–806.

Spangler, J.B., Moraga, I., Jude, K.M., Savvides, C.S., and Garcia, K.C. (2019). A strategy for the selection of monovalent antibodies that span protein dimer interfaces. J Biological Chem *294*, 13876–13886.

Stumm, R.K., Zhou, C., Schulz, S., and Höllt, V. (2004). Neuronal types expressing mu- and delta-opioid receptor mRNA in the rat hippocampal formation. The Journal of Comparative Neurology *469*, 107–118.

Sun, F., Zeng, J., Jing, M., Zhou, J., Feng, J., Owen, S.F., Luo, Y., Li, F., Wang, H., Yamaguchi, T., et al. (2018). A Genetically Encoded Fluorescent Sensor Enables Rapid and Specific Detection of Dopamine in Flies, Fish, and Mice. Cell *174*, 481-496.e19.

Svoboda, K.R., and Lupica, C.R. (1998). Opioid Inhibition of Hippocampal Interneurons via Modulation of Potassium and Hyperpolarization-Activated Cation (Ih) Currents. J Neurosci *18*, 7084–7098.

Svoboda, K.R., Adams, C.E., and Lupica, C.R. (1999). Opioid receptor subtype expression defines morphologically distinct classes of hippocampal interneurons. J Neurosci Official J Soc Neurosci *19*, 85–95.

Syková, E., and Nicholson, C. (2008). Diffusion in Brain Extracellular Space. Physiol Rev *88*, 1277–1340.

Thorne, R.G., and Nicholson, C. (2006). In vivo diffusion analysis with quantum dots and dextrans predicts the width of brain extracellular space. Proc National Acad Sci *103*, 5567–5572.

Tichy, A.-M., Gerrard, E.J., Sexton, P.M., and Janovjak, H. (2019). Light-activated chimeric GPCRs: limitations and opportunities. Current Opinion in Structural Biology *57*, 196–203.

Toll, L., Berzetei-Gurske, I.P., Polgar, W.E., Brandt, S.R., Adapa, I.D., Rodriguez, L., Schwartz, R.W., Haggart, D., O'Brien, A., White, A., et al. (1998). Standard binding and functional assays

related to medications development division testing for potential cocaine and opiate narcotic treatment medications. NIDA Research Monograph *178*, 440–466.

Torrecilla, M., Marker, C.L., Cintora, S.C., Stoffel, M., Williams, J.T., and Wickman, K. (2002). G-Protein-Gated Potassium Channels Containing Kir3.2 and Kir3.3 Subunits Mediate the Acute Inhibitory Effects of Opioids on Locus Ceruleus Neurons. J Neurosci *22*, 4328–4334.

Trieu, B.H., Remmers, B.C., Toddes, C., Brandner, D.D., Lefevre, E.M., Kocharian, A., Retzlaff, C.L., Dick, R.M., Mashal, M.A., Gauthier, E.A., et al. (2022). Angiotensin-converting enzyme gates brain circuit–specific plasticity via an endogenous opioid. Sci New York N Y eabl5130.

van den Pol, A.N. (2012). Neuropeptide Transmission in Brain Circuits. Neuron *76*, 98–115.

Veening, J.G., Gerrits, P.O., and Barendregt, H.P. (2012). Volume transmission of beta-endorphin via the cerebrospinal fluid; a review. Fluids Barriers Cns *9*, 16.

Waard, M.D., Liu, H., Walker, D., Scott, V.E., Gurnett, C.A., and Campbell, K.P. (1997). Direct binding of G-protein betagamma complex to voltage-dependent calcium channels. Nature *385*, 446–450.

Wan, R.Q., Wiegant, V.M., Jong, W. de, and Wied, D. de (1996). Alterations of β-endorphin-like immunoreactivity in CSF following behavioral training using a passive avoidance procedure. Psychoneuroendocrino *21*, 503–513.

Wang, D., Tawfik, V.L., Corder, G., Low, S.A., François, A., Basbaum, A.I., and Scherrer, G. (2018). Functional Divergence of Delta and Mu Opioid Receptor Organization in CNS Pain Circuits. Neuron.

Williams, J.T., Ingram, S.L., Henderson, G., Chavkin, C., Zastrow, M. von, Schulz, S., Koch, T., Evans, C.J., and Christie, M.J. (2013). Regulation of μ-opioid receptors: desensitization, phosphorylation, internalization, and tolerance. Pharmacological Reviews *65*, 223–254.

Wimpey, T.L., and Chavkin, C. (1991). Opioids activate both an inward rectifier and a novel voltage-gated potassium conductance in the hippocampal formation. Neuron *6*, 281–289.

Wimpey, T.L., and Chavkin, C. (1992). 8-Bromo-cAMP blocks opioid activation of a voltage-gated potassium current in isolated hippocampal neurons. Neurosci Lett *137*, 137–140.

Winters, B.L., Gregoriou, G.C., Kissiwaa, S.A., Wells, O.A., Medagoda, D.I., Hermes, S.M., Burford, N.T., Alt, A., Aicher, S.A., and Bagley, E.E. (2017). Endogenous opioids regulate moment-to-moment neuronal communication and excitability. Nature Communications *8*, 14611.

Wu, L.-G., and Saggau, P. (1997). Presynaptic inhibition of elicited neurotransmitter release. Trends in Neurosciences *20*, 204–212.

Wu, Z., He, K., Chen, Y., Li, H., Pan, S., Li, B., Liu, T., Xi, F., Deng, F., Wang, H., et al. (2021). A sensitive GRAB sensor for detecting extracellular ATP in vitro and in vivo. Neuron.

Xiong, H., Lacin, E., Ouyang, H., Naik, A., Xu, X., Xie, C., Youn, J., Kumar, K., Kern, T., Aisenberg, E., et al. (2021). Probing neuropeptide volume transmission in vivo by a novel all-optical approach. Biorxiv 2021.09.10.459853.

Yao, Z., Velthoven, C.T.J. van, Nguyen, T.N., Goldy, J., Sedeno-Cortes, A.E., Baftizadeh, F., Bertagnolli, D., Casper, T., Chiang, M., Crichton, K., et al. (2021). A taxonomy of transcriptomic cell types across the isocortex and hippocampal formation. Cell *184*, 3222-3241.e26.

Yoon, E.-J., Gerachshenko, T., Spiegelberg, B.D., Alford, S., and Hamm, H.E. (2007). Gβγ Interferes with Ca2+-Dependent Binding of Synaptotagmin to the Soluble N-Ethylmaleimide-Sensitive Factor Attachment Protein Receptor (SNARE) Complex. Mol Pharmacol *72*, 1210–1219.

Zakarian, S., and Smyth, D. (1979). Distribution of active and inactive forms of endorphins in rat pituitary and brain. Proc National Acad Sci *76*, 5972–5976.

Zhang, Z., and Pan, Z.Z. (2010). Synaptic Mechanism for Functional Synergism between δ- and μ-Opioid Receptors. J Neurosci *30*, 4735–4745.

Zubieta, J.-K., Gorelick, D.A., Stauffer, R., Ravert, H.T., Dannals, R.F., and Frost, J.J. (1996). Increased mu opioid receptor binding detected by PET in cocaine–dependent men is associated with cocaine craving. Nat Med *2*, 1225–1229.

Zurawski, Z., Gray, A.D., Brady, L.J., Page, B., Church, E., Harris, N.A., Dohn, M.R., Yim, Y.Y., Hyde, K., Mortlock, D.P., et al. (2019). Disabling the Gβγ-SNARE interaction disrupts GPCR-mediated presynaptic inhibition, leading to physiological and behavioral phenotypes. Science Signaling *12*.

CHAPTER 2. Convergent, functionally independent signaling by mu and delta opioid receptors in hippocampal parvalbumin interneurons

Abstract

Functional interactions between G protein-coupled receptors are poised to enhance neuronal sensitivity to neuromodulators and therapeutic drugs. Mu and Delta opioid receptors (MORs and DORs) can interact when overexpressed in the same cells, but whether co-expression of endogenous MORs and DORs in neurons leads to functional interactions is unclear. Here, in mice, we show that both MORs and DORs inhibit parvalbumin-expressing basket cells (PV-BCs) in hippocampal CA1 through partially occlusive signaling pathways that terminate on somato-dendritic potassium channels and presynaptic calcium channels. Using photoactivatable opioid neuropeptides, we find that DORs dominate the response to enkephalin in terms of both ligand-sensitivity and kinetics, which may be due to relatively low expression levels of MOR. Opioid-activated potassium channels do not show heterologous desensitization, indicating that MORs and DORs signal independently. In a direct test for heteromeric functional interactions, the DOR antagonist TIPP-Psi does not alter the kinetics or potency of either the potassium channel or synaptic responses to photorelease of the MOR agonist DAMGO. Thus, aside from largely redundant and convergent signaling, MORs and DORs do not functionally interact in PV-BCs in a way that impacts somato-dendritic potassium currents or synaptic transmission. These findings imply that crosstalk between MORs and DORs, either in the form of physical interactions or synergistic intracellular signaling, is not a preordained outcome of co-expression in neurons.

Introduction

G protein-coupled receptors (GPCRs) regulate cellular physiology through a diverse but limited number of intracellular signaling pathways. In neurons, signaling through multiple GPCRs expressed in the same cell can converge on the same molecular effectors (*e.g.* ion channels) to regulate neurophysiological properties such as cellular excitability and neurotransmitter release. Although GPCRs that engage the same family of G proteins ($G\alpha_s$, $G\alpha_{i/o}$ or $G\alpha_q$) are poised to functionally interact through convergent biochemical signaling, it is not clear *a priori* whether such interactions would actually occur. Examples of interactions include functional synergy, when activation of one receptor subtype enhances activity at the other, or reciprocal occlusion, when the receptor subtypes compete for the same pool of effector molecules. Alternatively, GPCRs have been proposed to functionally interact through the formation of receptor heteromers, such that conformational changes due to ligand binding at one receptor shape agonist-driven signaling at the other.

Mu and delta opioid receptors (MORs and DORs) are both $G\alpha_{i/o}$-coupled GPCRs that are activated by endogenous opioid neuropeptides such as enkephalin to suppress neuronal excitability and synaptic output. MORs are the primary target of widely used opiate analgesics (*e.g.* morphine, fentanyl) that are plagued by tolerance, high potential for addiction, and a propensity to cause respiratory depression. MORs and DORs have been proposed to functionally interact such that DOR-targeting drugs could reduce the clinical liabilities of MOR-targeting analgesics. For example, either pharmacological suppression or genetic removal of DOR attenuates morphine tolerance (Abdelhamid *et al.*, 1991; Sánchez-Blázquez, García-España and Garzón, 1997; Zhu *et al.*, 1999). Furthermore, co-administration of MOR and DOR agonists produces spinal, supraspinal and peripheral analgesic synergy (Porreca *et al.*, 1987; Schuster *et*

al., 2015; Bruce *et al.*, 2019). In contrast, antagonism of one receptor has been reported to enhance agonist-driven activity at the other receptor in assays using heterologous receptor expression. These observations have been interpreted to support the existence of MOR/DOR heteromers that interact through direct allosteric coupling (Fujita, Gomes and Devi, 2015; Cahill and Ong, 2018). MOR/DOR heteromers have been specifically implicated as potential therapeutic targets for the treatment of pain, as intrathecal co-administration of the DOR-selective antagonist TIPP-Psi with morphine produces stronger analgesia than morphine alone (Gomes *et al.*, 2004). Due to the clinical potential of therapeutic approaches that simultaneously engage MORs and DORs, understanding the mechanisms that underlie their potential for functional interactions is of great importance.

Relatively few studies have investigated functional interactions between endogenous MORs and DORs using sensitive measurements of cellular physiology with the single-cell resolution required to implicate cell-autonomous interactions, as opposed to circuit-level effects. In recordings from neurons in the nucleus raphe magnus after upregulation of DORs in response to chronic morphine treatment, MORs and DORs were found to synergistically suppress inhibitory synaptic transmission through a PKA-dependent pathway, but evidence of heteromers was not observed (Zhang and Pan, 2010). Also supporting functionally independent signaling, using both electrophysiological and receptor trafficking experiments, a more recent study of spinal dorsal horn neurons that co-express MOR and DOR did not find evidence for co-internalization or co-degradation after intrathecal administration of either the DOR-selective agonist SNC80 or the MOR-selective agonist [D-Ala^2, NMe-Phe^4, Gly-ol^5]enkephalin (DAMGO) (Wang *et al.*, 2018). In contrast, recordings from ventral tegmental area neurons suggested MOR/DOR interactions consistent with heteromer formation (Margolis *et al.*, 2017).

In that study, TIPP-Psi enhanced DAMGO-evoked membrane potential hyperpolarization, and the MOR antagonist CTOP enhanced hyperpolarization evoked by the DOR agonists DPDPE and deltorphin II. However, at least some of the recordings were from dopamine neurons, which have been shown not to express *Oprm1* mRNA (Galaj *et al.*, 2020). Thus, in naïve mice, unequivocal evidence for functional interactions between endogenous MORs and DORs in the same neurons, and in particular, for the existence of MOR/DOR heteromers that impact neuronal physiology, is lacking.

In some brain regions, including the hippocampus, MORs and DORs are established to be co-expressed in the same neurons, such that the receptors and their downstream intracellular signaling pathways are poised to interact (Chieng, Christie and Osborne, 2006; Erbs *et al.*, 2015). In the hippocampus, activation of MORs in GABA neurons contributes to stress-induced memory deficits (Shi *et al.*, 2020), whereas DORs may contribute to spatial contextual cue-related memory retrieval (Le Merrer *et al.*, 2011, 2012, 2013). Recently, we reported that MORs and DORs both contribute to opioid-mediated suppression of perisomatic inhibition in the CA1 region of hippocampus, consistent with previous studies of MOR and DOR modulation of synaptic transmission (Glickfeld, Atallah and Scanziani, 2008; Piskorowski and Chevaleyre, 2013; Banghart, He and Sabatini, 2018). In fact, MORs and DORs are well established to regulate inhibitory synaptic transmission in CA1 (Zieglgänsberger *et al.*, 1979; Nicoll, Alger and Jahr, 1980; Lupica and Dunwiddie, 1991; Lupica, Proctor and Dunwiddie, 1992; Lupica, 1995; Svoboda and Lupica, 1998; Svoboda, Adams and Lupica, 1999; Rezaï *et al.*, 2012). Although a substantial body of work indicates co-expression of MOR and DOR in CA1 parvalbumin basket cells (PV-BCs), which are a primary source of perisomatic inhibition (Stumm *et al.*, 2004; Erbs

et al., 2012; Faget *et al.*, 2012; Yao *et al.*, 2021), a direct comparison of their neurophysiological actions has not been conducted.

In this study, we explored potential interactions between MORs and DORs in CA1 PV-expressing basket cells using recordings from hippocampal slices. In order to obtain precise and sensitive measures of receptor function, we optically probed native MORs and DORs using photoactivatable (caged) opioid neuropeptides (Banghart and Sabatini, 2012; Banghart, He and Sabatini, 2018). Using this approach, we found that MORs and DORs activate partially overlapping pools of somato-dendritic potassium channels in PV-BCs, and suppress synaptic output from PV-BCs in a mutually occlusive manner. Despite their co-expression and functional redundancy, we did not find evidence of synergy or for heteromers, indicating that MOR and DOR signal in a parallel, functionally independent manner in PV-BCs.

Results

Occlusive suppression of hippocampal perisomatic inhibition by MORs and DORs

We first confirmed that both MORs and DORs are co-expressed in PV-BCs using fluorescence in-situ hybridization, which revealed that 78% (171/218) of *Pvalb* mRNA-containing neurons with cell bodies in and around stratum pyramidale contain both *Oprm1* and *Oprd1* mRNA (**Figure 2.1A, B**). To determine if both MORs and DORs are functional in PV-BCs, we virally expressed the light-gated cation channel Chronos in a Cre recombinase-dependent manner in the CA1 region of $Pvalb^{Cre}$ mice and measured the effects of the selective MOR and DOR agonists DAMGO and SNC162, respectively, on light-evoked synaptic transmission using electrophysiological recordings from pyramidal cells (PCs) in acute hippocampal slices (Klapoetke *et al.*, 2014). We chose SNC162 due to its exceptional selectivity

for DOR over MOR (Knapp *et al.*, 1996). To maximize the relative contribution of perisomatic inhibition from PV basket cells, as opposed to dendrite-targeting PV bistratified cells, we restricted the area of illumination to a small region of stratum pyramidale around the recorded PC (**Figure 2.2A**). Bath perfusion of either DAMGO (1 μM) or SNC162 (1 μM) strongly reduced the optically-evoked IPSC (oIPSC) to a similar degree (**Figure 2.2B-D**). Sequential drug application only slightly increased the degree of suppression compared to either drug alone (DAMGO: 0.69 ± 0.05, n = 9 cells; SNC162: 0.70 ± 0.05, n = 9 cells; both: 0.76 ± 0.03, n = 18 cells; no significant differences, Ordinary one-way ANOVA) (**Figure 2.2D, Figure 2.1F**). In both cases, application of pairs of optical stimuli (50 ms apart) revealed small increases in the paired-pulse ratio (PPR) in the presence of the opioid agonist, consistent with a presynaptic mechanism of action for the opioid receptor (BL: 0.47 ± 0.08; DAMGO: 0.68 ± 0.14; n = 9 pairs; p = 0.0078, Wilcoxon matched-pairs signed rank test; BL: 0.42 ± 0.05; SNC162: 0.56 ± 0.07; n = 8 pairs; p = 0.016, Wilcoxon matched-pairs signed rank test) (**Figure 2.2E**). With sustained application, both the effects of DAMGO and SNC162 appeared to desensitize slightly, with DAMGO showing greater desensitization (**Figure 2.1H, I**) ($DAMGO_{early}$: 0.69 ± 0.05; $DAMGO_{late}$: 0.44 ± 0.07; n = 9 pairs; p = 0.0038, Paired t test; $SNC162_{early}$: 0.70 ± 0.05; $SNC162_{late}$: 0.61 ± 0.06; n = 9 pairs; p = 0.048, Paired t test). These results reveal that both MORs and DORs suppress the output of PV-BCs in a mutually occlusive manner.

To avoid complications due to optical cross-talk between optogenetic tools and photoactivatable peptides in subsequent experiments, we established an electrical stimulation protocol for preferential activation of PV-BC terminals by placing a small bipolar stimulating electrode in stratum pyramidale immediately adjacent to the recorded PC (**Figure 2.2F**). Recordings were made from PCs near stratum oriens, as these have been shown to receive BC

input that is biased towards PV-BCs, as opposed to CCK-BCs (Lee *et al.*, 2014). Whereas fast-spiking, presumably PV-BCs have been shown to be opioid, but not cannabinoid sensitive, output from regular-spiking CCK-BCs is suppressed by CB1R, but not MOR activation (Glickfeld, Atallah and Scanziani, 2008). Consistent with only a minor contribution to the electrically evoked IPSC (eIPSC) from CB1R-expressing CCK-BCs, bath application of the CB1R agonist WIN55 (1 μM) resulted in only modest eIPSC suppression (0.25 ± 0.07, n = 8 cells), and application of WIN55 in the presence of DAMGO produced only slightly more suppression than DAMGO alone, although this effect was not significant, suggesting some occlusion (DAMGO: 0.67 ± 0.02, n = 12 cells; WIN+DAMGO: 0.79 ± 0.03, n = 8 cells; p = 0.14, Ordinary one-way ANOVA with Tukey's multiple comparison test) (**Figure 2.1C-E**). Under these electrical stimulation conditions, DAMGO and SNC162 again suppressed the eIPSC to a similar degree, with DAMGO, but not SNC162, producing slight desensitization **(Figure 2.1H)** ($DAMGO_{early}$: 0.70 ± 0.03; $DAMGO_{late}$: 0.41 ± 0.05; n = 13 pairs; p < 0.0001, Paired t test; $SNC162_{early}$: 0.63 ± 0.06; $SNC162_{late}$: 0.57 ± 0.05; n = 9 pairs; p = 0.10, Paired t test). For both eIPSCs and oIPSCs, DAMGO resulted in more desensitization than SNC162 (**Figure 2.1I**) (eIPSC DAMGO: 0.28 ± 0.04; oIPSC DAMGO: 0.25 ± 0.06; eIPSC SNC162: 0.07 ± 0.04; oIPSC SNC162: 0.09 ± 0.04; Skillings-Mack non-parametric test for grouped data (Mack and Skillings, 1980), p < 0.0001 for column effects (DAMGO vs SNC162), p = 0.13 for row effects (eIPSC vs oIPSC)). As with optogenetic stimulation, DAMGO and SNC162 exhibited strong mutual occlusion of the eIPSC (DAMGO: 0.69 ± 0.02, n = 14 cells; SNC162: 0.63 ± 0.06, n = 9 cells; both: 0.75 ± 0.04, n = 14 cells; no significant differences, Ordinary one-way ANOVA), and a small increase in PPR was produced by DAMGO but not SNC162 (BL: 0.67 ± 0.03; DAMGO: 0.80 ± 0.04; n = 11 pairs; p = 0.019, Wilcoxon matched-pairs signed rank test; BL:

0.65 ± 0.02; SNC162: 0.77 ± 0.04; n = 9 pairs; p = 0.055, Wilcoxon matched-pairs signed rank test) (**Figure 2.2F-J, Figure 2.1F**). Although it is possible that an opioid-sensitive population of non-PV interneurons contributes to the opioid sensitive component of the eIPSC, the effects of DAMGO and SNC162 on the eIPSC and oIPSC were indistinct (no significant difference, Two-way ANOVA) (**Figure 2.1G)**.

MOR and DOR are thought to exhibit similar affinity for enkephalin, but how this translates to ligand efficacy at native receptors in neurons is not clear. In addition, receptor signaling kinetics could prove to be a sensitive means of detecting functional interactions. To compare the ligand sensitivity and receptor signaling kinetics of MORs and DORs, we turned to photoactivatable derivatives of the MOR and DOR agonist [Leu^5]-enkephalin (LE) (**Figure 2.3A, top**) (Banghart and Sabatini, 2012). For quantitative pharmacology, we chose to use *N*-MNVOC-LE, which is highly inactive at both DOR and MOR (Banghart, He and Sabatini, 2018). In the presence of *N*-MNVOC-LE (6 μM), which is optimized for simultaneous activation of MORs and DORs, application of a strong 5 ms UV light flash 2 sec prior to an eIPSC produced a rapid, transient suppression of the eIPSC that recovered within 1-2 minutes (**Figure 2.3A, B**). Varying UV light intensity in a graded fashion allowed us to rapidly obtain power-response curves within a single recording. To assess the potency of LE at MORs and DORs, and the relative contributions of the receptors to the eIPSC suppression by LE, we recorded power-response curves in the absence and presence of the MOR- and DOR-selective antagonists CTOP (1 μM) and TIPP-Psi (1 μM), respectively (**Figure 2.3C**). We chose CTOP over its analog CTAP due to its higher selectivity for MORs. Whereas LE uncaging at the highest light power (84 mW) in the absence of opioid antagonists suppressed synaptic transmission by 63 ± 4%, activation of MORs or DORs alone, which were isolated by antagonizing with TIPP-Psi or

CTOP, respectively, suppressed synaptic output by ~40% each. Although the extent of suppression achieved with caged LE was somewhat less than with bath application (**Figure 2.2I**), the relative contributions of MORs and DORs were similar in both experiments and consistent with mutual occlusion. The power-response curve revealed that LE exhibits ~3-fold greater potency for DORs than MORs in regulating perisomatic inhibition (EC_{50} values in the absence (black, 3.28±0.47 mW) and presence of either CTOP (red, 2.29±0.61 mW) or TIPP-Psi (blue, 9.30±1.40 mW)). Moreover, DOR activation largely accounts for the actions of LE in the absence of antagonists. This could reflect greater affinity for DORs, or more efficacious signaling by DORs than MORs (**Figure 2.3D**).

We evaluated receptor signaling kinetics using the photoactivatable LE derivative CYLE, which photolyzes within tens of microseconds, such that receptor activation is rate-limiting (Banghart and Sabatini, 2012; Banghart, He and Sabatini, 2018). In order to sample synaptic transmission at frequencies sufficient to resolve receptor signaling kinetics, we drove eIPSCs in 5 s bouts at 10, 20 and 50 Hz, and photolyzed CYLE (6 μM) after synaptic depression had stabilized to a steady state (**Figure 2.3E**). To obtain the time-constants of synaptic suppression for each receptor, we repeated this experiment in the presence of the selective antagonists and fit the post-flash eIPSC amplitudes with a single exponential function (**Figure 2.3F**). The time constants we obtained for each pharmacological condition were similar for all three stimulus frequencies (**Figure 2.3G**). At 20 Hz, DOR (CTOP at 20 Hz, tau = 419 ± 105 ms, n = 11 cells) exhibited kinetics indistinct from the drug-free condition (ACSF at 20 Hz, tau = 259 ± 30 ms, n = 8 cells), but the time-constant of MOR-mediated suppression was surprisingly slow (TIPP-Psi at 20 Hz, tau = 683 ± 36 ms, n = 6 cells; p = 0.0046, Kruskal-Wallis test with Dunn's multiple comparisons). At other frequencies, although the MOR kinetics trended toward slower time

constants, statistical significance was not observed. We also observed that the extent of eIPSC suppression correlated inversely with the frequency of synaptic stimulation, and that this was most pronounced in the absence of antagonists (**Figure 2.3H**).

Together, these results suggest that MOR and DOR suppress output from overlapping populations of PV-BC presynaptic terminals, and that this suppression is dominated by DOR, both in terms of sensitivity to LE and response kinetics.

MORs and DORs suppress GABA release by inhibiting voltage-gated Ca^{2+} channels

At least two mechanisms of presynaptic inhibition by $G\alpha_{i/o}$-coupled GPCRs have been established, but the pathways engaged by opioid receptors in PV-BCs are not known. One potential mechanism involves the inhibition of voltage-sensitive calcium channels (VSCCs) by Gβγ proteins (Bean, 1989), whereas the other involves direct suppression of SNARE proteins by Gβγ binding to the C-terminus of SNAP25 (Blackmer *et al.*, 2001; Gerachshenko *et al.*, 2005; Zurawski *et al.*, 2019; Hamm and Alford, 2020). The observed frequency-dependent synaptic suppression is consistent with both mechanisms, as Gβγ binding to VSCCs is reversed by strong depolarization, and elevated Ca^{2+} facilitates displacement of Gβγ from the SNARE complex by Ca^{2+}-bound synaptotagmin (Park and Dunlap, 1998; Brody and Yue, 2000; Yoon *et al.*, 2007).

To ask if MOR and DOR inhibit presynaptic VSCCs in PV-BCs, we imaged action potential-induced Ca^{2+} transients in presynaptic boutons of PV-BCs using two-photon laser scanning microscopy. PV-BCs were targeted for whole cell current clamp recordings in *Pvalb^{Cre}*/*Rosa26-lsl-tdTomato* (Ai14)) mice with the small molecule Ca^{2+} indicator Fluo5F included in the recording pipette (**Figure 2.4A**). Line scans across putative boutons were

obtained while triggering either one or five action potentials, before and after bath application of DAMGO, SNC162 or both drugs together (**Figure 2.4B**).

Individually, DAMGO and SNC162 both caused a ~30% reduction in the peak ΔF/F evoked by either stimulation protocol (DAMGO 27.27% for 1 AP, 17.73% for 5 APs, SNC162 31.18% for 1 AP, 26.55% for 5 APs). When DAMGO and SNC162 were applied together, these presynaptic Ca^{2+} transients were suppressed by ~40%, on average (DAMGO then SNC162 40.95% for 1 AP, 38.92% for 5 APs, SNC162 then DAMGO 46.08% for 1 AP, 40.85% for 5 APs) (**Figure 2.4C, D**). Under the conditions employed, peak ΔF/F is linearly correlated with Ca^{2+} concentration (Higley and Sabatini, 2008). Given the nonlinear Ca^{2+}-dependence of vesicular fusion, a 30% reduction in presynaptic Ca^{2+} is consistent with the strong suppression of PV-BC IPSCs by MORs and DORs (Wu and Saggau, 1997). These results indicate that the inhibition of VSCCs by both MORs and DORs is the most likely mechanism accounting for their effects on inhibitory transmission. Furthermore, the marginal effect of adding a second drug suggests convergence on the same pool of VSCCs.

Enkephalin generates large outward somato-dendritic currents in PV-BCs primarily through DORs rather than MORs

$G\alpha_{i/o}$-coupled GPCRs, including both MORs and DORs, often hyperpolarize neurons by activating G protein-coupled inward rectifier K^+ (GIRK) channels, as well as voltage-gated K+ channels, or by suppressing hyperpolarization gated cyclic nucleotide (HCN) channels (Williams, Egan and North, 1982; North *et al.*, 1987; Wimpey and Chavkin, 1991; Svoboda and Lupica, 1998). Although MORs were previously reported to activate outward currents in the somato-dendritic compartment of fast spiking CA1 BCs, the role of DORs has not been explored

(Glickfeld, Atallah and Scanziani, 2008). To address this, we performed voltage-clamp recordings of opioid-evoked currents in tdTom-labeled cells in *Pvalb*^{Cre}/*Rosa26-lsl-tdTomato* mice (**Figure 2.5A**). At a holding potential of -55 mV, *N*-MNVOC-LE photoactivation using strong (84 mW) light flashes applied to the soma and proximal dendrites of the recorded neuron evoked rapidly rising outward currents that decayed over ~1 min, similar to previous observations in locus coeruleus (**Figure 2.5B, C**) (Banghart and Sabatini, 2012). Surprisingly, blocking MORs with CTOP had no measurable effect on the light-evoked current (ACSF: 81.7 ± 9.6 pA, n = 9 cells; CTOP: 82.5 ± 12.8 pA, n = 10 cells; not significant). In contrast, blocking DOR with TIPP-Psi greatly reduced the current amplitude (TIPP-Psi: 26.4 ± 4.8 pA, n = 11 cells; p = 0.016), and addition of both drugs completely abolished it (CTOP + TIPP-Psi: 7.1 ± 0.09 pA, n = 5 cells; p = 0.0009; Kruskal-Wallis test with Dunn's multiple comparisons). Power-response curves in the presence of each antagonist revealed a larger DOR-mediated than MOR-mediated current (**Figure 2.5D**). Similar to our observations with presynaptic receptors, LE exhibited greater potency at DORs than MORs in generating outward currents (EC50 values of ACSF: 17.55 ± 2.98 mW, CTOP: 7.59 ± 1.26 mW, TIPP-Psi: 28.03 ± 7.14 mW) (**Figure 2.5E**). Assessment of current activation kinetics with CYLE (6 µM) revealed that, whereas DOR-mediated currents activated with kinetics similar to the MOR currents previously observed in LC neurons, somato-dendritic MOR currents in CA1 PV-BCs activated 3-fold more slowly, similar to the rate observed for presynaptic MOR in these neurons (ACSF: 275.9 ± 35.7 ms, n = 11 cells; CTOP: 395.3 ± 109.6 ms, n = 6 cells; TIPP-Psi: 844.1 ± 105.2 ms, n = 9 cells; p = 0.019, Kruskal-Wallis test with Dunn's multiple comparisons) (**Figure 2.5F, G**) (Ingram *et al.*, 1997; Banghart and Sabatini, 2012). The small MOR-mediated currents, coupled with similarly slow

signaling kinetics in both the presynaptic and somato-dendritic compartments, suggest that MOR signaling is relatively inefficient in CA1 PV-BCs.

To identify the ion channels underlying the MOR- and DOR-mediated outward currents, we applied the GIRK channel blocker Ba^{2+} (1 mM) while delivering strong light flashes to uncage *N*-MNVOC-LE, in the absence and presence of CTOP or TIPP-Psi. Consistent with a primary role of GIRK channels, Ba^{2+} blocked the majority, but notably not all, of the current mediated by both MOR and DOR to the same extent (**Figure 2.6A, B**) (Ba^{2+} in ACSF: 67.9 ± 4.9 %, n = 8 cells; Ba^{2+} in CTOP: 59.6 ± 9.7 %, n = 10 cells; Ba^{2+} in TIPP-Psi: 67.7 ± 9.1 %, n = 11 cells; no significant differences, Ordinary one-way ANOVA). At DORs, inclusion of the HCN channel blocker ZD7288 (1 µM) did not further block the current, suggesting the involvement of additional ion channels (Ba^{2+}, Zd70288 in CTOP: 74.0 ± 5.6 %, n = 9 cells; no significant difference, Unpaired t test). Due to the small size of the Ba^{2+}-insensitive MOR-mediated current, we did not examine the effect of ZD7288 at MOR.

One possible explanation for the slow kinetics and low efficacy of MOR-mediated GIRK activation, as well as slow kinetics of synaptic suppression, is relatively low cell surface expression of MORs in comparison to DORs. In LC, reducing available surface MORs with a covalent antagonist leads to a reduction not only in the amplitude of MOR-mediated currents, but also a slowing of activation kinetics (Williams, 2014). To test this hypothesis, we virally overexpressed human MOR (hMOR) with an mCherry tag in *Pvalb*^{Cre} mice and probed the resulting enhanced MOR signaling with CYLE in TIPP-Psi (Liu *et al.*, 2021) (**Figure 2.5H, I**). As predicted, hMOR overexpression enhanced both the magnitude (57.5 ± 7.8 pA, n = 8 cells, $p < 0.0001$, Unpaired t-test) and the kinetics (421.8 ± 68.7 ms, n = 8 cells, $p = 0.0052$, Unpaired t-test) of the MOR-mediated current evoked with a strong light flash in comparison to those

recorded from *Pvalb*^{Cre}/*Rosa26-lsl-tdTomato* mice (**Figure 2.5I-K**). Both parameters correlated strongly with mCherry fluorescence as an indicator of expression level (Peak: r = 0.8314, Tau on: r = -0.8538, Pearson's correlation coefficient) (**Figure 2.6C, D**). These results indicate that low MOR expression levels can account for the surprisingly modest effects of MOR activation in the somato-dendritic compartment of PV-BCs.

MORs and DORs do not functionally interact in CA1 PV-BCs

The apparent co-expression of MORs and DORs in the somato-dendritic compartment is a minimal requirement for functional interactions between receptors. We therefore asked if MORs and DORs undergo heterologous desensitization such that desensitization of one receptor perturbs the function of the other. We first confirmed that prolonged exposure to DAMGO (1 µM) caused desensitization of the resulting outward current (**Figure 2.7A**). After incubating slices in DAMGO for at least 10 minutes to maximally desensitize MOR, power-response curves were obtained in the presence of DAMGO, such that subsequent photorelease of LE would only activate DORs (**Figure 2.7B**). We compared these responses to those evoked in naïve slices bathed in the MOR antagonist CTOP. Indicative of a lack of heterologous desensitization, neither the efficacy or potency of LE at DORs was affected by MOR desensitization (EC50 value of LE in the presence of DAMGO: 5.12 ± 0.38 mW, n = 9 cells; CTOP: 6.00 ± 0.42 mW, n = 7 cells) (**Figure 2.7C, D**). Similarly, prolonged exposure to deltorphin II (1 µM) caused desensitization of the outward current (**Figure 2.7E**). Desensitization of DORs using deltorphin II did not affect the ability of LE to elicit somato-dendritic outward currents compared to naïve slices bathed in the DOR antagonist TIPP-Psi (EC50 value of LE in the presence of Delt II:

13.47 ± 1.10 mW, n = 7 cells; TIPP-Psi: 13.47 ± 1.10 mW, n = 11 cells) . These results reveal that MORs and DORs do not undergo heterologous desensitization in CA1 PV-BCs.

MORs and DORs have been proposed to functionally interact through the formation of heteromeric receptors such that a selective antagonist for one receptor enhances signaling at the other (Gomes *et al.*, 2004). To directly probe for functional interactions of this type, we developed a new photoactivatable analogue of the MOR-selective agonist DAMGO, CNV-Y-DAMGO (Ma, He and Banghart, 2021). We hypothesized that if these interactions are present, inclusion of TIPP-Psi in the bath would lead to a leftward shift in the optical power-response curves of CNV-Y-DAMGO, and possibly an increase in the response kinetics. We tested this by uncaging CNV-Y-DAMGO (1 µM) while measuring somato-dendritic currents in PV-BCs (**Figure 2.8A-E**) and eIPSCs in pyramidal neurons (**Figure 2.8F-J**). In both cases, TIPP-Psi did not alter either the kinetics of the response to DAMGO photorelease (GIRK tau on CNV-Y-DAMGO: 917.6 ± 75.7 ms, n = 11 cells; CNV-Y-DAMGO + TIPP-Psi: 808.8 ± 46.5 ms, n = 7 cells; no significant difference, Mann-Whitney test; eIPSC tau on CNV-Y-DAMGO: 476.4 ± 36.9 ms, n = 8 cells; CNV-Y-DAMGO + TIPP-Psi: 441.6 ± 28.1 ms, n = 7 cells; no significant difference, Mann-Whitney test) (**Figure 2.8C, H**), its maximal effect (**Figure 2.8D, I**), or its power-dependence (EC50 values for GIRKs in CNV-Y-DAMGO: 6.86 ± 0.68 mW, n = 8 cells; CNV-Y-DAMGO + TIPP-Psi: 8.53 ± 0.64 mW, n = 7 cells; EC50 values for eIPSCs in CNV-Y-DAMGO: 2.79 ± 0.44 mW, n = 9 cells; CNV-Y-DAMGO + TIPP-Psi: 3.06 ± 0.38 mW, n = 9 cells) (**Figure 2.8E, J**). These results indicate that MORs and DORs do not interact in PV-BCs in a manner consistent with MOR/DOR heteromers. To confirm the lack of TIPP-Psi effect on DAMGO-mediated suppression of PV-BC output in a cell-specific manner, we optogenetically stimulated PV-BCs with Chronos, as in Figure 1, and asked if TIPP-Psi enhanced the effect of a

sub-maximal concentration of DAMGO (300 nM, **Figure 2.9**). Consistent with the uncaging data obtained using electrical stimulation, TIPP-Psi was again without effect (300 nM DAMGO: 0.33 ± 0.05; 300 nM DAMGO in TIPP-Psi: 0.30 ± 0.08; no significant difference, Unpaired t test).

Discussion

Identification of the delta opioid receptor as the primary target of enkephalin in CA1 PV-BCs

Prior models of neuromodulator actions on hippocampal interneurons have emphasized MOR expression as a primary distinctive feature of PV-BCs, as opposed to CCK-BCs (Freund and Katona, 2007). This results from an electrophysiological study in CA1 BCs that used the MOR agonist DAMGO to elicit outward somato-dendritic currents and suppress synaptic output (Glickfeld, Atallah and Scanziani, 2008). Although multiple studies have demonstrated the expression of DORs, in addition to MORs, in CA1 PV neurons, the relative contributions of the two receptors to opioid modulation of CA1 PV-BCs has not been established (Stumm *et al.*, 2004; Erbs *et al.*, 2012; Faget *et al.*, 2012). Our findings, using caged leucine-enkephalin to activate both MORs and DORs, indicate that DORs dominate cellular and synaptic responses to enkephalin, in particular at low concentrations that may be most physiologically relevant. Notably, MOR-mediated currents of > 2 pA were evoked in 22/25 cells using caged LE in TIPP-Psi, which suggests that the presence of a subpopulation of cells lacking MOR entirely do not account for the small effect. Reinforcing the dominant role of DOR, the somato-dendritic currents obtained with maximal photorelease of caged DAMGO, a full agonist of MOR G protein signaling (Williams *et al.*, 2013), were also smaller than those produced by LE uncaging in CTOP (currents were apparent in 19/19 cells). Power-response curves with caged enkephalin revealed that LE activates DORs with ~3-fold greater potency than MORs in both the somato-dendritic and presynaptic compartments. Strikingly, the power-response relationships observed

in the absence of antagonist closely match those obtained with MORs blocked, which underscores the dominant role of DORs in the integrated response to enkephalin. While this may reflect a greater binding affinity of LE for DORs (Toll *et al.*, 1998), because somato-dendritic DOR-mediated currents are much larger than MOR-mediated currents when both receptors are saturated, this preferential recruitment of DOR signaling is also likely to result in much stronger inhibition of cellular excitability. In presynaptic terminals of PV-BCs, the strong reciprocal occlusion of synaptic suppression by saturating doses of selective MOR and DOR agonists suggests that because DOR activation by LE occurs at lower concentrations, it will occlude subsequent actions of MOR at higher doses. Given that local sources of the MOR-selective neuropeptide β-endorphin are apparently lacking in CA1 (Bjorklund and Hokfelt, 1986), this raises the question as to why PV-BCs express MORs at all. One possible explanation is that diurnal variation in the levels of brain-wide β-endorphin in the cerebrospinal fluid contribute to the resting excitability and tune the strength of synaptic output via PV-BC MORs, while dynamic, local release of enkephalin in CA1 produces stronger, temporally-precise inhibition of cellular output through activation of DORs (Dent *et al.*, 1981; Barreca *et al.*, 1986).

A recent study in CA2 implicated enkephalin release from vasoactive-intestinal peptide (VIP) interneurons in social memory (Leroy *et al.*, 2021). This effect was attributed to DOR-mediated LTD at PV-BC synapses onto PCs (Piskorowski and Chevaleyre, 2013). It is currently not clear if CA2 PV-BCs also express MOR, and if their activation also drives LTD. In contrast to CA2, enkephalin-mediated presynaptic suppression of PV-BCs is reversible in CA1. Given that hippocampal DORs contribute to memory formation, and possibly, cue-related retrieval as well (Le Merrer *et al.*, 2011, 2012, 2013), and that hippocampal MORs are implicated in stress-induced memory deficits, one possibility is that MOR activation in response to stress-induced

beta-endorphin release (Millan *et al.*, 1981) occludes enkephalin actions at DOR to perturb DOR-dependent memory formation and/or retrieval. Understanding the behavioral significance of the interplay between DOR and MOR signaling will require the identification of behavior contexts that result in endogenous enkephalin release in CA1.

Enkephalin suppresses synaptic transmission with sub-second kinetics

Although GPCRs are well established to engage effector pathways within 100 ms of exposure to agonists, data describing the kinetics of synaptic suppression by $G\alpha_{i/o}$-coupled GPCRs are sparse. A study in rat cerebellum reported rapid and transient $GABA_B$-mediated suppression of an excitatory synapse that peaked 300 ms after application of a high frequency stimulus to drive GABA release, with detectable reduction in presynaptic Ca^{2+} 100 ms after the stimulus (Dittman and Regehr, 1997). A similarly structured study in rat striatum observed a maximal suppression of corticostriatal transmission 500 ms after stimulating striatal neurons to release endogenous opioid neuropeptides (Blomeley and Bracci, 2011). Both of these studies involved relatively small quantities of neuromodulator such that rapid clearance likely obscured the intrinsic kinetics of the presynaptic signaling pathway. Here, we found that photorelease of enkephalin during high frequency stimulation of synaptic transmission produced suppression that peaked between 1-2 s after the light flash. The high sample frequency we employed facilitated rate determination, yielding an average time constant of ~300 ms at 10 Hz. A potential caveat to our approach is that our measurements were taken from synapses that were already in a partially depressed state. Nonetheless, we observed a striking difference in the kinetics of synaptic suppression by DORs and MORs that closely matched the time constants determined for the activation of outward current in the somato-dendritic compartment. In both cases, MORs

exhibited much slower kinetics (tau ~800 ms) than DORs. This was not ligand-dependent, as the same time constants were obtained using caged DAMGO (**Figure 2.8C, H**). This stands in contrast to prior measurements of the kinetics of GIRK activation by MORs in other cell types that found faster time constants, similar to our measurements of DOR-mediated responses (Ingram *et al.*, 1997; Banghart and Sabatini, 2012; Williams, 2014). Interestingly, in the somato-dendritic compartment, we found that increasing MOR expression increased the MOR-evoked current activation rate. Thus, differences in MOR kinetics observed for other brain regions or cell types is likely to reflect differences in relative levels of MOR expression.

It is also notable that relatively strong activity-dependent synaptic depression due to high frequency stimulation did not dramatically occlude synaptic suppression, indicating that release of a relatively depleted readily-releasable pool of vesicles is still prone to attenuation by $G\alpha_{i/o}$-coupled GPCRs that inhibit presynaptic $Ca2^{+}$ channels. We observed a modest but significant negative correlation between the extent of synaptic suppression and the frequency of stimulation, which is consistent with voltage-dependent unbinding of $G\beta\gamma$ from VSCCs (Bean, 1989; Brody *et al.*, 1997).

Lack of cross-talk between MORs and DORs in CA1 PV-BCs

MORs and DORs have been suggested to physically interact via the formation of heterodimers when expressed in the same cell. Although most of the mechanistic work on MOR/DOR heteromers has been performed in cultured cells with overexpressed receptors, multiple studies have also found evidence for their occurrence in naïve brain tissue (Gomes *et al.*, 2004; Gupta *et al.*, 2010; Kabli *et al.*, 2014; Erbs *et al.*, 2015). The pharmacological framework for detecting MOR/DOR functional interactions emerges from studies in cultured

cells showing that ligands for one receptor can increase the binding (in terms of B_{max} but not K_d) and signaling efficacy of agonists for the other (Gomes *et al.*, 2000). Specifically, both the DOR selective agonist deltorphin II and the selective antagonist TIPP-Psi were observed to enhance binding of DAMGO, which was accompanied by a decrease in DAMGO's EC_{50} in a functional assay of MOR activation. Conversely, DAMGO, as well as the MOR antagonist CTOP, enhanced binding and reduced the EC_{50} of deltorphin II. Similar enhancements of MOR activation in the presence of DOR antagonist have been observed in brain tissue using multiple functional assays of MOR signaling, including antinociceptive behavior (Gomes *et al.*, 2004).

Additional evidence supporting the existence of endogenous MOR/DOR heteromers has emerged from the observation that the efficacy of bivalent MOR-DOR ligands is highly dependent on the length of the linker connecting them, which is consistent with action at a receptor complex (Daniels *et al.*, 2005). Numerous studies of receptor trafficking in cultured cells indicate substantial co-localization of MORs and DORs, as well as co-internalization upon exposure to certain agonists for one of the two receptors (*e.g.* He *et al.*, 2011; Derouiche *et al.*, 2020). In addition, biochemical studies have reported co-immunoprecipitation from naïve brain tissue using an antibody for either MORs or DORs (Gomes *et al.*, 2000), or an antibody that specifically recognizes MOR/DOR heteromers (Gupta *et al.*, 2010).

In contrast to these prior studies that focus on heteromers, we found no evidence for functional interactions between MORs and DORs in CA1 PV-BCs. Rather than synergistic, supralinear signaling, we observed largely parallel signaling and occlusion. If LE elicited synergistic signaling between MORs and DORs, we would predict that the power-response curve for LE with both receptors intact (control conditions) would sit to the left of the curves obtained for either receptor in isolation using selective antagonists. This was not the case. Instead, in both

subcellular compartments, DOR activation accounted for the low end of the power-response curves, with MORs contributing only at higher concentrations. Strong occlusion at presynaptic terminals was observed, as simultaneous application of small molecule agonists for both receptors only slightly increased the extent of synaptic modulation in comparison to either drug alone (from 70% to ~75% suppression). Similar occlusion was also observed while monitoring presynaptic Ca^{2+} transients. Interestingly, only unidirectional occlusion was observed in the somato-dendritic compartment, where MOR block had no effect on outward currents driven by high doses of LE, while DOR block dramatically reduced them. This observed sub-linear signaling indicates that DORs have access to a larger pool of GIRKs than MORs, and that GIRKs activated by MORs are completely shared between both receptor types. These results are summarized graphically in **Figure 2.10**.

In addition, we did not observe heterologous desensitization between MORs and DORs in the somato-dendritic compartment. In general, presynaptic inhibitory GPCRs do not desensitize (Pennock, Dicken and Hentges, 2012). Due to the relatively small amount of presynaptic desensitization observed (~20% with DAMGO), we did not attempt to study heterologous desensitization at presynaptic terminals. Given the strong occlusion we observed between MOR and DOR in presynaptic terminals, it remains possible that some heterologous desensitization may occur in this compartment. In opioid-naïve animals, desensitization appears to occur at the level of the receptor, likely due to C-terminus phosphorylation, rather than through the effectors (Llorente *et al.*, 2012; Leff, Arttamangkul and Williams, 2020). Nonetheless, because desensitization can lead to endocytosis, and possibly conformational changes, if the receptors were physically interacting, desensitization of one receptor may be expected to impact signaling at the other.

Similarly, our findings argue against the presence of native MOR/DOR heteromers that influence cellular physiology in either the somato-dendritic or presynaptic compartments of CA1 PV-BCs, since TIPP-Psi had no effect on DAMGO potency or signaling kinetics, both of which serve as sensitive measures of receptor function. This lack of interaction between MORs and DORs is consistent with our previous observation in striatal indirect pathway neurons, wherein their actions were strictly additive, and genetic removal of either receptor neither enhanced nor suppressed the efficacy of the other (Banghart *et al.*, 2015). A possible explanation is that MOR/DOR heteromers present in PV-BCs are retained in the Golgi apparatus due to a lack of Rtp4 expression (*Allen Brain Atlas API*; Décaillot *et al.*, 2008; Saunders *et al.*, 2018). As this may involve sequestering MORs, it may also contribute to the surprisingly small somato-dendritic MOR-mediated GIRK currents we observed. While MOR/DOR functional interactions may be more prominent in other brain regions, our findings indicate that co-expression and co-localization in subcellular compartments do not guarantee receptor crosstalk at the cell surface.

In conclusion, DORs in CA1 PV-BCs, rather than MORs, are the primary target of the opioid neuropeptide enkephalin. Although signaling at both receptors converges on largely overlapping populations of effectors within the same subcellular compartments, MORs and DORs appear to signal predominantly in a parallel, functionally-independent manner. These results imply that functional redundancy between multiple GPCRs expressed in the same neuron may be a common feature in the nervous system. Additional research is necessary to further delineate mechanisms that determine whether or not heteromers form when heterophilic receptors are present in close proximity within cells.

Key Resources Table

Key Resources Table				
Reagent type (species) or resource	**Designation**	**Source or reference**	**Identifiers**	**Additional information**
Strain, strain background (*M. musculus*, male and female)	C57Bl/6	The Jackson Laboratory	Cat # 000664 RRID:IMSR_JAX:000664	
Strain, strain background (*M. musculus*, male and female)	*Pvalb*^{Cre}	The Jackson Laboratory	Cat # 012358 RRID:IMSR_JAX:012358	
Strain, strain background (*M. musculus*, male and female)	*Rosa26-lsl-tdTomato* (Ai14)	The Jackson Laboratory	Cat # 007914 RRID:IMSR_JAX:007914	
Recombinant DNA reagent	AAV1-Syn-FLEX-Chronos-GFP	Addgene	Cat # 62722 RRID:Addgene_62722	
Recombinant DNA reagent	AAVDJ-hSyn1-FLEX-mCh-T2A-FLAG-hMOR-WPRE	Banghart Lab	Addgene Plasmid #166970	
Commercial assay or kit	RNAscope Fluorescent Multiplex Kit	ACD bio / Bio-Techne	Cat # 320850	

Commercial assay or kit	*Pvalb* FISH probe	ACD bio / Bio-Techne	Cat # 421931-C3	
Commercial assay or kit	*Oprd1* FISH probe	ACD bio / Bio-Techne	Cat # 427371-C2	
Commercial assay or kit	*Oprm1* FISH probe	ACD bio / Bio-Techne	Cat # 315841	
Chemical compound, drug	*N*-MNVOC-LE	Banghart Lab		Banghart, He, and Sabatini, 2018
Chemical compound, drug	CYLE	Banghart Lab and NIDA Drug Supply Program	MPSP-117 (NDSP)	Banghart and Sabatini, 2012
Chemical compound, drug	CNV-Y-DAMGO	Banghart Lab		Ma, He, and Banghart, 2021
Chemical compound, drug	NBQX	HelloBio	Cat # HB0443	
Chemical compound, drug	(R)-CPP	HelloBio	Cat # HB0021	
Chemical compound, drug	TIPP-Psi	NIDA Drug Supply Program	MPSP-056	
Chemical compound, drug	CTOP	Tocris	Cat # 1578	
Chemical compound, drug	DAMGO	Tocris	Cat # 1171	

Chemical compound, drug	SNC162	Tocris	Cat # 1529	
Chemical compound, drug	AlexaFluor 547	Thermo Fisher	Cat # 10438	
Chemical compound, drug	Fluo5F	Thermo Fisher	Cat # F14221	
Chemical compound, drug	Picrotoxin	Sigma	Cat # P1675	
Chemical compound, drug	Tetrodotoxin citrate (TTX)	HelloBio	Cat # HB1035	
Chemical compound, drug	WIN55	Tocris	Cat # 1038	
Chemical compound, drug	Deltorphin II	NIDA Drug Supply Program	MPSP-036	
Chemical compound, drug	ZD7288	Tocris	Cat # 1000	
Software, algorithm	MatLab	Mathworks Inc	RRID:SCR_001622	
Software, algorithm	ScanImage		RRID:SCR_014307	(Pologruto, Sabatini and Svoboda, 2003)
Software, algorithm	Igor Pro	WaveMetrics	RRID:SCR_000325	
Software, algorithm	ImageJ		RRID:SCR_003070	

Software, algorithm	Illustrator CC	Adobe Systems Inc	RRID:SCR_010279	
Software, algorithm	Prism 7	GraphPad Inc	RRID:SCR_002798	
Software, algorithm	Excel	Microsoft	RRID:SCR_016137	

Brain Slice Preparation. Animal handling protocols were approved by the UC San Diego Institutional Animal Care and Use Committee. Most experiments were conducted using postnatal day 15-32 mice of both males and females on a C57Bl/6 background. For experiments that required viral expression (Figure1A-E, Figure 4H-K, and Figure S3), older mice of postnatal day 25-41 (both males and females) were used. Mice were anesthetized with isoflurane and decapitated, and the brain was removed, blocked, and mounted in a VT1000S vibratome (Leica Instruments). Horizontal slices (300 μm) were prepared in ice-cold choline-ACSF containing (in mM) 25 $NaHCO_3$, 1.25 NaH_2PO_4, 2.5 KCl, 7 $MgCl_2$, 25 glucose, 0.5 $CaCl_2$, 110 choline chloride, 11.6 ascorbic acid, and 3.1 pyruvic acid, equilibrated with 95% O_2/5% CO_2. Slices were transferred to a holding chamber containing oxygenated artificial cerebrospinal fluid (ACSF) containing (in mM) 127 NaCl, 2.5 KCl, 25 $NaHCO_3$, 1.25 NaH_2PO_4, 2 $CaCl_2$, 1 $MgCl_2$, and 10 glucose, osmolarity 290. Slices were incubated at 32 °C for 30 min and then left at room temperature until recordings were performed.

Electrophysiology. All recordings were performed within 5 h of slice cutting in a submerged slice chamber perfused with ACSF warmed to 32 °C and equilibrated with 95% O_2/5% CO_2. Whole-cell voltage clamp recordings were made with an Axopatch 700B amplifier (Axon Instruments). Data were filtered at 3 kHz, sampled at 10 kHz, and acquired using National

Instruments acquisition boards and a custom version of ScanImage written in MATLAB (Mathworks). Cells were rejected if holding currents exceeded −200 pA or if the series resistance (<25 MΩ) changed during the experiment by more than 20%. For recordings measuring K+ currents in PV cells (Figure 1), patch pipets (open pipet resistance 2.0−3.0 MΩ) were filled with an internal solution containing (in mM) 135 KMeSO4, 5 KCl, 5 HEPES, 1.1 EGTA, 4 MgATP, 0.3 Na2GTP, and 10 Na2phosphocreatine (pH 7.25, 286 mOsm/kg). Cells were held at −55 mV, and synaptic transmission was blocked with the addition to the ACSF of 2,3-dihydroxy-6-nitro-7-sulfamoyl-benzo(f)quinoxaline (NBQX; 10 μM), R,S-3-(2-carboxypiperazin-4-yl)propyl-1-phosphonic acid (CPP; 10 μM), picrotoxin (10 μM), and TTX (1 μM). TdTomato-expressing neurons were visualized through a Cy3 filter cube (Semrock Cy3-4040C) upon illumination with an iCoolLED pE-300. For recordings measuring inhibitory synaptic transmission in mouse hippocampus, patch pipets (2.5−3.5 MΩ) were filled with an internal solution containing (in mM) 135 CsMeSO3, 10 HEPES, 1 EGTA, 3.3 QX-314 (Cl^- salt), 4 Mg-ATP, 0.3 Na-GTP, and 8 Na_2phosphocreatine (pH 7.3, 295 mOsm/kg). Cells were held at 0 mV to produce outward currents. Excitatory transmission was blocked by the addition to the ACSF of NBQX (10 μM) and CPP (10 μM).To electrically evoke IPSCs, stimulating electrodes pulled from theta glass with ∼5 μm tip diameters were placed at the border between stratum pyramidale and straum oriens nearby the recorded cell (∼50−150 μm) and a two brief pulses (0.5 ms, 50−300 μA, 50 ms interval) were delivered every 20 s. The experimenters were not blinded to the pharmacological conditions employed.

UV Photolysis. Uncaging was carried out using 5 ms flashes of collimated full-field illumination with a 355 nm laser, as previously described. Light powers in the text correspond to

measurements of a 10 mm diameter collimated beam at the back aperture of the objective. Beam size coming out of the objective onto the sample was 3,900 μm^2.

Optogenetics. AAV encoding Chronos-GFP was injected into the hippocampus of *Pvalb*^{Cre} pups P0-3. The virus was allowed to express for 4 weeks and then acute hippocampal slices were made as described above. For optogenetic stimulation of PV basket cell terminals, two 2 ms pulses from a blue LED (iCoolLED pE-300, filtered through a 472/30 nm bandpass, Semrock (FF02-472/30-25)) were applied over the cell body of the recorded pyramidal cell. The field stop of the LED was narrowed to 6,600 μm^2 in order to limit the excitation to only the immediate axons surrounding the cell body, such that the power reaching the sample was 5 - 20 mW/mm^2 .

Two-photon calcium imaging. Two-photon imaging of axonal boutons was performed using a custom-built two-photon laser-scanning microscope (Carter and Sabatini, 2004; Bloodgood and Sabatini, 2007). First, PV neurons in the CA1 region of the hippocampus were visualized using epifluorescence in a *Pvalb*^{Cre}/*Rosa26-lsl-tdTomato* line and targeted recordings were made under infrared differential interference contrast (IR-DIC) on an Olympus BX51 microscope. Whole cell current clamp recordings were made with a potassium (K)-methanesulfonate internal consisting of (in mM): 135 KMeSO4, 5 KCl, 5 HEPES, 4 MgATP, 0.3 Na_2GTP, and 10 Na_2phosphocreatine. The internal also contained the Ca^{2+}-sensitive green fluorophore Fluo-5F (300 μM) and Ca-insensitive red fluorophore Alexa Fluor-594 (30 μM). After a patch was made, the cell was allowed at least 15 minutes for the dye and indicator to fill the axons. Then an 800 nm laser was used to locate axonal boutons based on morphology. Once

identified, line scans were made across 1-2 boutons while evoking 1 or 5 action potentials by injecting voltage into the cell body. Calcium transients were averaged across 30 trials, before and after drug addition. Stimulus-evoked changes in fluorescence (and the Ca signal) were reported as %ΔG/Gsat, reflecting measurements of ΔG/R normalized to G/R in saturating $Ca^{2}+$ as described previously (Bloodgood and Sabatini, 2007).

Data Analysis. Electrophysiology data were analyzed in Igor Pro (Wavemetrics). Peak current amplitudes were calculated by averaging over a 200 ms (GIRK) or 2 ms (synaptic transmission) window around the peak. Activation time constants for GIRKs were calculated by fitting the rising phases of light evoked currents to an exponential function. To determine magnitude of modulation by enkephalin uncaging (%IPSC suppression), the IPSC peak amplitude immediately after a flash was divided by the average peak amplitude of the three IPSCs preceding the light flash. Kinetics of synaptic modulation (Figure 3) were determined by averaging 3 stimulus trains before uncaging (at 10 Hz, 20 Hz, and 50 Hz) and fitting a bi-exponential curve describe the synaptic depression. The curve was then divided from the stimulus train with uncaging to get the traces seen in Figure 3B. The time constant was then extracted from a mono-exponential was fit to the suppression from the time of uncaging. The effects of drugs on IPSC suppression were calculated as the average %IPSC suppression 1-3 minutes after drug addition. PPR was determined by dividing Peak 2 / Peak 1, where Peak 2 was calculated by subtracting the residual Peak 1 current (1 ms before second stimulus) from the absolute peak amplitude of Peak 2. Summary values are reported as mean ± SEM. Data were tested for normality using the D'Agostino and Pearson test, and the appropriate statistical tests (parametric or non-parametric) were carried out based on those results. All statistical tests were

performed in GraphPad Prism except for the Skilling-Mack test, which was performed in Matlab using code developed by Thomas Pingel (https://github.com/thomaspingel/mackskill-matlab). Specific statistical tests and corrections are described for each figure in the text and figure legends.

Fluorescence in-situ hybridization. Mice were deeply anesthetized with isoflurane and decapitated, and their brains were quickly removed and frozen in tissue freezing medium on dry ice. Brains were cut on a cryostat (Leica CM 1950) into 8 μm sections, adhered to SuperFrost Plus slides (VWR), and stored at -80°C. Samples were fixed 4% paraformaldehyde, processed according to ACD RNAscope Fluorescent Multiplex Assay manual, and coverslipped with ProLong antifade reagent *(*Molecular Probes*).* Sections were imaged on a Keyence BZ-X710 Microscope at 60x magnification. The images were acquired and manually scored for the presence of fluorescent puncta and colocalization using ImageJ.

Acknowledgements

We thank the National Institute on Drug Abuse Drug Supply Program (NDSP) for generously providing pharmacological reagents; L Sancho and E Campbell for training and assistance with two-photon microscopy; BK Lim for reagents for adenoassociated virus production; E Berg for genotyping, animal husbandry, adenoassociated virus production and administrative assistance; J Isaacson, W Birdsong, J Williams, M Lovett-Barron, and members of the Banghart Lab for helpful discussions.

Competing interests

The authors declare no competing interests.

Funding

Funder	Grant reference number	Author
National Institute on Drug Abuse	R00DA034648	Matthew R. Banghart
National Institute of General Medical Sciences	R35GM133802	Matthew R. Banghart
BRAIN Initiative, National Institute of Neurological Disorders and Stroke , National Institute of Mental Health	U01NS113295	Matthew R. Banghart
Brain & Behavior Research Foundation	NARSAD Young Investigator Award	Matthew R. Banghart
Esther A. & Joseph Klingenstein Fund & Simons Foundation	Klingenstein-Simons Fellowship in Neuroscience	Matthew R. Banghart
National Institute of General Medical Sciences	T32GM007240	Xinyi J. He
National Institute of Neurological Disorders and Stroke	R01NS111162	Brenda L. Bloodgood

The funders had no role in study design, data collection and interpretation, or the decision to submit the work for publication

Author ORCIDs

Matthew R. Banghart: 0000-0001-7248-2932

Xinyi Jenny He: 0000-0002-388400596

Janki Patel: 000-0002-8140-9347

Connor E. Weiss: 0000-0002-2597-9636

Xiang Ma: 0000-0002-9164-8608

Brenda L. Bloodgood: 0000-0002-4797-9119

Ethics

Animal experimentation: All procedures were performed in accordance with protocols approved by the University of California San Diego Institutional Animal Care and Use Committee (IACUC) following guidelines described in the the US National Institutes of Health Guide for Care and Use of Laboratory Animals (UCSD IACUC protocol S16171). All surgery was performed under isoflurane anesthesia.

Chapter 2, in full, is a reprint of the material as it appears in He, X. J., Patel, J, Weiss, C, Ma, X., Bloodgood, B. L., Banghart, M. R. “Convergent, functionally independent signaling by mu and delta opioid receptors in hippocampal parvalbumin interneurons”. *Elife* **10**, e69746 (2021). The dissertation author was the primary investigator and author of this paper.

Figure 2.1. Opioid receptor mRNA in CA1 parvalbumin interneurons and characterization of the neuromodulator-sensitivity of CA1 basket cell synaptic output.
A. Example fluorescence *in situ* hybridization image of *Pvalb*, *Oprm1*, and *Oprd1* mRNA in the CA1 pyramidal layer of mouse hippocampus. Scale bar = 20 μm. **B.** Summary of *Pvalb*, *Oprm1*, and *Oprd1* mRNA co-localization images acquired from 5 mice. **C.** Schematic of recording configuration for electrical stimulation depicting two populations of basket cells and their distinguishing neuromodulator receptors. **D.** Baseline-normalized, average eIPSC amplitude over time during bath application of the CB1R agonist WIN55 (n=9 cells from 3 mice). **E.** Summary data of WIN55 and DAMGO flow-in experiments (DAMGO data replotted from Figure 1I), revealing only a small contribution to the eIPSC from CCK-BCs that are suppressed by CB1R but not MOR. **F.** Example double flow-in experiments with optogenetic stimulation (top) and electrical stimulation (bottom) of synaptic transmission. **G.** Summary data of IPSC suppression by DAMGO and SNC162, comparing electrical to optogenetic stimulation (data are replotted from Figure 1D and 1I). **H.** Pairedesensitization data plotting the early phase of IPSC suppression (1-3 minutes after drug addition) compared to the late phase of IPSC suppression (8-10 minutes after drug addition) for both DAMGO and SNC162 and both stimulation protocols. **I.** The change in IPSC suppression between early phase and late phase on a cell by cell basis for both DAMGO and SNC162 and both stimulation protocols.

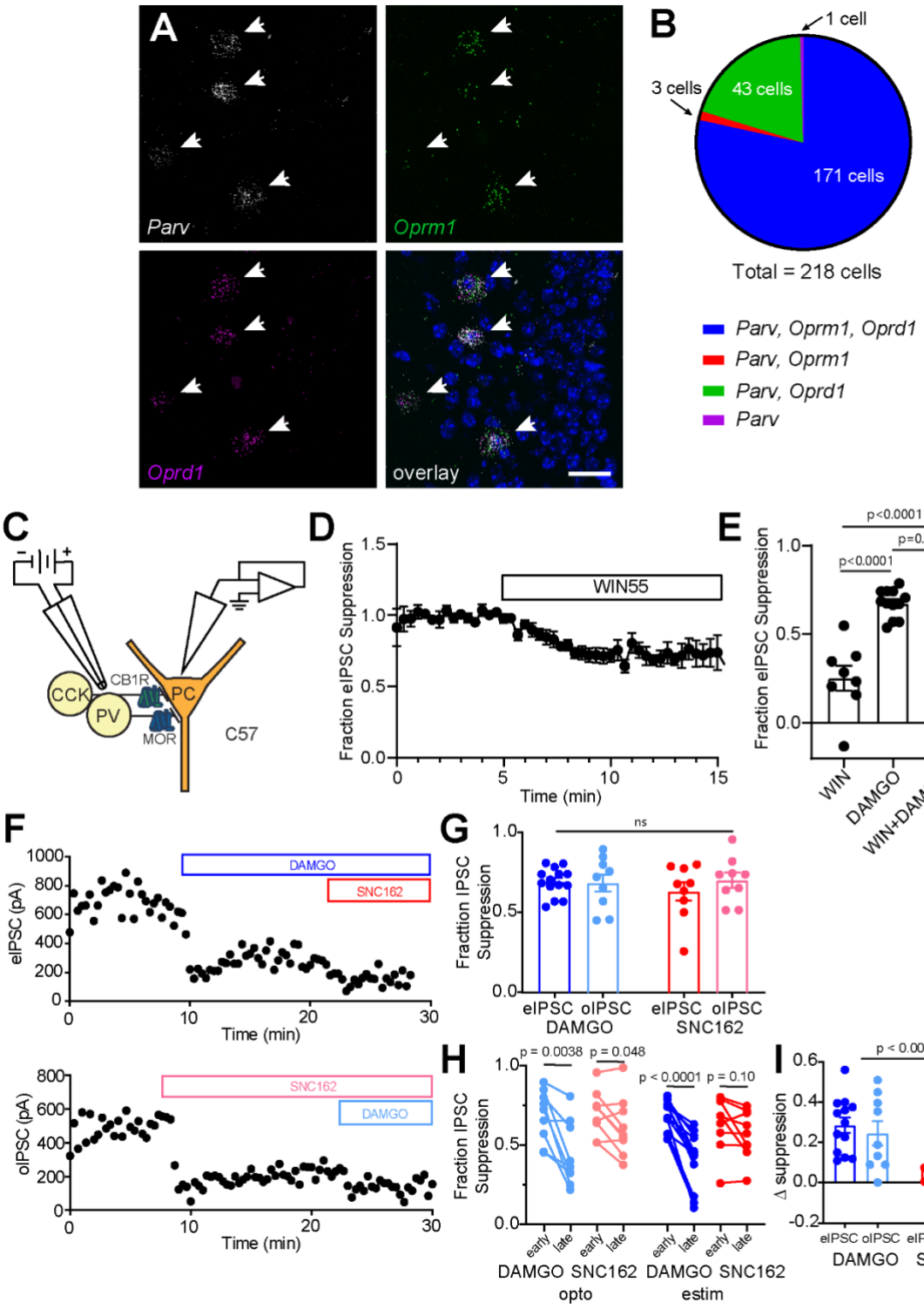
A
Parv
Oprm1
Oprd1
overlay
B
1 cell
3 cells
43 cells
171 cells
Total = 218 cells
Parv, Oprm1, Oprd1
Parv, Oprm1
Parv, Oprd1
Parv
C
CCK
CB1R
PV
PC
MOR
C57
D
WIN55
Fraction eIPSC Suppression
Time (min)
E
p<0.0001
p=0.14
p<0.0001
Fraction eIPSC Suppression
WIN
DAMGO
WIN+DAMGO
F
DAMGO
SNC162
eIPSC (pA)
Time (min)
SNC162
DAMGO
oIPSC (pA)
Time (min)
G
ns
Fraction IPSC Suppression
eIPSC oIPSC eIPSC oIPSC
DAMGO
SNC162
H
p = 0.0038
p = 0.048
p < 0.0001
p = 0.10
Fraction IPSC Suppression
early late early late early late early late
DAMGO SNC162 DAMGO SNC162
opto
estim
I
p < 0.0001
Δ suppression
eIPSC oIPSC eIPSC oIPSC
DAMGO
SNC162

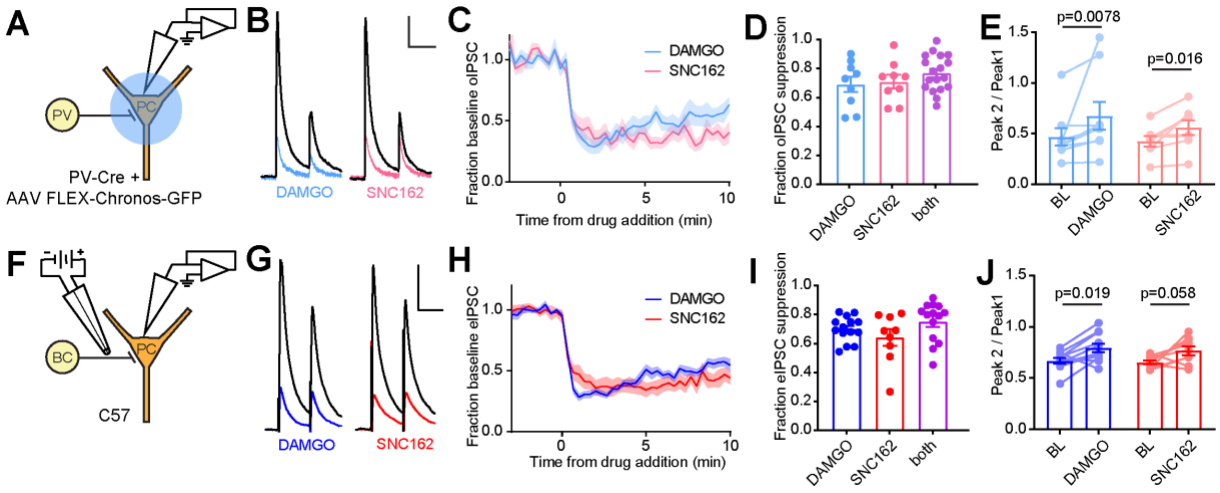

Figure 2.2. Electrophysiological recordings of opioid-sensitive synaptic output from hippocampal parvalbumin basket cells.

A. Schematic of the experimental configuration for recording optogenetically-evoked inhibitory synaptic transmission in PV-Cre mice. **B.** Representative oIPSC pairs (50 ms interval) recorded from a pyramidal cell. Black traces are the average of 6 baseline sweeps, and colored traces are the average of 6 sweeps after addition of either DAMGO (1 uM, blue) or SNC162 (1 uM, red). Scale bars: x = 40 ms, y = 100 pA. **C.** Baseline-normalized, average oIPSC amplitude over time during bath application of DAMGO (n = 9 cells from 6 mice) or SNC162 (n = 9 cells from 7 mice). **D.** Summary data of double flow-in experiments, comparing oIPSC suppression by DAMGO or SNC162 alone, followed by the other drug. **E.** oIPSC paired pulse ratios (Peak 2/Peak 1), before (baseline, BL) and after drug addition. **F.** Schematic of the experimental configuration for recording electrically-evoked inhibitory synaptic transmission in wild type mice. **G.** Representative eIPSC pairs (50 ms interval) recorded from a pyramidal cell (as in **B**). Scale bars: x = 40 ms, y = 200 pA. **H.** Baseline-normalized, average eIPSC amplitude over time during bath application of DAMGO (n = 15 cells from 13 mice) or SNC162 (n = 9 cells from 5 mice). **I.** Summary data of double flow-in experiments with electrical stimulation (as in **D**). **J.** eIPSC paired pulse ratios (Peak 2/Peak 1), before and after drug addition.

Figure 2.3. Characterization of the potency and kinetics of synaptic modulation by [Leu^5]-enkephalin at mu and delta opioid receptors using caged peptides.
A. Left: Schematic of the experimental configuration for photo-uncaging of opioid neuropeptides while recording electrically-evoked inhibitory synaptic transmission in wild type mice. **Right:** Schematic of photoreleasing [Leu^5]-enkephalin (cyan) from *N*-MNVOC-LE or CYLE (cyan with purple caging group) in the presence of selective antagonists to isolate its action on either MOR (blue, in TIPP-Psi) or DOR (red, in CTOP). **B.** Example recording showing graded suppression of inhibitory synaptic transmission by uncaging *N*-MNVOC-LE at various light intensities. **Inset:** Example eIPSCs before (black) and after LE uncaging at each light intensity. Scale bars: x = 20 ms, y = 100 pA **C.** Linear optical power-response curves of eIPSC suppression as a function of light intensity, in the absence (black, n = 6 -12 cells per laser intensity) and presence of either CTOP (red, n = 5-8 cells) or TIPP-Psi (blue, n = 4-10 cells). **D.** Logarithmic optical power-response curves of the data in **C** normalized to the maximal eIPSC suppression observed in each condition. **E.** Representative recording from a pyramidal cell demonstrating rapid suppression of eIPSC amplitude in response to photoactivation of CYLE during 10 Hz trains of electrical stimuli. Purple arrow represents CYLE uncaging at 2 seconds into the 10 Hz train. Outward stimulus artifacts are removed for clarity. Scale bars: x = 1 sec, y = 100 pA **F.** Average, baseline subtracted and baseline-normalized eIPSC amplitude showing the kinetics of synaptic suppression with electrical stimulation at 10 Hz in the absence (ACSF, n = 9 cells from 6 mice) and presence of either CTOP (n = 12 cells from 7 mice) or TIPP-Psi (n = 8 cells from 6 mice). **G.** Time constants of synaptic suppression in response to CYLE photoactivation with an 84 mW light flash at the indicated frequencies of synaptic stimulation. At 20 Hz, the time constant in TIPP-Psi was significantly greater than the time constant without any antagonists. **H.** Plot of eIPSC suppression as a function of synaptic stimulation frequency.

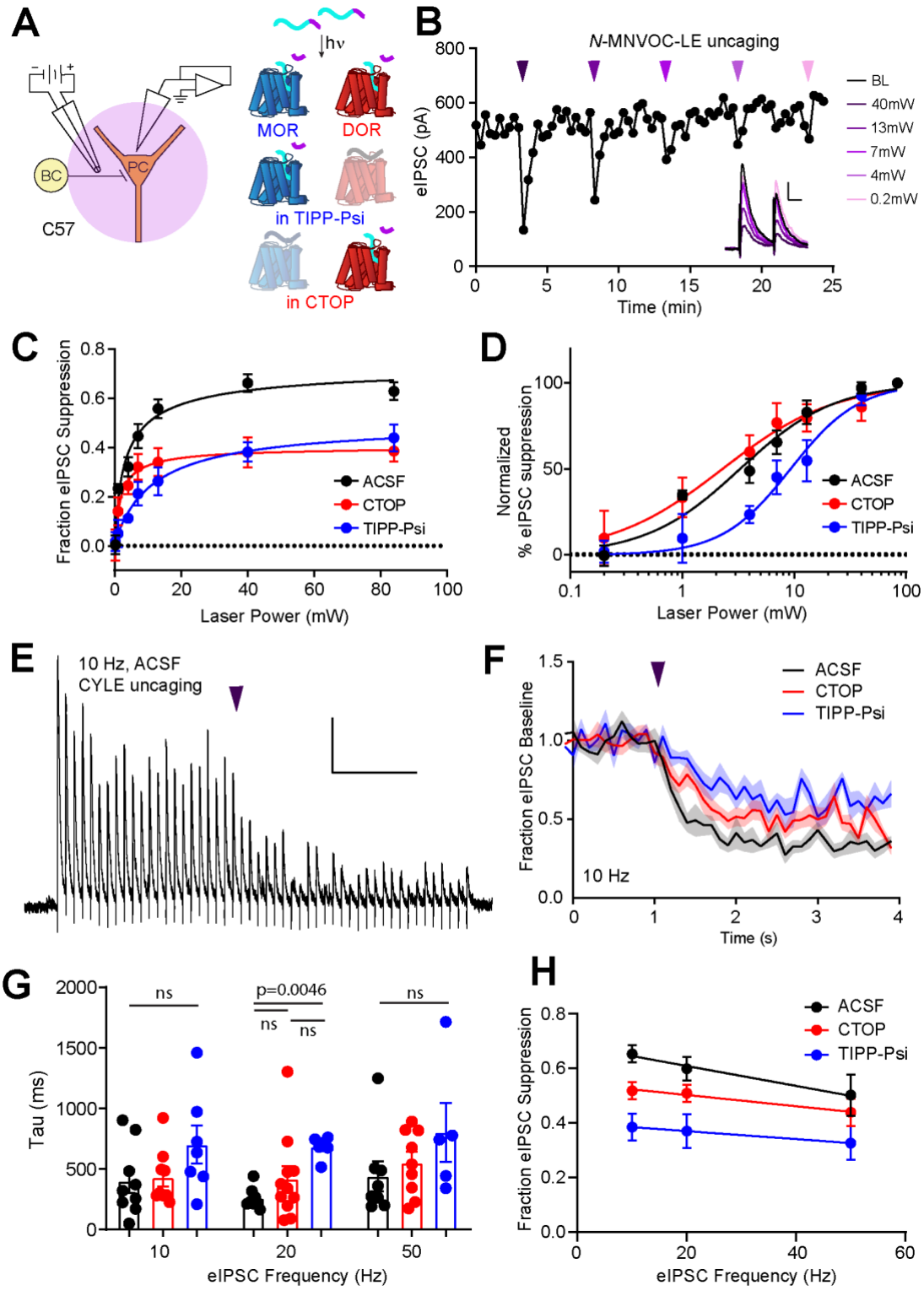
A
hν
MOR
DOR
in TIPP-Psi
in CTOP
BC
PC
C57
B
N-MNVOC-LE uncaging
eIPSC (pA)
Time (min)
BL
40mW
13mW
7mW
4mW
0.2mW
C
Fraction eIPSC Suppression
Laser Power (mW)
ACSF
CTOP
TIPP-Psi
D
Normalized
% eIPSC suppression
Laser Power (mW)
ACSF
CTOP
TIPP-Psi
E
10 Hz, ACSF
CYLE uncaging
F
Fraction eIPSC Baseline
10 Hz
Time (s)
ACSF
CTOP
TIPP-Psi
G
Tau (ms)
ns
p=0.0046
ns
ns
ns
eIPSC Frequency (Hz)
H
Fraction eIPSC Suppression
eIPSC Frequency (Hz)
ACSF
CTOP
TIPP-Psi

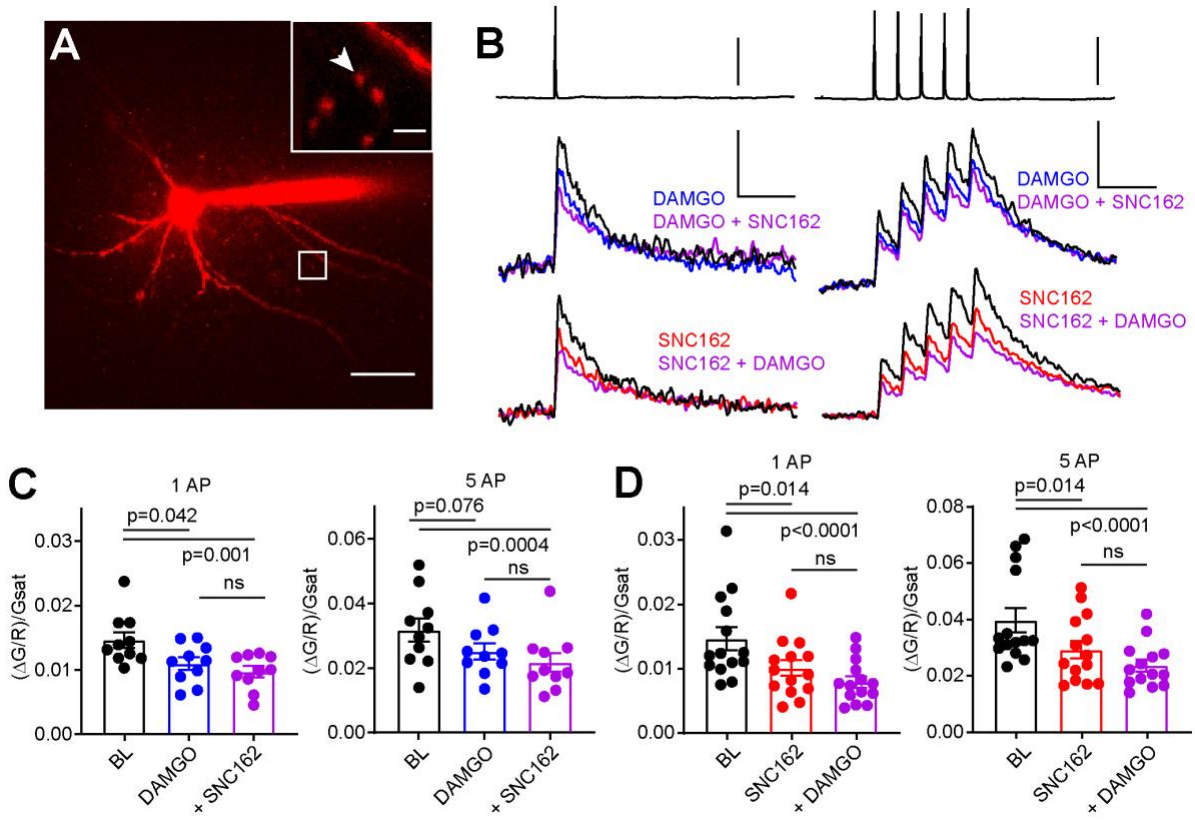

Figure 2.4. Axonal calcium imaging reveals that both mu and delta opioid receptors suppress presynaptic voltage-gated calcium channels

A. Two-photon image of a tdTomato-expressing basket cell filled with 30 µM Alexa 594 and 300 µM Fluo-5F in a brain slice taken from a PV-Cre; tdTom mouse. Scale bar: 50 µm. Inset shows the two axonal boutons where the line scan was carried out, with the orientation of the line scan indicated by the arrow. Scale bar: 5 µm. **B.** Example of either a single action potential (left) or five action potentials (right) triggered in the cell body (top), and the resulting averaged, presynaptic Ca^{2+} transients, before and after application of DAMGO (top, blue, n = 8 cells, 16 boutons), SNC162 (red bottom, n = 7 cells, 14 boutons), and both drugs (top and bottom, purple). The transients are measured as the change in green signal (ΔG) over red signal (R), divided by ΔG in saturating Ca^{2+} conditions (ΔG^{sat}). Scale bars: top, 50 mV; bottom, x = 100 ms, y = 0.01 (left) or 0.02 (right) (ΔG/R)/Gsat. **C.** Summary of peak Ca^{2+} transients for DAMGO application in response to 1 AP (left) or 5 APs (right). 1 AP: BL 0.014 ± 0.001; DAMGO 0.011 ± 0.001; DAMGO+ SNC162 0.010 ± 0.001 (p = 0.042 and p = 0.0001, n = 10 pairs, Friedman test with Dunn's multiple comparisons) 5AP: BL 0.032 ± 0.004; DAMGO 0.025 ± 0.002, DAMGO + SNC162 0.022 ± 0.003 (p = 0.076 and p = 0.0004, n = 10 pairs). **D.** Summary of peak Ca^{2+} transients for SNC162 application in response to 1 AP (left) or 5 APs (right). 1AP: BL 0.014 ± 0.002; SNC162 0.010 ± 0.002; SNC162 + DAMGO 0.008 ± 0.001 (p = 0.014 and p < 0.0001, n = 14 pairs, Friedman test with Dunn's multiple comparisons). 5AP: BL 0.039 ± 0.004; SNC162 0.029 ± 0.003; SNC162 + DAMGO 0.023 ± 0.002 (p = 0.014 and p < 0.0001, n = 14 pairs)

Figure 2.5. Enkephalin evokes outward currents in CA1 parvalbumin interneurons through both mu and delta opioid receptors

A. Schematic of whole-cell voltage clamp recording configuration from PV interneurons with peptide uncaging. **B.** Average outward currents evoked by photoactivation of *N*-MNVOC-LE (6μM) with an 84 mW light flash in the absence (black, ACSF, n = 9 cells from 5 mice) and presence of mu and delta opioid receptor antagonists (red, CTOP, n = 10 cells from 6 mice; blue, TIPP-Psi, n = 11 cells from 6 mice; purple, CTOP + TIPP-Psi, n = 5 cells from 3 mice). Scale bar: x = 5 sec, y = 20 pA. **C.** Summary of peak current amplitudes shown in **B**. **D.** Linear optical power-response curve of peak current as a function of light intensity, in the absence (ACSF, black, n = 9 cells per laser intensity) and presence of either CTOP (red, n = 10 cells) or TIPP-Psi (blue, n = 11 cells) **E.** Logarithmic optical power-response curves of the data in **D** normalized to the maximal peak current observed in each condition. **F.** Rising phase of the average peak-normalized outward currents evoked by photoactivation of CYLE (6μM) with an 84mW light flash in the absence (black, ACSF, n = 11 cells from 4 mice) and presence of mu and delta opioid receptor antagonists (red, CTOP, n = 10 cells from 4 mice; blue, TIPP-Psi, n = 12 cells from 4 mice). **G.** Time constants of current activation in response to photoactivation of CYLE from **F**. **H.** Schematic of viral Cre-dependent mu opioid receptor over-expression in CA1 of PV-Cre mice. **I.** Average outward currents evoked by photoactivation of CYLE by an 84 mW light flash in the presence of TIPP-Psi in either PV-Cre; tdTom mice (blue, data from **B**) or PV-Cre mice overexpressing the mu opioid receptor (purple, n = 8 cells from 3 mice). Scale bar: x = 10 sec, y = 20 pA. **J.** Summary of current amplitudes shown in **I**. **K.** Time constants of current activation in response to photoactivation of CYLE.

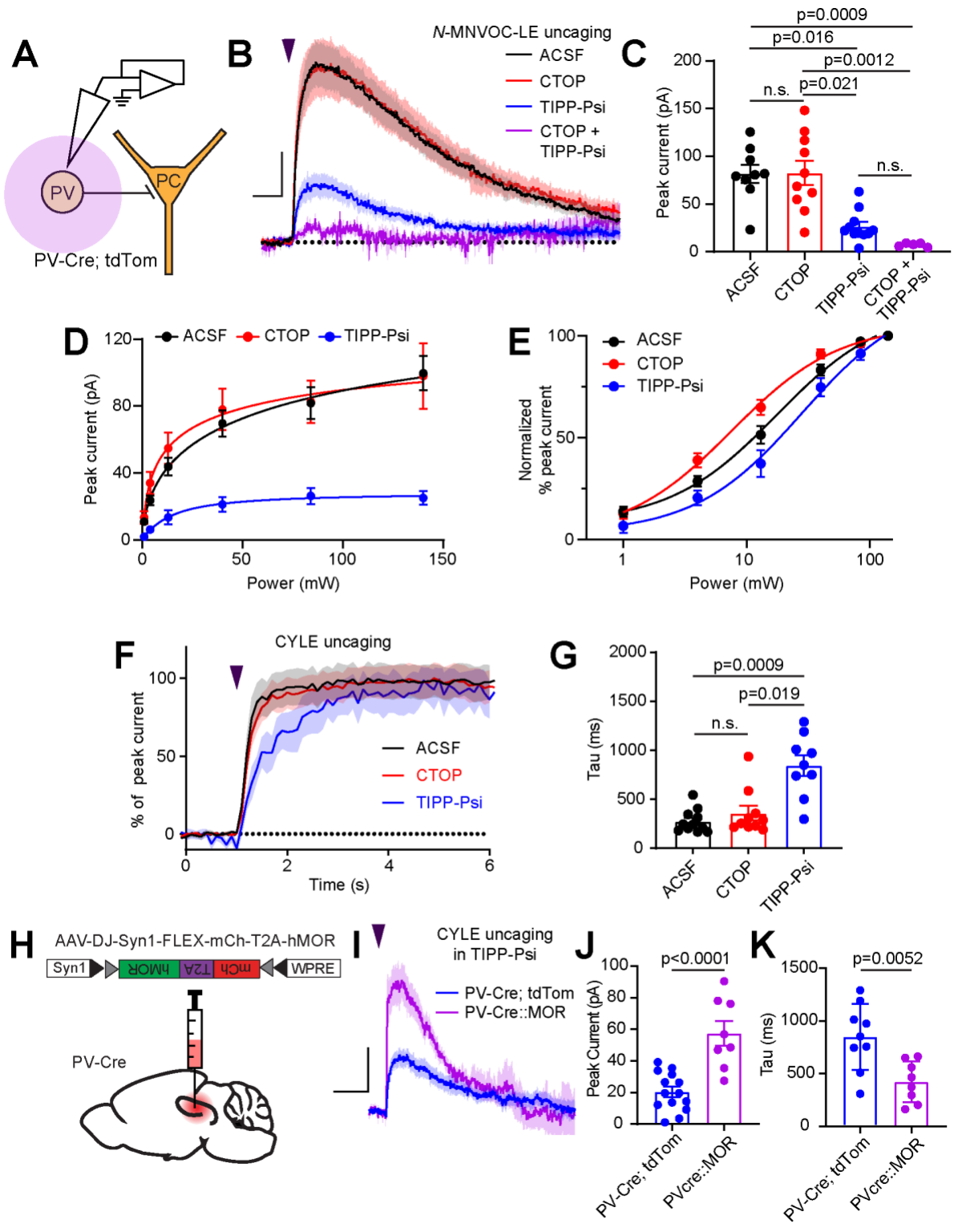
A
PV
PC
PV-Cre; tdTom
B
N-MNVOC-LE uncaging
ACSF
CTOP
TIPP-Psi
CTOP + TIPP-Psi
C
p=0.0009
p=0.016
p=0.0012
n.s.
p=0.021
n.s.
Peak current (pA)
ACSF
CTOP
TIPP-Psi
CTOP + TIPP-Psi
D
ACSF
CTOP
TIPP-Psi
Peak current (pA)
Power (mW)
E
ACSF
CTOP
TIPP-Psi
Normalized % peak current
Power (mW)
F
CYLE uncaging
% of peak current
ACSF
CTOP
TIPP-Psi
Time (s)
G
p=0.0009
p=0.019
n.s.
Tau (ms)
ACSF
CTOP
TIPP-Psi
H
AAV-DJ-Syn1-FLEX-mCh-T2A-hMOR
Syn1
hMOR
T2A
mCh
WPRE
PV-Cre
I
CYLE uncaging in TIPP-Psi
PV-Cre; tdTom
PV-Cre::MOR
J
p<0.0001
Peak Current (pA)
PV-Cre; tdTom
PVcre::MOR
K
p=0.0052
Tau (ms)
PV-Cre; tdTom
PVcre::MOR

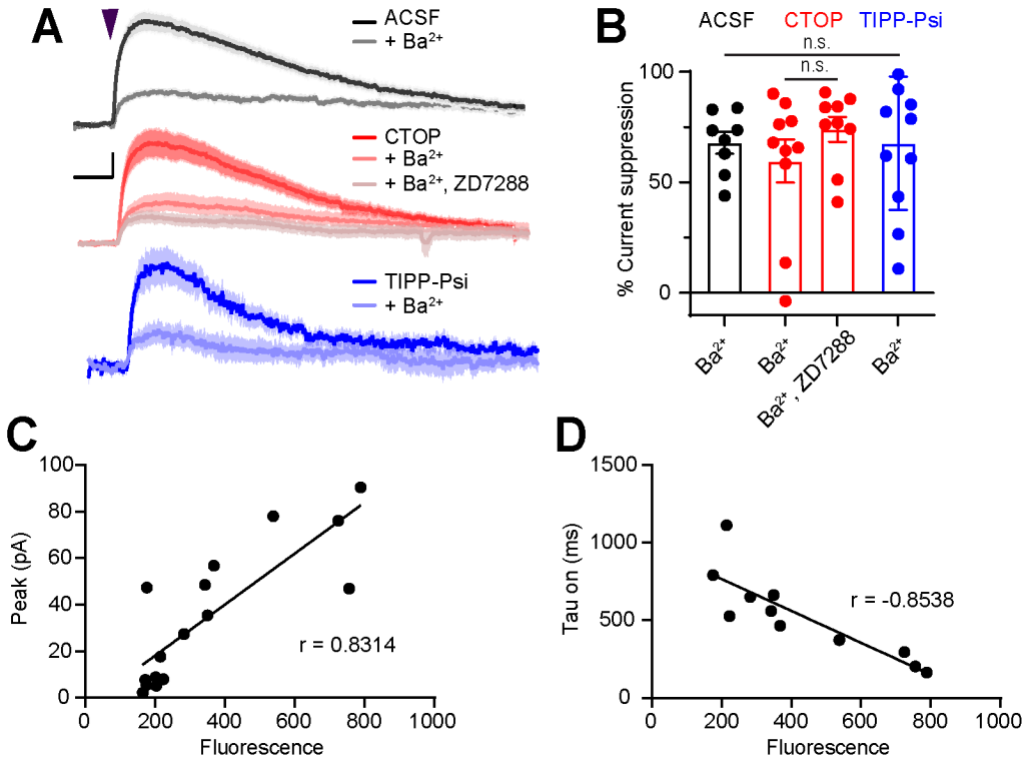

Figure 2.6. Sensitivity of somato-dendritic currents to the GIRK blocker Ba^{2+} and mu opioid receptor expression level.
A. Average outward currents evoked by photoactivation of CYLE with a 84 mW light flash in the absence (black, ACSF, n = 13 cells from 7 mice) and presence of mu and delta opioid receptor antagonists (red, CTOP, n = 14 cells from 10 mice; TIPP-Psi, n = 13 cells from 9 mice), as well as Ba^{2+} (1 mM) (gray, ACSF + Ba^{2+}, n = 8 cells from 2 mice; light red, CTOP + Ba^{2+}, n = 10 cells from 4 mice; light blue, TIPP-Psi + Ba^{2+}, n = 10 cells from 4 mice), and the HCN blocker ZD7288 (lightest red, CTOP + Ba^{2+}, ZD7288, n = 9 cells from 3 mice), as indicated. Scale bar: x = 5 sec, y = 25% of current without Ba^{2+} or ZD7288. **B.** Summary of the percentage of the average peak current amplitude that is blocked in each condition shown in **A**. **C.** Peak amplitude of the MOR-current in *Pvalb*^{Cre} neurons expressing mCh-2A-hMOR vs red fluorescence in the recorded cell, as well as the Pearson's correlation coefficient. For this comparison, all cells were used regardless of fluorescence level. Meanwhile, in **Figure 4I-K**, only cells that had fluorescence > 250 were included. **D.** Time constant of MOR-current activation in *Pvalb*^{Cre} neurons expressing mCh-2A-hMOR vs red fluorescence in the recorded cell, as well as the Pearson's correlation coefficient.

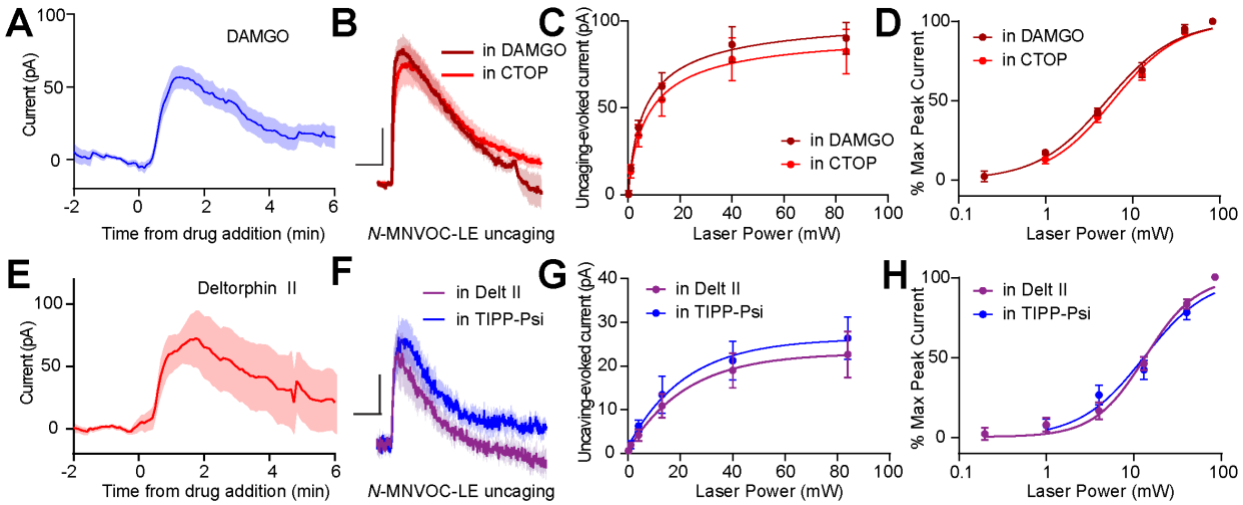

Figure 2.7. Somato-dendritic mu and delta opioid receptors do not exhibit heterologous desensitization

A. Average outward current evoked by sustained bath application of DAMGO (n = 9 cells from 6 mice). **B.** Average outward currents evoked by photoactivation of *N*-MNVOC-LE either in the presence of CTOP (red, data from **4B**) or in the presence of DAMGO, after desensitization (brick red, n = 9 cells from 4 mice). Scale bars: x = 10 sec, y = 25 pA. **C.** Linear optical power-response curve of peak current as a function of light intensity, in the presence of either CTOP (red, n = 10 cells, data from **4C**) or DAMGO (brick red, n = 9 cells) **D.** Logarithmic optical power-response curves of the data in **C** normalized to the maximal peak current observed in each condition. **E.** Average outward current evoked by sustained bath application of deltorphin II (n = 12 cells from 6 mice). **F.** Average outward currents evoked by photoactivation of *N*-MNVOC-LE either in the presence of TIPP-Psi (blue, data from **4B**) or in the presence of deltorphin II, after desensitization (purple, n = 8 cells from 4 mice). Scale bars: x = 10 sec, y = 10 pA. **G.** Linear optical power-response curve of peak current as a function of light intensity, in the presence of either TIPP-Psi (blue, n=11 cells, data from **4C**) or deltorphin II (purple, n = 8 cells) **H.** Logarithmic optical power-response curves of the data in **F** normalized to the maximal peak current observed in each condition.

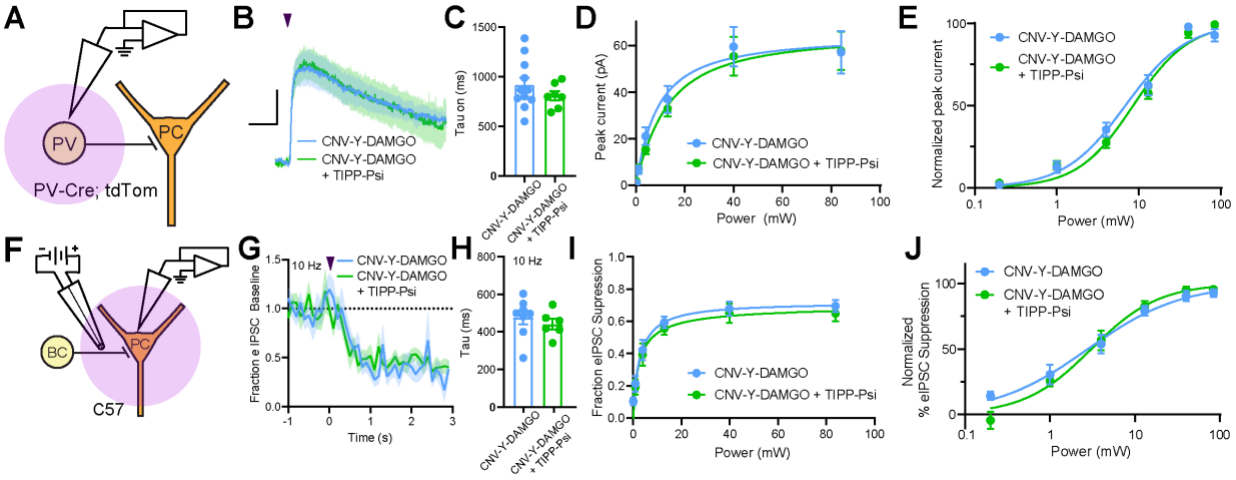

Figure 2.8. Mu and delta opioid receptors do not signal as heteromers in CA1 PV neurons. **A.** Schematic of whole-cell voltage clamp recording configuration from PV interneurons with peptide uncaging. **B.** Average outward currents evoked by photoactivation of CNV-Y-DAMGO with an 84 mW light flash either in the absence (sky blue, n = 8 from 5 mice) or presence (green, n = 7 cells from 4 mice) of TIPP-Psi. Scale bar: x = 10 sec, y = 20 pA. **C.** Time constants of current activation in response to photoactivation of CNV-Y-DAMGO in the absence or presence of TIPP-Psi. **D.** Linear optical power-response curve of peak current as a function of light intensity, in the absence (sky blue) or presence (green) of TIPP-Psi. **E.** Logarithmic optical power-response curves of the data in **D** normalized to the maximal peak current observed in each condition. **F.** Schematic of the experimental configuration for photo-uncaging of opioid neuropeptides while recording electrically-evoked inhibitory synaptic transmission in wild type mice. **G.** Average, baseline subtracted and baseline-normalized eIPSC amplitude showing the kinetics of synaptic suppression with electrical stimulation at 10 Hz in the absence (sky blue, n = 8 cells from 4 mice) or presence of TIPP-Psi (green, n = 8 cells from 4 mice). **H.** Time constants of synaptic suppression at 10 Hz stimulation in response to photoactivation of CNV-Y-DAMGO in the absence or presence of TIPP-Psi. **I.** Linear optical power-response curve of eIPSC suppression as a function of light intensity, in the absence (sky blue) or presence (green) of TIPP-Psi. **J.** Logarithmic optical power-response curves of the data in **I** normalized to the maximal eIPSC suppression observed in each condition.

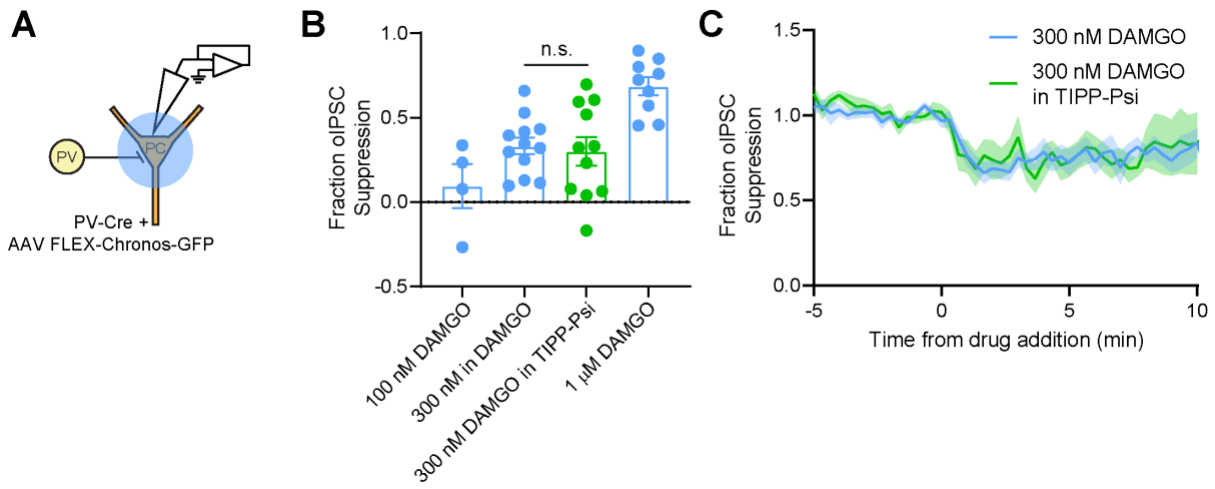

Figure 2.9. Optogenetic activation confirms that MOR and DOR do not signal as heteromers in PV terminals.

A. Schematic of the experimental configuration for recording optogenetically-evoked inhibitory synaptic transmission in *Pvalb*^{Cre} mice. **B.** Summary data showing fraction of oIPSC suppression by 100 nM DAMGO (n = 4 cells from 2 mice), 300 nM DAMGO (n = 12 cells from 6 mice), 300 nM DAMGO in 1 μM TIPP-Psi (green, n = 11 cells from 5 mice), and 1 μM DAMGO (n = 9 cells from 6 mice, same data as Figure 1D) for comparison. **C.** Baseline-normalized, average oIPSC amplitude over time during bath application of 300 nM DAMGO (n = 12 cells from 6 mice) or 300 nM DAMGO in the presence of 1 μM TIPP-Psi (n = 11 cells from 5 mice).

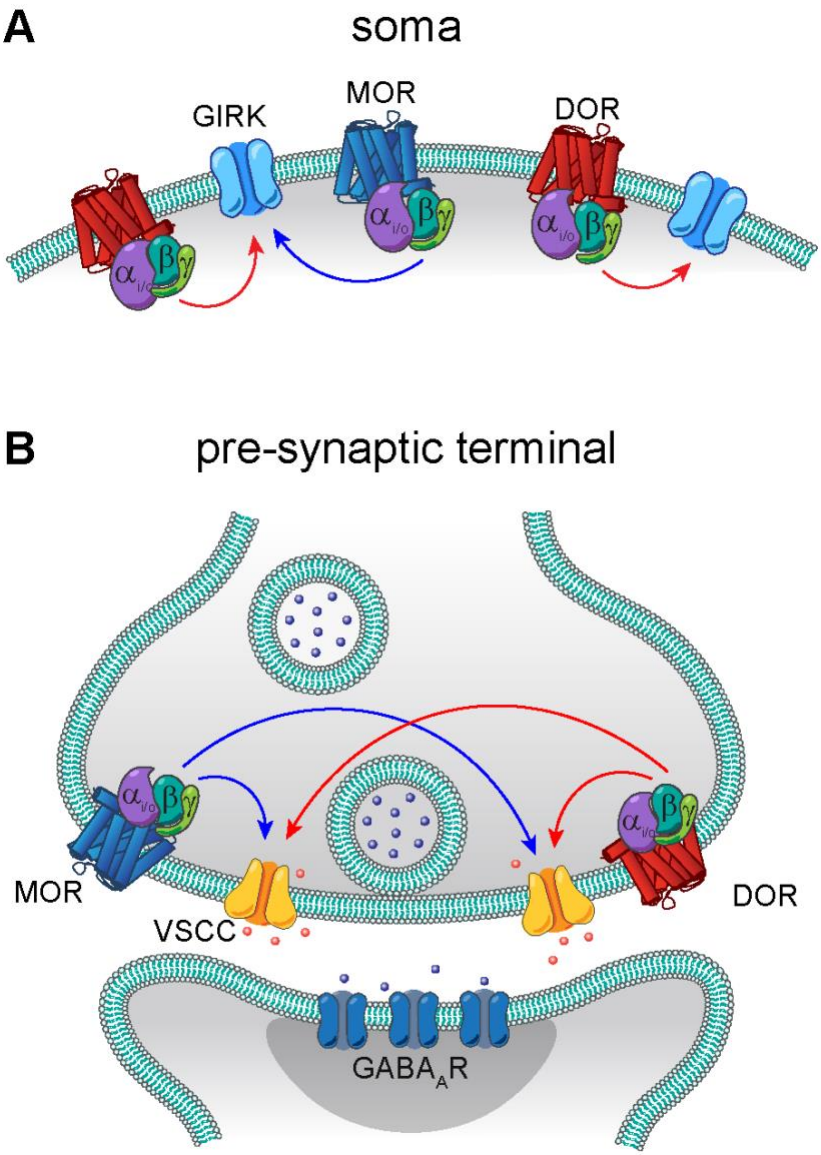

Figure 2.10. Models of MOR and DOR signaling in the soma and the pre-synaptic terminal **A.** In the soma, both MORs (blue) and DORs (red) signal through GIRK channels. MORs are expressed at lower levels than DORs, as the somato-dendritic currents evoked by activation of MORs alone are small and are increased by increasing MOR expression. The unidirectional occlusion observed suggests that MORs only have access to a subset of GIRKs, whereas DORs have access to larger pool that encompasses the MOR-pool. **B.** In the pre-synaptic terminal, MORs and DORs both act on VSCCs to suppress Ca^{2+} influx and inhibit vesicle release. Unlike somatic MORs and DORs, pre-synaptic MORs and DORs are bidirectionally occlusive, so that both MORs and DORs have access to the majority of VSCCs.

References

Abdelhamid, E. E., Sultana, M., Portoghese, P. S., and Takemori, A. E. (1991) 'Selective blockage of delta opioid receptors prevents the development of morphine tolerance and dependence in mice', *Journal of Pharmacology and Experimental Therapeutics*. J Pharmacol Exp Ther, 258(1), pp. 299–303.

Allen Institute for Brain Science (2015). *Allen Brain Atlas API. Available from: brain-map.org/api/index.html* [Accessed April 9, 2021].

Banghart, M. R. Neufeld, S. Q., Wong, N. C., and Sabatini, B. L. (2015) 'Enkephalin Disinhibits Mu Opioid Receptor-Rich Striatal Patches via Delta Opioid Receptors', *Neuron*, 88(6), pp. 1227–1239. doi: 10.1016/j.neuron.2015.11.010.

Banghart, M. R., He, X. J., and Sabatini, B. L. (2018) 'A Caged Enkephalin Optimized for Simultaneously Probing Mu and Delta Opioid Receptors.', *ACS chemical neuroscience*, 9(4), pp. 684–690. doi: 10.1021/acschemneuro.7b00485.

Banghart, M. R. and Sabatini, B. L. (2012) 'Photoactivatable neuropeptides for spatiotemporally precise delivery of opioids in neural tissue.', *Neuron*, 73(2), pp. 249–59. doi: 10.1016/j.neuron.2011.11.016.

Barreca, T., Siani C., Franceschini, R., Francaviglia, N., Messina, V., Perria, C., and Rolandi, E. (1986) 'Diurnal beta-endorphin changes in human cerebrospinal fluid', *Life Sciences*. Life Sci, 38(24), pp. 2263–2267. doi: 10.1016/0024-3205(86)90579-5.

Bean, B. P. (1989) 'Neurotransmitter inhibition of neuronal calcium currents by changes in channel voltage dependence', *Nature*, 340(6229), pp. 153–156. doi: 10.1038/340153a0.

Bjorklund, A. and Hokfelt, T. (1986) *Gaba and Neuropeptides in the Cns, Part I (Handbook of Chemical Neuroanatomy) (Pt. 1)*. 1st edn. New York: Elsevier Science Ltd.

Blackmer, T., Larsen E. C., Takahashi M., Martin T. F., Alford S., and Hamm H. E. (2001) 'G protein βγ subunit-mediated presynaptic inhibition: Regutation of exocytotic fusion downstream of Ca2+ entry', *Science*, 292(5515), pp. 293–297. doi: 10.1126/science.1058803.

Blomeley, C. P. and Bracci, E. (2011) 'Opioidergic interactions between striatal projection neurons.', *The Journal of neuroscience : the official journal of the Society for Neuroscience*, 31(38), pp. 13346–56. doi: 10.1523/JNEUROSCI.1775-11.2011.

Bloodgood, B. L. and Sabatini, B. L. (2007) 'Nonlinear Regulation of Unitary Synaptic Signals by CaV2.3 Voltage-Sensitive Calcium Channels Located in Dendritic Spines', *Neuron*. Neuron, 53(2), pp. 249–260. doi: 10.1016/j.neuron.2006.12.017.

Brody, D. L., Patil, P. G., Mulle, J. G., Snutch, T. P., and Yue, D. T. (1997) 'Bursts of action potential waveforms relieve G-protein inhibition of recombinant P/Q-type Ca2+ channels in

HEK 293 cells.', *The Journal of Physiology*. Blackwell Publishing Ltd, 499(3), pp. 637–644. doi: 10.1113/jphysiol.1997.sp021956.

Brody, D. L. and Yue, D. T. (2000) 'Relief of G-protein inhibition of calcium channels and short-term synaptic facilitation in cultured hippocampal neurons', *Journal of Neuroscience*. Society for Neuroscience, 20(3), pp. 889–898. doi: 10.1523/jneurosci.20-03-00889.2000.

Bruce, D. J., Peterson, C. D., Kitto, K. F., Akgün, E., Lazzaroni, S, Portoghese, P. S., Fairbanks, C. A., Wilcox, G. L. (2019) 'Combination of a δ-opioid Receptor Agonist and Loperamide Produces Peripherally-mediated Analgesic Synergy in Mice', *Anesthesiology*. NLM (Medline), 131(3), pp. 649–663. doi: 10.1097/ALN.0000000000002840.

Cahill, C. M. and Ong, E. (2018) 'Evidence and function relevance of native DOR–MOR heteromers', in *Handbook of Experimental Pharmacology*. Springer New York LLC, pp. 115–127. doi: 10.1007/164_2018_112.

Carter, A. G. and Sabatini, B. L. (2004) 'State-dependent calcium signaling in dendritic spines of striatal medium spiny neurons.', *Neuron*, 44(3), pp. 483–93. doi: 10.1016/j.neuron.2004.10.013.

Chieng, B. C. H., Christie, M. J. and Osborne, P. B. (2006) 'Characterization of neurons in the rat central nucleus of the amygdala: Cellular physiology, morphology, and opioid sensitivity', *Journal of Comparative Neurology*. J Comp Neurol, 497(6), pp. 910–927. doi: 10.1002/cne.21025.

Daniels, D. J., Lenard, N. R., Etienne, C. L., Law, P-Y., Roerig, S. C., and Portoghese, P. S. (2005) 'Opioid-induced tolerance and dependence in mice is modulated by the distance between pharmacophores in a bivalent ligand series', *Proceedings of the National Academy of Sciences of the United States of America*. Proc Natl Acad Sci U S A, 102(52), pp. 19208–19213. doi: 10.1073/pnas.0506627102.

Décaillot, F. M., Rozenfeld, R., Gupta, A., and Devi, L. A. (2008) 'Cell surface targeting of μ-δ opioid receptor heterodimers by RTP4', *Proceedings of the National Academy of Sciences of the United States of America*. National Academy of Sciences, 105(41), pp. 16045–16050. doi: 10.1073/pnas.0804106105.

Dent, R. R. M., Guilleminault, C., Albert, L., Posner, B. I., Cox, B. M., and Goldstein, A. (1981) 'Diurnal rhythm of plasma immunoreactive β-endorphin and its relationship to sleep stages and plasma rhythms of cortisol and prolactin', *Journal of Clinical Endocrinology and Metabolism*. J Clin Endocrinol Metab, 52(5), pp. 942–947. doi: 10.1210/jcem-52-5-942.

Derouiche, L., Pierre, F., Doridot, S., Ory, S., and Massotte, D. (2020) 'Heteromerization of endogenous mu and delta opioid receptors induces ligand-selective co-targeting to lysosomes', *Molecules*. MDPI AG, 25(19). doi: 10.3390/molecules25194493.

Dittman, J. S. and Regehr, W. G. (1997) 'Mechanism and kinetics of heterosynaptic depression at a cerebellar synapse.', *The Journal of neuroscience : the official journal of the Society for*

Neuroscience, 17(23), pp. 9048–59.

Erbs, E., Faget, L., Scherrer, G., Kessler, P., Hentsch, D., Vonesch, J-L., Matifas, A., Kieffer, B. L., and Massotte, D. (2012) 'Distribution of delta opioid receptor-expressing neurons in the mouse hippocampus', *Neuroscience*. NIH Public Access, 221, pp. 203–213. doi: 10.1016/j.neuroscience.2012.06.023.

Erbs, E., Faget, L., Scherrer, G., Matifas, A., Filliol, D., Vonesch, J-L., Koch, M., Kessler, P., Hentsch, D., Birling, M-C., Koutsourakis, M., Vasseur, L., Veinante, P., Kieffer, B. L., and Massotte, D. (2015) 'A mu–delta opioid receptor brain atlas reveals neuronal co-occurrence in subcortical networks', *Brain Structure and Function*. Springer Verlag, 220(2), pp. 677–702. doi: 10.1007/s00429-014-0717-9.

Faget, L., Erbs, E., Le Merrer, J., Scherrer, G., Matifas, A., Benturquia, N., Noble, F., Decossas, M., Koch, M., Kessler, P., Vonesch, J-L., Schwab, Y., Kieffer, B. L., and Massotte, D. (2012) 'In vivo visualization of delta opioid receptors upon physiological activation uncovers a distinct internalization profile', *Journal of Neuroscience*, 32(21), pp. 7301–7310. doi: 10.1523/JNEUROSCI.0185-12.2012.

Freund, T. F. and Katona, I. (2007) 'Perisomatic Inhibition', *Neuron*. Cell Press, pp. 33–42. doi: 10.1016/j.neuron.2007.09.012.

Fujita, W., Gomes, I. and Devi, L. A. (2015) 'Heteromers of μ-δ Opioid receptors: New pharmacology and novel therapeutic possibilities', *British Journal of Pharmacology*. John Wiley and Sons Inc., pp. 375–387. doi: 10.1111/bph.12663.

Galaj, E., Han, X., Shen, H., Jordan, C. J., He, Y., Humburg, B., Bi, G-H., Xi, and Z-X. (2020) 'Dissecting the role of GABA neurons in the VTA versus SNr in opioid reward', *Journal of Neuroscience*. Society for Neuroscience, 40(46), pp. 8853–8869. doi: 10.1523/JNEUROSCI.0988-20.2020.

Gerachshenko, T., Blackmer, T., Yoon, E-J., Bartleson, C., Hamm, H. E., and Alford, S. (2005) 'Gβγ acts at the C terminus of SNAP-25 to mediate presynaptic inhibition', *Nature Neuroscience*, 8(5), pp. 597–605. doi: 10.1038/nn1439.

Glickfeld, L. L., Atallah, B. V. and Scanziani, M. (2008) 'Complementary modulation of somatic inhibition by opioids and cannabinoids', *Journal of Neuroscience*, 28(8), pp. 1824–1832. doi: 10.1523/JNEUROSCI.4700-07.2008.

Gomes, I., Jordan, B. A., Gupta, A., Trapaidze, N., Nagy, V., and Devi, L. A. (2000) 'Heterodimerization of mu and delta opioid receptors: A role in opiate synergy.', *The Journal of neuroscience : the official journal of the Society for Neuroscience*. J Neurosci, 20(22). doi: 10.1523/jneurosci.20-22-j0007.2000.

Gomes, I., Gupta, A., Filipovska, J., Szeto, H. H., Pintar, J. E., and Devi, L. A. (2004) 'A role for heterodimerization of μ and δ opiate receptors in enhancing morphine analgesia', *Proceedings of*

the National Academy of Sciences of the United States of America. Proc Natl Acad Sci U S A, 101(14), pp. 5135–5139. doi: 10.1073/pnas.0307601101.

Gupta, A., Mulder, J., Gomes, I., Rozenfeld, R., Bushlin, I., Ong, E., Lim, M., Maillet, E., Junek, M., Cahill, C. M., Harkany, T., and Devi, L. A. (2010) 'Increased abundance of opioid receptor heteromers after chronic morphine administration', *Science Signaling*. American Association for the Advancement of Science, 3(131). doi: 10.1126/scisignal.2000807.

Hamm, H. E. and Alford, S. T. (2020) 'Physiological roles for neuromodulation via Gi/o GPCRs working through Gβγ–SNARE interaction', *Neuropsychopharmacology*. Springer Nature, p. 221. doi: 10.1038/s41386-019-0497-2.

He, S. Q., Zhang, Z-N., Guan, J-S., Liu, H-R., Zhao, B., Wang, H-B., Li, Q., Yang, H., Luo, J., Li, Z-Y., Wang, Q., Lu, Y-J., Bao, L., and Zhang, X. 2011. (2011) 'Facilitation of μ-Opioid Receptor Activity by Preventing δ-Opioid Receptor-Mediated Codegradation', *Neuron*. Neuron, 69(1), pp. 120–131. doi: 10.1016/j.neuron.2010.12.001.

Higley, M. J. and Sabatini, B. L. (2008) 'Calcium Signaling in Dendrites and Spines: Practical and Functional Considerations', *Neuron*, 59(6), pp. 902–913. doi: 10.1016/J.NEURON.2008.08.020.

Ingram, S., Wilding, T. J., McCleskey, E. W., and Williams, J. T. (1997) 'Efficacy and kinetics of opioid action on acutely dissociated neurons', *Molecular Pharmacology*. American Society for Pharmacology and Experimental Therapy, 52(1), pp. 136–143. doi: 10.1124/mol.52.1.136.

Kabli, N., Fan, T., O'Dowd, B. F., and George, S. R. (2014) 'M-Δ Opioid Receptor Heteromer-Specific Signaling in the Striatum and Hippocampus.', *Biochemical and biophysical research communications*. Elsevier Inc., 450(1), pp. 906–911. doi: 10.1016/j.bbrc.2014.06.099.

Klapoetke, N.C., Murata, Y., Kim, S.S., Pulver, S.R., Birdsey-Benson, A., Cho, Y.K., Morimoto, T.K., Chuong, A.S., Carpenter, E.J., Tian, Z., Wang, J., Xie, Y., Yan, Z., Zhang, Y., Chow, B. Y., Surek, B., Melkonian, M., Jayaraman, V., Constantine-Paton, M., Wong, GK.-S., and Boyden, E. S. (2014). Independent optical excitation of distinct neural populations. Nature Methods *11*, 338–346.

Knapp, R.J., Santoro, G., Leon, I.A.D., Lee, K.B., Edsall, S.A., Waite, S., Malatynska, E., Varga, E., Calderon, S.N., Rice, K.C., Rothman, R. B., Porreca, F., Roeske, W. R., and Yamamura, H. I. (1996). Structure-activity relationships for SNC80 and related compounds at cloned human delta and mu opioid receptors. J Pharmacol Exp Ther *277*, 1284–1291.

Le Merrer, J., Plaza-Zabala, A., Del Boca, C., Matifas, A., Maldonado, R., and Kieffer, B. L. (2011) 'Deletion of the δ opioid receptor gene impairs place conditioning but preserves morphine reinforcement', *Biological Psychiatry*. Biol Psychiatry, 69(7), pp. 700–703. doi: 10.1016/j.biopsych.2010.10.021.

Le Merrer, J., Faget, L., Matifas, A., and Kieffer, B. L. (2012) 'Cues predicting drug or food

reward restore morphine-induced place conditioning in mice lacking delta opioid receptors', *Psychopharmacology*. Psychopharmacology (Berl), 223(1), pp. 99–106. doi: 10.1007/s00213-012-2693-1.

Le Merrer, J., Rezai, X., Scherrer, G., Becker, J. A. J., and Kieffer, B. L. (2013) 'Impaired hippocampus-dependent and facilitated striatum-dependent behaviors in mice lacking the delta opioid receptor', *Neuropsychopharmacology*, 38(6), pp. 1050–1059. doi: 10.1038/npp.2013.1.

Lee, S.-H., Marchionni, I., Bezaire, M., Varga, C., Danielson, N., Lovett-Barron, M., Losonczy, A., and Soltesz, I. (2014). Parvalbumin-Positive Basket Cells Differentiate among Hippocampal Pyramidal Cells. Neuron *82*, 1129–1144.

Leff, E. R., Arttamangkul, S. and Williams, J. T. (2020) 'Chronic treatment with morphine disrupts acute kinase-dependent desensitization of GPCRs', *Molecular Pharmacology*. American Society for Pharmacology and Experimental Therapy, 98(4), pp. 497–507. doi: 10.1124/mol.119.119362.

Leroy, F., Solis, C.A. de, Boyle, L.M., Bock, T., Lofaro, O.M., Buss, E.W., Asok, A., Kandel, E.R., and Siegelbaum, S.A. (2021). Enkephalin release from VIP interneurons in the hippocampal CA2/3a region mediates heterosynaptic plasticity and social memory. *Molecular Psychiatry* **1**:01124-y.

Liu, S., Kim, D.-I., Oh, T.G., Pao, G.M., Kim, J.-H., Palmiter, R.D., Banghart, M.R., Lee, K.-F., Evans, R.M., and Han, S. (2021) 'Neural basis of opioid-induced respiratory depression and its rescue', *Proceedings of the National Academy of Sciences of the United States of America*. Proc Natl Acad Sci U S A, 118(23). doi: 10.1073/pnas.2022134118.

Llorente, J., Lowe, J. D., Sanderson, H. S., Tsisanova, E., Kelly, E., Henderson, G., and Bailey, C. P. (2012) 'μ-Opioid receptor desensitization: homologous or heterologous?', *European Journal of Neuroscience*. John Wiley & Sons, Ltd, 36(12), pp. 3636–3642. doi: 10.1111/ejn.12003.

Lupica, C. R. (1995) 'δ and μ enkephalins inhibit spontaneous GABA-mediated IPSCs via a cyclic AMP-independent mechanism in the rat hippocampus', *Journal of Neuroscience*. Society for Neuroscience, 15(1 II), pp. 737–749. doi: 10.1523/jneurosci.15-01-00737.1995.

Lupica, C. R. and Dunwiddie, T. V. (1991) 'Differential effects of mu- and delta-receptor selective opioid agonists on feedforward and feedback GABAergic inhibition in hippocampal brain slices', *Synapse*. Synapse, 8(4), pp. 237–248. doi: 10.1002/syn.890080402.

Lupica, C. R., Proctor, W. R. and Dunwiddie, T. V. (1992) 'Dissociation of μ and δ opioid receptor-mediated reductions in evoked and spontaneous synaptic inhibition in the rat hippocampus in vitro', *Brain Research*, 593(2), pp. 226–238. doi: 10.1016/0006-8993(92)91312-3.

Ma, X., He, X. J. and Banghart, M. R. (2021) 'A caged DAMGO for selective photoactivation of

endogenous mu opioid receptors', *bioRxiv*, p. 2021.09.13.460181. doi: 10.1101/2021.09.13.460181.

Mack, G. A. and Skillings, J. H. (1980) 'A Friedman-Type Rank Test for Main Effects in a 2-Factor Anova', *Journal of the American Statistical Association*, 75(372), pp. 947–951. Available at: https://www.tandfonline.com/doi/abs/10.1080/01621459.1980.10477577.

Margolis, E. B., Fujita, W., Devi, L. A., and Fields, H. L. (2017) 'Two delta opioid receptor subtypes are functional in single ventral tegmental area neurons, and can interact with the mu opioid receptor', *Neuropharmacology*. Elsevier Ltd, 123, pp. 420–432. doi: 10.1016/j.neuropharm.2017.06.019.

Millan, M. J., Przewlock, R., Jerlicz, M., Gramsch, Ch, Höllt, V., and Herz, A. (1981) 'Stress-induced release of brain and pituitary β-endorphin: Major role of endorphins in generation of hyperthermia, not analgesia', *Brain Research*. Brain Res, 208(2), pp. 325–338. doi: 10.1016/0006-8993(81)90561-8.

Nicoll, R. A., Alger, B. E. and Jahr, C. E. (1980) 'Enkephalin blocks inhibitory pathways in the vertebrate CNS', *Nature*, 287(5777), pp. 22–25. doi: 10.1038/287022a0.

North, R. A., Williams, J. T., Surprenant, A., and Christie, M. J. (1987) 'μ and δ receptors belong to a family of receptors that are coupled to potassium channels', *Proceedings of the National Academy of Sciences of the United States of America*. Proc Natl Acad Sci U S A, 84(15), pp. 5487–5491. doi: 10.1073/pnas.84.15.5487.

Park, D. and Dunlap, K. (1998) 'Dynamic regulation of calcium influx by G-proteins, action potential waveform, and neuronal firing frequency', *Journal of Neuroscience*. Society for Neuroscience, 18(17), pp. 6757–6766. doi: 10.1523/jneurosci.18-17-06757.1998.

Pennock, R. L., Dicken, M. S. and Hentges, S. T. (2012) 'Multiple inhibitory G-protein-coupled receptors resist acute desensitization in the presynaptic but not postsynaptic compartments of neurons', *Journal of Neuroscience*, 32(30), pp. 10192–10200. doi: 10.1523/JNEUROSCI.1227-12.2012.

Piskorowski, R. A. and Chevaleyre, V. (2013) 'Delta-opioid receptors mediate unique plasticity onto parvalbumin-expressing interneurons in area CA2 of the hippocampus', *Journal of Neuroscience*. Society for Neuroscience, 33(36), pp. 14567–14578. doi: 10.1523/JNEUROSCI.0649-13.2013.

Pologruto, T. A., Sabatini, B. L. and Svoboda, K. (2003) 'ScanImage: Flexible software for operating laser scanning microscopes', *BioMedical Engineering Online*. Biomed Eng Online, 2. doi: 10.1186/1475-925X-2-13.

Porreca, F., Heyman, J. S., Mosberg, H. I., Omnaas, J. R., and Vaught, J. L. (1987) 'Role of mu and delta receptors in the supraspinal and spinal analgesic effects of [D-Pen2, D-Pen5]enkephalin in the mouse.', *Journal of Pharmacology and Experimental Therapeutics*,

241(2).

Rezaï, X., Faget, L., Bednarek, E., Schwab, Y., Kieffer, B. L., and Massotte, D. (2012) 'Mouse delta opioid receptors are located on presynaptic afferents to hippocampal pyramidal cells', *Cellular and Molecular Neurobiology*. Springer New York LLC, 32(4), pp. 509–516. doi: 10.1007/s10571-011-9791-1.

Sánchez-Blázquez, P., García-España, A. and Garzón, J. (1997) 'Antisense oligodeoxynucleotides to opioid mu and delta receptors reduced morphine dependence in mice: Role of delta-2 opioid receptors', *Journal of Pharmacology and Experimental Therapeutics*. J Pharmacol Exp Ther, 280(3), pp. 1423–1431.

Saunders, A., Macosko, E.Z., Wysoker, A., Goldman, M., Krienen, F.M., Rivera, H. de, Bien, E., Baum, M., Bortolin, L., Wang, S., Goeva, A., Nemesh, J., Kamitaki, N., Brumbaugh, S., Kulp, D., and McCarroll, S. A. (2018) 'Molecular Diversity and Specializations among the Cells of the Adult Mouse Brain', *Cell*. Elsevier, 174(4), pp. 1015-1030.e16. doi: 10.1016/J.CELL.2018.07.028.

Schuster, D. J., Metcalf, M. D., Kitto, K. F., Messing, R. O., Fairbanks, C. A., and Wilcox, G. L. (2015) 'Ligand requirements for involvement of PKCε in synergistic analgesic interactions between spinal μ and δ opioid receptors', *British Journal of Pharmacology*. John Wiley and Sons Inc., 172(2), pp. 642–653. doi: 10.1111/bph.12774.

Shi, M.-M., Fan, K.-M., Qiao, Y.-N., Xu, J.-H., Qiu, L.-J., Li, X., Liu, Y., Qian, Z.-Q., Wei, C.-L., Han, J., et al. (2020). Hippocampal μ-opioid receptors on GABAergic neurons mediate stress-induced impairment of memory retrieval. Mol Psychiatr *25*, 977–992.

Shi, M. M., Fan, K.-M., Qiao, Y.-N., Xu, J.-H., Qiu, L.-J., Li, X., Liu, Y., Qian, Z.-Q., Wei, C.-L., Han, J., Fan, J., Tian, Y.-F., Ren, W., Liu, Z.-Q. (2020) 'Hippocampal μ-opioid receptors on GABAergic neurons mediate stress-induced impairment of memory retrieval', *Molecular Psychiatry*. Springer Nature, 25(5), pp. 977–992. doi: 10.1038/s41380-019-0435-z.

Stumm, R. K., Zhou, C., Schulz, S., and Höllt, V. (2004) 'Neuronal Types Expressing μ- and δ-Opioid Receptor mRNA in the Rat Hippocampal Formation', *Journal of Comparative Neurology*, 469(1), pp. 107–118. doi: 10.1002/cne.10997.

Svoboda, K. R., Adams, C. E. and Lupica, C. R. (1999) 'Opioid receptor subtype expression defines morphologically distinct classes of hippocampal interneurons', *Journal of Neuroscience*. Society for Neuroscience, 19(1), pp. 85–95. doi: 10.1523/jneurosci.19-01-00085.1999.

Svoboda, K. R. and Lupica, C. R. (1998) 'Opioid inhibition of hippocampal interneurons via modulation of potassium and hyperpolarization-activated cation (I(h)) currents', *Journal of Neuroscience*. Society for Neuroscience, 18(18), pp. 7084–7098. doi: 10.1523/jneurosci.18-18-07084.1998.

Toll, L., Berzetei-Gurske, I.P., Polgar, W.E., Brandt, S.R., Adapa, I.D., Rodriguez, L., Schwartz, R.W., Haggart, D., O'Brien, A., White, A., Kennedy, J. M., Craymer, K., Farrington, L., and

Auh, J. S. (1998). Standard binding and functional assays related to medications development division testing for potential cocaine and opiate narcotic treatment medications. *NIDA Research Monograph 178*, 440–466. Available at: http://www.ncbi.nlm.nih.gov/pubmed/9686407 (Accessed: 1 December 2017).

Wang, D., Tawfik, V.L., Corder, G., Low, S.A., François, A., Basbaum, A.I., and Scherrer, G. (2018) 'Functional Divergence of Delta and Mu Opioid Receptor Organization in CNS Pain Circuits', *Neuron*. Cell Press, 98(1), pp. 90-108.e5. doi: 10.1016/j.neuron.2018.03.002.

Williams, J. T., Ingram, S. L., Henderson, G., Chavkin, C., von Zastrow, M., Schulz, S., Koch, T., Evans, C. J., and Christie, M. J. (2013) 'Regulation of μ-opioid receptors: Desensitization, phosphorylation, internalization, and tolerance', *Pharmacological Reviews*. Pharmacol Rev, pp. 223–254. doi: 10.1124/pr.112.005942.

Williams, J. T. (2014) 'Desensitization of Functional -Opioid Receptors Increases Agonist Off-Rate', *Molecular Pharmacology*, 86(1), pp. 52–61. doi: 10.1124/mol.114.092098.

Williams, J. T., Egan, T. M. and North, R. A. (1982) 'Enkephalin opens potassium channels on mammalian central neurones', *Nature*. Nature, 299(5878), pp. 74–77. doi: 10.1038/299074a0.

Wimpey, T. L. and Chavkin, C. (1991) 'Opioids activate both an inward rectifier and a novel voltage-gated potassium conductance in the hippocampal formation.', *Neuron*, 6(2), pp. 281–9.

Wu, L. G. and Saggau, P. (1997) 'Presynaptic inhibition of elicited neurotransmitter release', *Trends in Neurosciences*. Elsevier Ltd, 20(5), pp. 204–212. doi: 10.1016/S0166-2236(96)01015-6.

Yao, Z., Velthoven, C.T.J. van, Nguyen, T.N., Goldy, J., Sedeno-Cortes, A.E., Baftizadeh, F., Bertagnolli, D., Casper, T., Chiang, M., Crichton, K., Ding, S.-L., Fong, O., Garren, E., Glandon, A., Gouwens, N. W., Gray, J., Graybuck, L. T., Hawrylycz, M. J., Hirschstein, D., Kroll, M., Lathia, K., Lee, C., Levi, B., McMillen, D., Mok, S., Pham, T., Ren, Q., Rimorin, C., Shapovalova, N., Sulc, J., Sunkin, S. M., Tieu, M., Torkelson, A., Tung, H., Ward, K., Dee, N., Smith, K. A., Tasic, B. T., and Zeng, H. (2021) 'A taxonomy of transcriptomic cell types across the isocortex and hippocampal formation', *Cell*. Cell, 184(12), pp. 3222-3241.e26. doi: 10.1016/J.CELL.2021.04.021.

Yoon, E. J., Gerachshenko, T., Spiegelberg, B. D., Alford, S., and Hamm, H. E. (2007) 'Gβγ interferes with Ca2+-dependent binding of synaptotagmin to the soluble N-ethylmaleimide-sensitive factor attachment protein receptor (SNARE) complex', *Molecular Pharmacology*. American Society for Pharmacology and Experimental Therapeutics, 72(5), pp. 1210–1219. doi: 10.1124/mol.107.039446.

Zhang, Z. and Pan, Z. Z. (2010) 'Synaptic mechanism for functional synergism between δ- And μ-opioid receptors', *Journal of Neuroscience*, 30(13), pp. 4735–4745. doi: 10.1523/JNEUROSCI.5968-09.2010.

Zhu, Y., King, M.A., Schuller, A.G.P., Nitsche, J.F., Reidl, M., Elde, R.P., Unterwald, E., Pasternak, G.W., and Pintar, J.E. (1999) 'Retention of supraspinal delta-like analgesia and loss of morphine tolerance in δ opioid receptor knockout mice', *Neuron*. Cell Press, 24(1), pp. 243–252. doi: 10.1016/S0896-6273(00)80836-3.

Zieglgänsberger, W., French, E. D., Siggins, G. R., and Bloom, F. E. (1979) 'Opioid peptides may excite hippocampal pyramidal neurons by inhibiting adjacent inhibitory interneurons', *Science*, 205(4404), pp. 415–417. doi: 10.1126/science.451610.

Zurawski, Z., Gray, A.D., Brady, L.J., Page, B., Church, E., Harris, N.A., Dohn, M.R., Yim, Y.Y., Hyde, K., Mortlock, D.P., Jones, C. K., Winder, D. G., Alford, S., and Hamm, H. E. (2019) 'Disabling the Gβγ-SNARE interaction disrupts GPCR-mediated presynaptic inhibition, leading to physiological and behavioral phenotypes', *Science Signaling*. American Association for the Advancement of Science, 12(569). doi: 10.1126/scisignal.aat8595.

CHAPTER 3. Visualizing the dynamics of neuropeptide signaling using novel sensors

Introduction

Neuropeptide signaling has historically been challenging to study because of the lack of robust tools to evoke and measure release. Because of that, we lack answers to basic questions such as – when and where are neuropeptides released? What conditions drive release? What is released from dense core vesicles when multiple neuropeptides are expressed in a single neuron? With advances in neuroscience tools and technology, we will soon be able to address these questions more directly. This study takes advantage of two novel tools – neuropeptide sensors and photoactivatable peptides – to ask the question of how far neuropeptides spread once they are released.

A recent preprint used a similar approach to control release of somatostatin (SST) by use of photosensitive nanovesicles and measurement of activity using a new cell-based neurotransmitter fluorescent engineered reporter (CNiFER) for SST (Xiong et al., 2021). Their approach demonstrated the power of these tools, but the applications are limited by the need to implant the CNiFER and the nanovesicles. Genetically encoded fluorescent sensors for neuropeptides can be expressed by injection of AAV into any brain area. Sensors for many neuropeptides are being developed and are now published, primarily by two groups. We are collaborating with Lin Tian's group at UC Davis to characterize novel sensors based on opioid receptors MOR, DOR, and KOR. In this study, we focused on the KOR-based sensor kLight to detect dynorphin after photorelease of a caged dynorphin, CNB-Y-Dyn-8 (CYD8) (Banghart and Sabatini, 2012). We characterized multiple sensor variants to determine the highest performing sensor, and then used photoactivation while imaging to measure the apparent diffusion

coefficient of dynorphin. This diffusion coefficient can then be used to determine how far the peptide spreads based on any starting concentration of the peptide.

Characterizing efficacy and sensitivity of kLight variants.

Our collaborators developed several variants of kLight that differ in properties such as membrane trafficking and binding affinity to ligands. To determine which variant would be best suited for our purposes, we first tested several of these variants using assays for dynamic range, sensitivity, and buffering capacity. An adeno-associated virus (AAV) encoding the various kLight variants was injected into the dorsal striatum of C57 pups (P0 – P6) and allowed to express for a minimum of 4 weeks (**Figure 3.1A**). Acute coronal slices were then prepared using a vibratome and the tissue was imaged using video recordings with a 60x objective (**Figure 3.1A-B**). In some experiments, a 355 nm laser was applied through the objective to uncage photoactivatable peptides (**Figure 3.1A**).

To compare the efficacies of the kLight variants, we first bath applied 1 μM dynorphin-8 (dyn8) while video imaging at 0.2 hz. Dyn8 caused increases in fluorescence with all the kLight variants, with the greatest dF/F changes from kLight1.3 (0.27 ± 0.02, n = 4 videos), followed by kLight1.2a (0.17 ± 0.04, n = 7 videos) (**Figure 3.1C-D**). The fluorescence change was completely blocked by the presence of opioid antagonist naloxone (NLX) (-0.003 ± 0.001, n = 5 videos, p = 0.045, Kruskal-Wallis test with Dunn's multiple comparisons), demonstrating that this effect was due to engagement of opioid receptors. We proceeded with the top two variants, kLight1.2a and kLight1.3, to generate dose-response curves by bath applying differing concentrations of dyn8. We found that while kLight1.3 showed greater dF/F at 1 μM, kLight1.2a has a greater affinity to dyn8 in slices (EC50 of kLight1.2a = 358 ± 123 nM, n = 5 – 8 videos;

EC50 of kLight1.3 = 1677 ± 1198 nM, n = 4 – 8 videos) (**Figure 3.1E-F**). This highlights kLight1.2a as a likely candidate for the best performing variant to carry forth our studies.

Characterizing kinetics of kLight engagement using dynorphin uncaging.

Because endogenous dynorphin release is yet to be reliably achieved, we took advantage of photoactivable dynorphin, CYD8, to measure kinetics of signaling and eventually mimic endogenous release. We used a collimated 355 nm laser to illuminate a large portion of the imaged tissue and analyzed the fluorescence change over the entire video frame (**Figure 3.2A**). CYD8 (5 μM) was circulated in the bath and then a 50 ms laser pulse was delivered to the tissue while video imaging at 1 hz (**Figure 3.2B**). This was repeated for all the kLight variants to find that kLight1.3 yielded the greatest dF/F (0.11 ± 0.01, n = 6 videos), with kLight 1.2a (0.091 ± 0.008, n = 24 videos) and kLight1.1 (0.093 ± 0.014, n = 4 videos) following it (**Figure 3.2C**). The uncaging response of kLight1.1 was completely blocked by the presence of NLX (0.005 ± 0.001, n = 3 videos; p = 0.017, Kruskal-Wallis test with Dunn's multiple comparisons), showing that the fluorescence change is due to engagement of opioid receptors and not an artifact of the UV laser.

While kLight1.3 had the greatest dF/F, we noticed that its response took remarkably longer to decay compared to the other variants (**Figure 3.2B**). We hypothesize that this is due to its higher buffering capacity, which is the ability for the kLight receptor to bind to a molecule of dynorphin and trap it, leading to continuous fluorescence and preventing the peptide from further diffusion and action. This property is an intrinsic limitation to all biosensors of this design, and while it can be seen for all the kLight variants, the buffering tendency of kLight1.3 is noticeably stronger. For kLight1.3, we found that this can impact the dF/F observed after uncaging, and the

time constant of decay. The background fluorescence of the tissue was found to be negatively correlated with dF/F ($r^2 = 0.4366$) (**Figure 3.2D**) and positively correlated with the time constant of decay ($r^2 = 0.8791$) (**Figure 3.2E**). Because of these issues, we chose not to continue with kLight1.3 for the purpose of our study.

To study onset kinetics of kLight, we repeated uncaging with the collimated laser, but restricted analysis to a smaller region of interest (ROI) to limit the effects of diffusion (**Figure 3.2F**). To more accurately estimate the rise time, we imaged only the first few seconds after uncaging at a higher temporal resolution of 50 hz (**Figure 3.2G**). A total of 3 frames (60 ms) were lost during uncaging because the light from the laser eclipsed any kLight signal. Double exponential functions were fit to these time courses to extract the two time constants $Tau_{on}1$ and $Tau_{on}2$ (**Figure 3.2H**). We believe $Tau_{on}1$ reflects the immediate rise time of the receptor at the site of uncaging, while $Tau_{on}2$ reflects dF/F changes due to diffusion in the z-axis. Both time constants were similar across all three variants tested ($Tau_{on}1$ for kLight1.2a = 54.5 ± 20.2 ms, kLight1.2b = 58.4 ± 19.4 ms, kLight1.2c = 59.0 ± 11.1 ms; $Tau_{on}2$ for kLight1.2a = 1.64 ± 0.55 s, kLight1.2b = 1.63 ± 0.21 s, kLight1.2c = 1.67 ± 0.21 s). With all these considerations, we confirmed kLight1.2a as the best performing variant to proceed in our studies.

kLight1.2a does not affect endogenous opioid receptor function

The intrinsic property of biosensors to buffer ligand can be a limitation on studying the ligand's effect on endogenous receptors. We wanted to address this potential limitation by using the assays discussed in Chapter 2 to ask if the effect of dynorphin uncaging on endogenous hippocampal opioid receptors is buffered by the presence of kLight1.2a. AAVs encoding kLight1.2a or GFP as a control were injected into the hippocampus of C57 pups (P0 – P3) and

allowed to express for a minimum of 3 weeks until acute slices were made for electrophysiology (**Figure 3.3A**). As discussed in Chapter 2, PV interneurons in CA1 region of the hippocampus express MOR and DOR which act presynaptically to suppress synaptic transmission. While dynorphin's primary target is KOR, it also binds strongly to MOR and DOR (Toll et al., 1998). Therefore, we can uncage dynorphin and ask if MOR and DOR function are affected by the expression of kLight1.2a.

To assay opioid receptor function, we recorded inhibitory currents (IPSCs) onto pyramidal cells by stimulating basket cell axons with a bipolar stimulating electrode (**Figure 3.3B**). The IPSCs were suppressed by uncaging of a photoactivatable dynorphin, MNV-D8, using a 5 ms 355 nm laser pulse (**Figure 3.3C**). Uncaging was performed using different powers of the UV laser to uncage differing concentrations of dyn8, for both tissue expressing kLight1.2a and GFP (**Figure 3.3D**). Although there was a slight trend for a smaller uncaging responses in tissue expressing kLight1.2a at higher laser powers, these effects were not significant ($p = 0.63$ at $11 \mu W/\mu m^2$, Multiple t tests with Holm-Sidak method to correct for multiple comparisons) (**Figure 3.3E**). There were also no significant differences in the recovery after uncaging (indicated by the tau_{off}) between kLight and GFP tissue, although there was a slight trend to longer recovery times for kLight at $0.89 \mu W/\mu m^2$ ($p = 0.07$, Multiple t tests with Holm-Sidak method to correct for multiple comparisons) (**Figure 3.3F**). Because kLight expression does not significantly change the responses of opioid receptors in this assay, this alleviates some of the concern for kLight buffering of endogenous receptors, at least in slice. Whether or not this applies to an *in vivo* context or endogenously released dynorphin will take further study.

Measuring neuropeptide diffusion through dynorphin uncaging

A fundamental question about neuromodulation is how far do peptides spread after they are released in the brain? While we have not yet achieved endogenous dynorphin release, we can use dynorphin uncaging to mimic release and measure its diffusion using kLight activation. Previous attempts at such questions use brief bath application or a picospritzer to puff on peptide and measure diffusion (Syková and Nicholson, 2008). Peptide uncaging is advantageous because it is almost instantaneous (i.e., photolysis is not the time limiting step) and does not apply any pressure onto the tissue. To measure dynorphin spread after uncaging, we used a focused 355 nm laser, steered to the side of the acquisition frame to maximize diffusion distance. Video recording was taken before and after laser flash and processed to obtain dF/F for each pixel in the video frame (**Figure 3.4A**). The averaged dF/F within the uncaging ROI was plotted to get the time constants of activation (τ_{on} = 1.54 sec) and decay (τ_{off} = 117 sec) at the site of uncaging (**Figure 3.4B**). As expected, the peak dF/F and kinetics of activation decrease as a function of distance from uncaging site (**Figure 3.4C**).

The video was further parsed to obtain the apparent diffusion coefficient (*D**), based on a derivation of Fick's law of diffusion that yields $\gamma_i^2 = 4D^*(t_i + t_0)$ (Nicholson and Tao, 1993). Based on this equation, *D** is the slope of the linear regression between $\gamma^2/4$ and time, as demonstrated by diffusion of dextrans molecules or quantum dots in the cortex (Thorne and Nicholson, 2006). A separate group used similar logic to calculate the diffusion coefficient of calcium in dendrites using the equation $D = \frac{1}{2} \cdot \frac{d[\sigma^2(t)]}{dt}$, where D is the slope of a plot of $\sigma^2/2$ against time (Soler-Llavina and Sabatini, 2006). They divided by a constant of 2 instead of 4 because they were describing two-dimensional spread in a dendrite. In this case, σ is used to describe to describe the width of the Gaussian distribution. Since our data is only half of a

Gaussian, we used an exponential curve to fit the data instead and used the half-width to describe the spread of fluorescence.

To do this, first the fluorescence profile was plotted as a function of distance from uncaging for each time frame post uncaging (**Figure 3.4D**). To reduce noise, we averaged 50 pixels in a column along the x-axis where uncaging had taken place. We also only analyzed the spread from the edge of the uncaging spot to around 100 μm away, where we thought the objective was most reliable. These fluorescence profiles were normalized and then fit to an exponential function to extract the half width, distance where dF/F decays to 50% of initial dF/F (**Figure 3.4E**). The half width squared, divided by 4, was plotted against time for each time frame, and the slope of the plot is D^* (**Figure 3.4F**). Across multiple uncaging trials in different tissue, the average D^* was found to be 1.44 ± 0.37 $\mu m^2/s$ (**Figure 3.4G**).

Discussion

The utilization of a novel peptide sensor along with photoactivatable peptide gives us tight control and insight over the spatiotemporal signaling dynamics of the neuropeptide dynorphin. It allows the instantaneous release of a controlled amount of dynorphin and imaging of actual receptor conformation change reflecting receptor activation. A literature search shows that estimated and measured diffusion coefficients for neuropeptides vary substantially. Estimates for the diffusion coefficient of dynorphin are 4×10^{-6} cm/s in water and 4×10^{-7} cm/s in brain tissue (Drake et al., 1994). The diffusion coefficient of a 3 kDa dextran molecule in cortical slice was found to be 8.1×10^{-7} cm^2/s, which converts to 8.1 $\mu m^2/s$ (Nicholson and Tao, 1993). A recent group had a similar approach of releasing somatostatin (SST) and measuring diffusion with CNiFERs and found the diffusion coefficient of SST to be 89 $\mu m^2/s$ (Xiong et al.,

2021). Another group used a novel oxytocin sensor to find the diffusion coefficient of endogenous oxytocin to be 4.7 x 10^3 $\mu m^2/s$ (Qian et al., 2022). Because of differences in methodology, it is difficult to compare values directly.

Because of kLight buffering, it is likely that our apparent diffusion coefficient is not the true diffusion coefficient of dynorphin in brain slices. We have experiments in mind to address this issue. We hypothesize that there is an inverse relationship between sensor expression (baseline fluorescence) and *D**, where the more sensor is present, the slower the diffusion. Therefore, if we obtain *D** at varying levels of sensor expression (baseline fluorescence), we would be able to extrapolate the value of *D** at zero sensor expression. We can also carry out various controls to determine how the *D** of dynorphin compares to other molecules. One example is to use a photoactivatable fluorescent dye and observe its diffusion in slices not expressing kLight. A more rigorous control would be to conjugate the dye to the caged peptide and image with or without kLight expression, to compare peptide diffusion with dye to peptide diffusion with sensor activation.

In the absence of a true diffusion coefficient, there is still much insight to be gleaned using our current methodology to compare diffusion coefficients under various conditions. One application is to compare *D** in striatum to other brain areas, such as the cortex. The apparent diffusion coefficient is related to the true diffusion coefficient and the tortuosity of the tissue, described by $\lambda = \sqrt{D/D^*}$, where λ is tortuosity (Syková and Nicholson, 2008). Because the striatum is a tortuous brain region, with fiber bundles of passage and microdomains like patch and matrix (Gerfen, 1992), we expect that a more homogenous brain region like the cortex would have a greater *D**. Another application is to measure *D** in the presence of peptidase inhibitors. Peptidases are enzymes that degrade peptides and are the primary way peptides are inactivated

and cleared from tissue (Coleman et al., 1994; Nässel, 2009). It's been shown that peptidase inhibitors enhance the signaling of neuropeptides (Banghart and Sabatini, 2012), sometimes even unveiling their effects (Trieu et al., 2022). We hypothesize that peptidase inhibitors will increase *D** by preventing peptide clearance and indeed we have preliminary evidence (not included in this dissertation) to support this.

This work done with peptide uncaging will greatly inform future studies to achieve the ultimate goal – imaging endogenous release in slice and *in vivo*. We have struggled to measure endogenous dynorphin release in slice using this assay as well as electrophysiological assays. But as our understanding of the types of stimuli that drive neuropeptide release grows, such as with substance P release (unpublished data from Banghart lab), we will be able to revisit dynorphin release with a more focused parameter space. Part of the issue is that the existing sensors may not be sensitive enough to detect endogenous release, which is thought to occur at the nanomolar level (Drake et al., 1994). We found that kLight1.2a has an EC50 of 358.3 nM in our assay, so we may need even more sensitive sensors to detect endogenous release. Our assay of imaging bulk fluorescence is also not the ideal configuration because of light scattering in the tissue. 2-photon or confocal microscopy may be better suited to detect brief, focused release events.

These experiments were also crucial in identifying the role of sensor expression and buffering in the kLight response. To obtain the maximal dF/F, we had to target recordings towards tissue of lower expression levels, deliberately moving away from areas of highest expression. While this is achievable in a slice, it can be challenging *in vivo* if fluorescence is used to target fiber optic implants. This could be a reason why *in vivo* dynorphin release has also been challenging to achieve despite producing stimuli that are thought to evoke it. One solution

would be to reduce buffering by using a sparse expression scheme to titrate the ideal amount of sensor expression. Such a system is already being developed by our collaborators and will be tested and implemented by us in the future.

Despite these limitations, kLight is still an extremely promising neuropeptide sensor that holds the potential to open up the field of neuropeptide signaling. We have shown that it performs well in brain slices to bath application of dynorphin and photoactivation of caged dynorphin. We have used these techniques to measure an apparent diffusion coefficient of dynorphin which can be compared to other contexts to answer biological questions relating to volume transmission. We have also identified the issue of buffering and proposed solutions to minimize its impact in future studies. With a few modifications in the sensor design or implementation, researchers will soon be able to utilize it as a direct readout of endogenous dynorphin *in vivo* which will have huge implications in the field of neuromodulation.

Methods

Key Resources Table

Reagent or Resource	Source	Identifier
Chemicals, Peptides, and Recombinant Proteins		
Dynorphin-8		
Naloxone		
MNV-D8	Banghart Lab	
CYD8	Banghart Lab and NIDA Drug Supply Program	
NBQX	HelloBio	Cat #HB0443
CPP	Tocris	Cat #0247
Experimental Models: Organisms/Strains		
C57/BL6J	The Jackson Laboratory	
Bacterial and Virus Strains		
AAV-DJ-CAG-GFP	Addgene	Plasmid #37825
AAV9-Syn-KOR-GIPH	Tian Lab	
AAV1-hSyn-kLight1.2a	Tian Lab	
AAV1-hSyn-kLight1.2b	Tian Lab	
AAV1-hSyn-kLight1.2c	Tian Lab	
Software and Algorithms		
MatLab	Mathworks Inc	https://www.mathworks.com
ScanImage	Pologruto et al, 2003	http://scanimage.vidriotechnologies.com/
Ocular	Qimaging	https://www.qimaging.com/ocular
Igor Pro	WaveMetrics	https://www.wavemetrics.com
ImageJ	Schneider et al, 2012	https://imagej.nih.gov/ij/index.html
Illustrator CC	Adobe Systems Inc.	https://www.adobe.com/
Prism 7	GraphPad Inc	https://www.graphpad.com
Excel	Microsoft	

Stereotaxic Intracranial Injection. Animal handling protocols were approved by the UC San Diego Institutional Animal Care and Use Committee. Male and female C57/B6J mice (postnatal day 0–7) were anesthetized with isoflurane and placed in a small animal stereotaxic frame (David Kopf Instruments). After puncturing the skin and skull under aseptic conditions, AAVs were injected (0.5–1 ml total volume) bilaterally through a pulled glass pipette at a rate of 100 nl/min using a UMP3 microsyringe pump (World Precision Instruments). Depending on the size of the mouse, injection coordinates ranged between 0 to +0.5 mm from bregma, 0.5 to 1.0

mm lateral, and 1.8 to 2.3 mm below pia for dorsal striatum. For targeting hippocampus, injection coordinates ranged from +0.3-0.5mm from lambda, 2.2-2.5mm lateral, and 1.4 to 2.0 below pia. After surgical procedures, mice were returned to their home cage for >30 days to allow for maximal gene expression.

Brain Slice Preparation. Postnatal day 30-60 mice were anesthetized with isoflurane and killed, and the brain was removed, blocked, and mounted in a VT1000S vibratome (Leica Instruments). For striatal imaging experiments, coronal slices (300 μm) were prepared in 34°C ACSF containing (in mM), 127 NaCl, 2.5 KCl, 25 NaHCO3, 1.25 NaH2PO4, 2 CaCl2, 1 MgCl2, and 25 glucose, osmolarity 307, equilibrated with 95% O2/5% CO2. For hippocampal electrophysiology recordings, horizontal slices (300 μm) were prepared in ice-cold choline-ACSF containing (in mM) 25 NaHCO3, 1.25 NaH2PO4, 2.5 KCl, 7 MgCl2, 25 glucose, 1 CaCl2, 110 choline chloride, 11.6 ascorbic acid, and 3.1 pyruvic acid, equilibrated with 95% O2/5% CO2. Slices were transferred to a holding chamber with oxygenated ACSF and incubated at 32 °C for 30 min and then left at room temperature until recordings were performed.

Video acquisition. All video recordings were performed within 5 h of slice cutting in a submerged slice chamber perfused with ACSF warmed to 32 °C and equilibrated with 95% O2/5% CO2. Infected tissue in the dorsal striatum was located and focused under a 60x objective. Ocular image acquisition software (Qimaging) was used to acquire videos using exposure times and frame rates as listed in the table below. For dynorphin flowins, 1 μM of dyn8 was added 3 minutes into the recording. For uncaging trials, 5 μM of CYD8 was circulated in the bath prior to beginning video acquisition. During uncaging trials, ScanImage was used to trigger

video acquisition and the UV laser. Uncaging was carried out using 10 or 50 ms flashes of collimated full-field illumination with a 355nm laser. Light powers in the text correspond to measurements of a 10mm diameter collimated beam at the back aperture of the objective.

Video acquisition specifications for different imaging configurations

	Dyn flow-in (Fig 3.1)	CYD8 uncaging (Fig 3.2A – E)	CYD8 kinetics (Fig 3.2F – H)
Exposure time	100 ms	100 ms	20 ms
Frame rate	0.2 hz	1 hz	50 hz
Blue LED power	20% ND2	20% ND2	20% ND2
UV Laser duration		50 ms	10 ms
UV Laser power		5 μW/μm^2	5 μW/μm^2
Total video duration	10 min	5 min	10 sec
Drug concentration	1 μM dyn8	5 μM CYD8	5 μM CYD8

Electrophysiology. All recordings were performed within 5 h of slice cutting in a submerged slice chamber perfused with ACSF warmed to 32 °C and equilibrated with 95% O2/5% CO2. Whole-cell voltage clamp recordings were made with an Axopatch 700B amplifier (Axon Instruments). Data were filtered at 3 kHz, sampled at 10 kHz, and acquired using National Instruments acquisition boards and a custom version of ScanImage written in MATLAB (Mathworks). Cells were rejected if holding currents exceeded −200 pA or if the series resistance (<25 MΩ) changed during the experiment by more than 20%. For recordings measuring inhibitory synaptic transmission in mouse hippocampus, patch pipets (2.8−3.5 MΩ) were filled with an internal solution containing (in mM) 135 CsMeSO3, 10 HEPES, 1 EGTA, 3.3 QX-314 (Cl − salt), 4 Mg-ATP, 0.3 Na-GTP, and 8 Na 2 phosphocreatine (pH 7.3, 295 mOsm/kg). Cells were held at 0 mV to produce outward currents. Excitatory transmission was blocked by the addition to the ACSF of NBQX (10 μM) and CPP (10 μM).To electrically evoke IPSCs, stimulating electrodes pulled from theta glass with ∼5 μm tip diameters were placed at the

border between stratum pyramidale and straum oriens nearby the recorded cell (~50−150 μm) and a two brief pulses (0.5 ms, 50−300 μA, 50 ms interval) were delivered every 20 s. 6 μM of MNV-D8 was circulated in the bath prior to uncaging. Uncaging was carried out using 5 ms flashes of collimated full-field illumination with a 355nm laser at different power densities.

Data Analysis. Video acquisition data were analyzed using ImageJ with follow up analysis in Igor Pro (Wavemetrics). For dynorphin flow-ins (Figure 1C), the mean brightness of the full frame was plotted per frame. The mean brightness of each frame was divided by the average baseline fluorescence of the first 3 minutes to get dF/F. Then, the first 3 minutes before drug addition was fit with a biexponential curve to estimate the rate of bleaching during the video acquisition. This was subtracted from the average brightness to get the curves in Figure 1C. For uncaging trials (Figure 1E), a 700μm^2 circle ROI was drawn at the center of the uncaging field and the mean brightness of this ROI was plotted per frame. The trace was then baseline normalized and subtracted as described above using the first minute of recording as baseline. For 50hz uncaging onset experiments (Figure 1G), 3 acquisitions with UV laser flash were taken before adding CYD8 into the bath to obtain average bleaching of the ROI. These 3 acquisitions were averaged and then subtracted from acquisition with uncaging in CYD8 to get the traces in Figure 1G. Note that a frame was lost during uncaging due to the UV laser oversaturating the frame. The resulting trace was fit to a biexponential curve to extract Tau_{on} 1 and Tau_{on} 2. Electrophysiology data were analyzed in Igor Pro (Wavemetrics). Peak current amplitudes were calculated by averaging over a 2 ms window around the peak. To determine magnitude of modulation by MNV-D8 uncaging (%IPSC suppression), the IPSC peak amplitude immediately after a flash was divided by the average peak amplitude of the three IPSCs

preceding the light flash. To determine the time constant of recovery (tau off), the IPSC amplitudes are fit to a monoexponential curve starting at the point of maximal IPSC suppression to when the IPSC amplitudes return to baseline.

Spot uncaging. For more details on acquisition and data analysis for spot uncaging (**Figure 3.4)**, see the appendix to this chapter.

Chapter 3 contains unpublished material coauthored with Tian, Lin and Banghart, Matthew. The dissertation author was the primary investigator and author of this chapter.

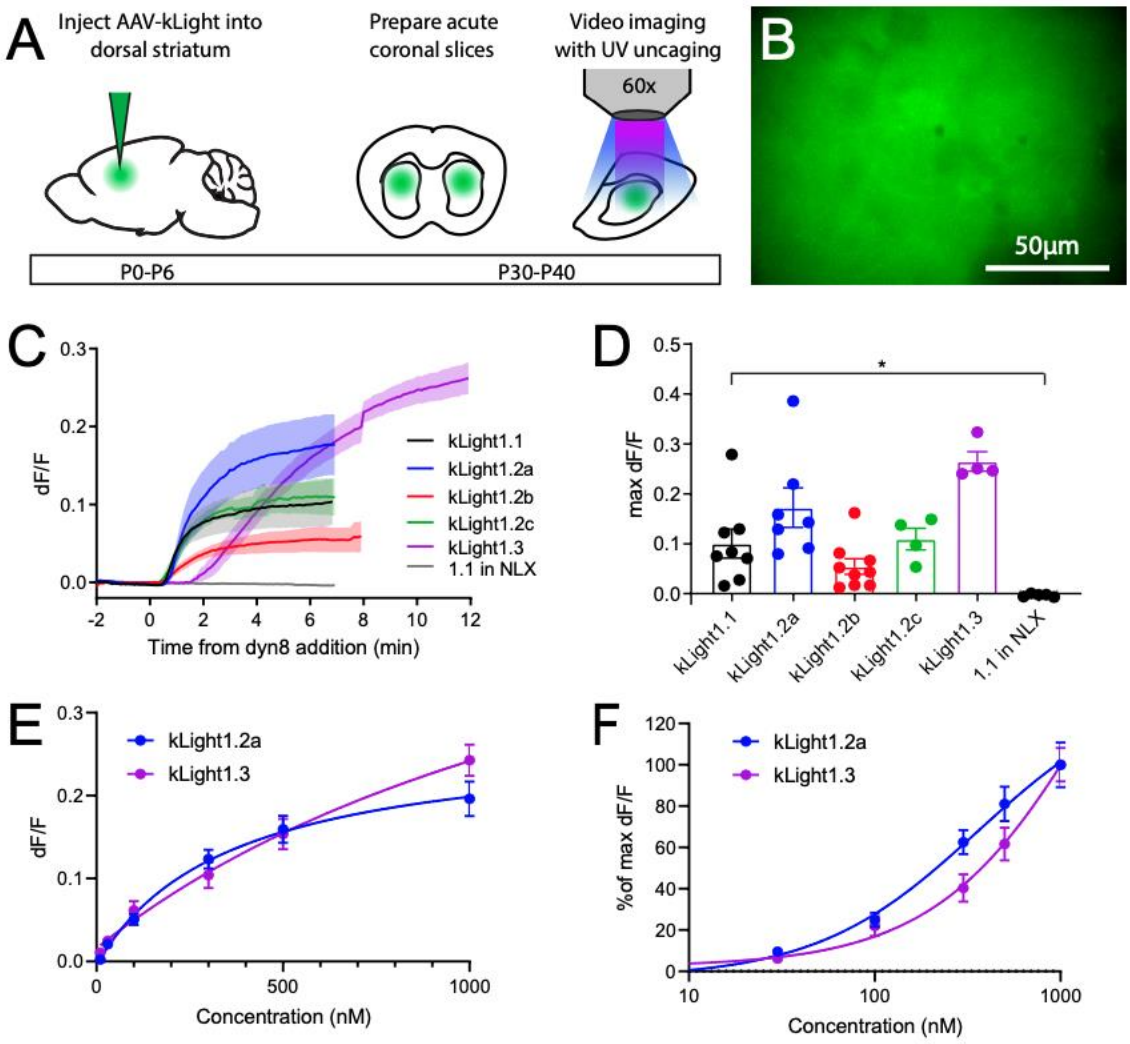

Figure 3.1. Characterization of kLight variants in acute striatal slices with bath application of dynorphin.

A. Schematic of experiment setup. C57/B6J pups are injected with AAV1-hSyn-kLight1.2a in the dorsal striatum. After 3-4 weeks, acute coronal slices were prepared and video imaged under a 60x objective. **B.** Single frame image of kLight infected tissue under settings used for video acquisition. **C.** Fluorescence change of different kLight variants during a 14 minute video acquisition at 0.2hz while 1 μM dyn8 is bath applied at 2 minutes into the recording. **D.** Summary of peak fluorescence increase of kLight variants. Error bars are standard error of the mean. Bath application of dyn8 in the presence of opioid antagonist naloxone (NLX) blocked the fluorescence increase of kLight1.1. **E.** Dose response curves of kLight1.2a (blue, n = 5-8 videos) and kLight1.3 (purple, n = 4-8 videos) constructed by bath applying various concentrations of dyn8. **F.** Dose response curves of kLight1.2a and kLight1.3 normalized to the maximal change in fluorescence and on a logarithmic scale. The EC50 for kLight1.2a is 358.3 nM compared to 1677 nM for kLight1.3.

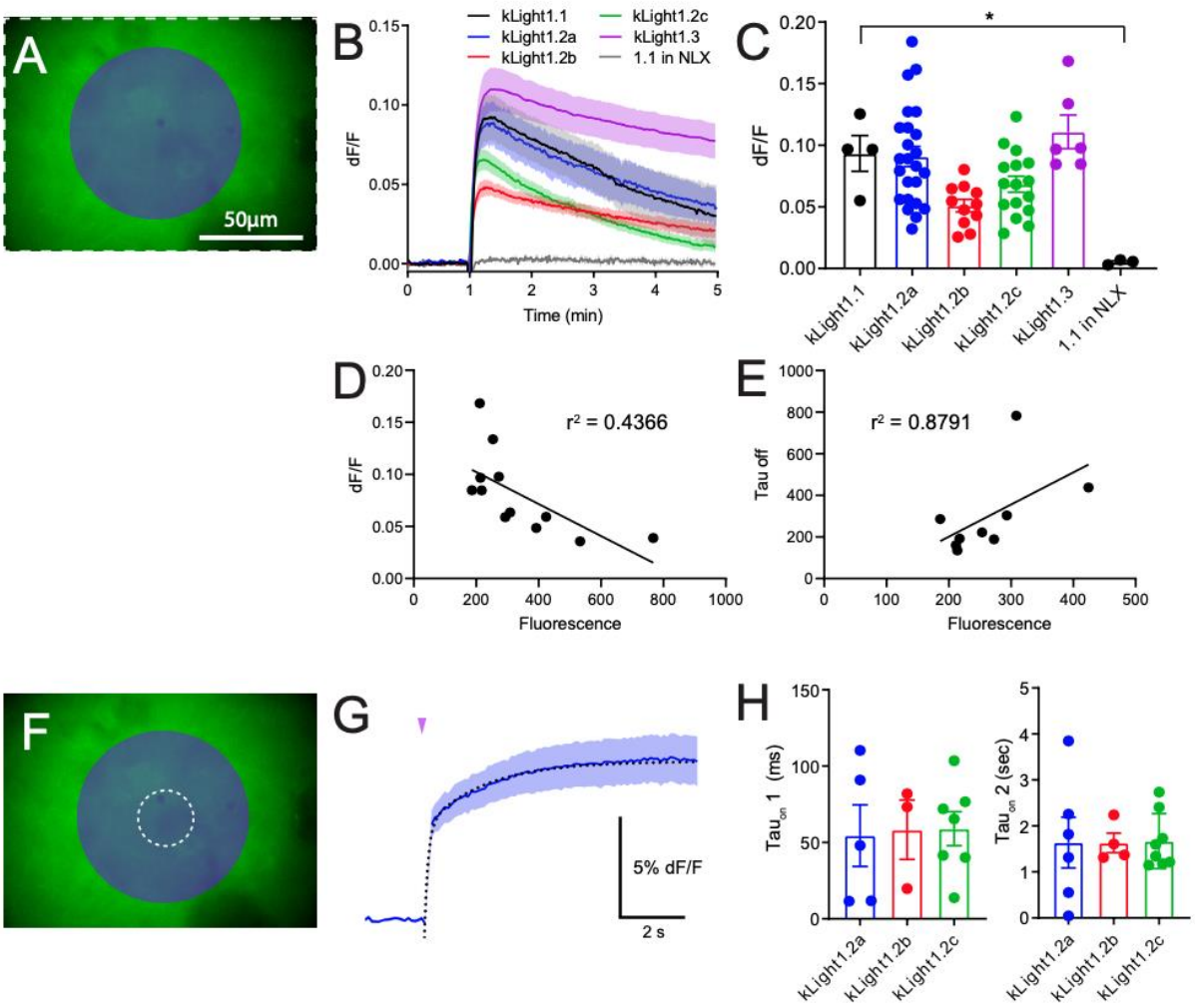

Figure 3.2. Characterization of kLight variants in acute striatal slices through photoactivation of caged dynorphin.

A. Image of tissue as acquired through video acquisition, with a semitransparent purple circle showing the field of uncaging with a collimated 355 nm laser. The dotted line shows the area of analysis (the entire field of view). **B.** Fluorescence change of kLight variants during a 50ms flash of UV laser at 5.1µW/µm^2, indicated by the purple arrow while imaging with video acquisition at 1 hz. **C.** Summary of peak fluorescence change of kLight variants after uncaging. kLight1.3 and kLight1.2a had the largest fluorescence increase. Uncaging in the presence of NLX blocked the change in fluorescence of kLight1.1. **D.** The relationship between baseline fluorescence and max dF/F for kLight 1.3 shows negative correlation (r^2 = 0.4366). **E.** The relationship between baseline fluorescence and the time constant of decay for kLight1.3 shows positive correlation (r^2 = 0.8791). **F.** Same field of view and field of uncaging as in A, but with a smaller ROI of analysis as shown by the dotted line. **G.** Average uncaging timecourse for kLight1.2a using 50 hz frame rate to resolve uncaging kinetics with a 10 ms UV flash at 5.1µW/µm^2 (purple arrow). Three frames had to be deleted during the UV flash due to an artifact from the laser itself. The curve was then fit to a biexponential (dotted line) with 2 time constants, tau1 and tau2, to describe the early rising phase and the late rising phase. **H.** Summary of tau1 (left) and tau2 (right) values show no difference between the kinetics of kLight variants.

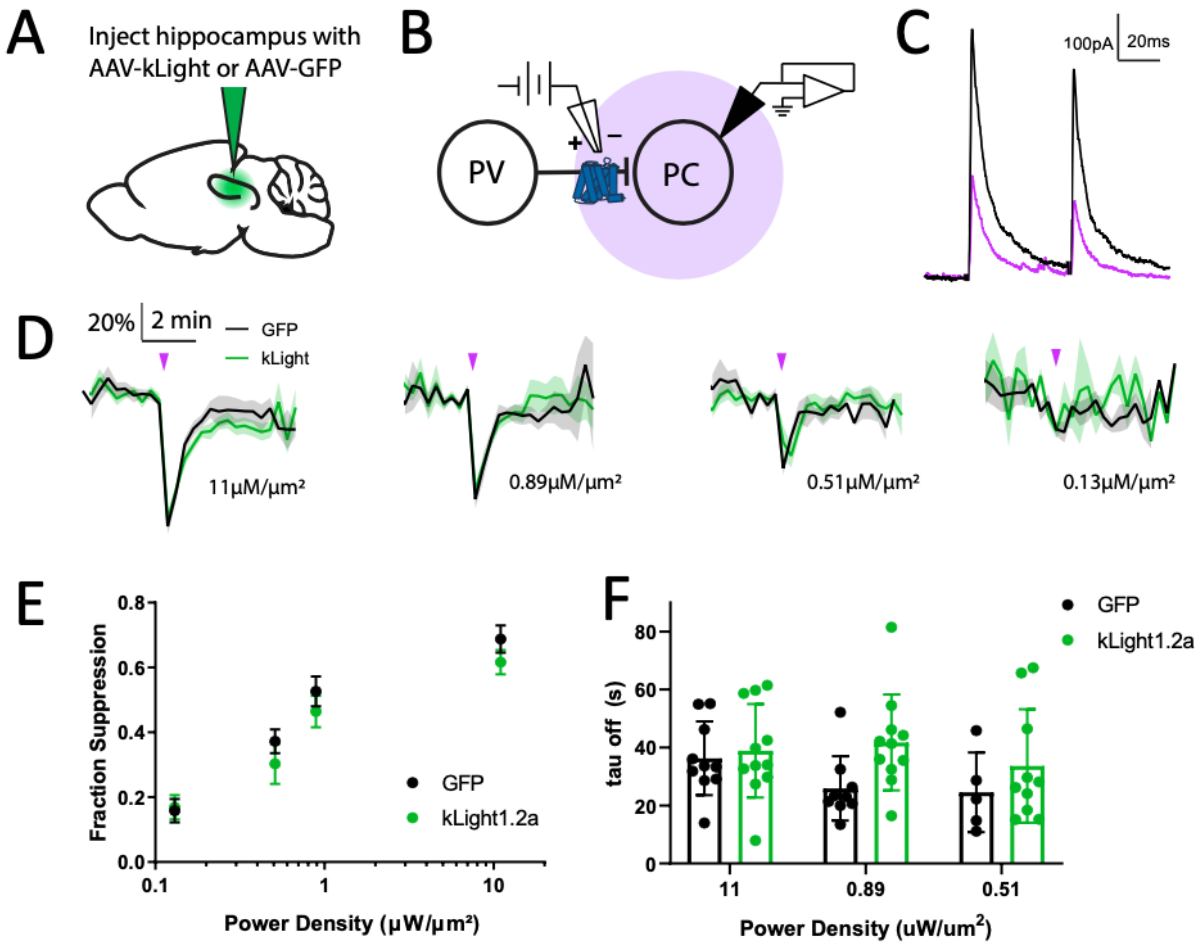

Figure 3.3. kLight1.2a does not significantly buffer opioid dependent synaptic suppression at endogenous opioid receptors.

A. Similar to 3.1A, C57/B6J pups are injected with AAV1-hSyn-kLight1.2a or AAV-DJ-CAG-GFP in the hippocampus and allowed to express for 3 weeks until acute slices are made for electrophysiology. **B.** Schematic for electrophysiology set-up. Pyramidal cells (PC) are patched and held at 0 mV while parvalbumin (PV) basket cell axons are stimulated with a bipolar electrode. Two pulses of electrical stimulus are elicited 50 ms apart to drive IPSCs in the PC. Then, with 5 μM MNV-D8 in the bath, a 5 ms flash of UV laser is used to uncage dynorphin which acts on the presynaptic opioid receptors on the PV cell to suppress the IPSC. **C.** Example of IPSC before (black) and after UV MNV-D8 uncaging (purple). **D.** Time course of dynorphin uncaging and recovery where the IPSC is probed every 20 sec to get the % of baseline IPSC peak before and after UV uncaging (purple arrow). The average timecourses are shown for varying UV powers for both GFP and kLight infected tissue. **E.** There is no difference between the fraction suppression evoked by uncaging dynorphin for GFP and kLight1.2a infected tissue. **F.** Average time constant of decay for the recovery of IPSC peak after dynorphin uncaging. While there is a trend for the time constant to be higher for kLight tissue at 0.89uW/um2, there were no differences found using multiple t-tests with Benjamini, Krieger and Yekutieli with Q=1% false discovery rate.

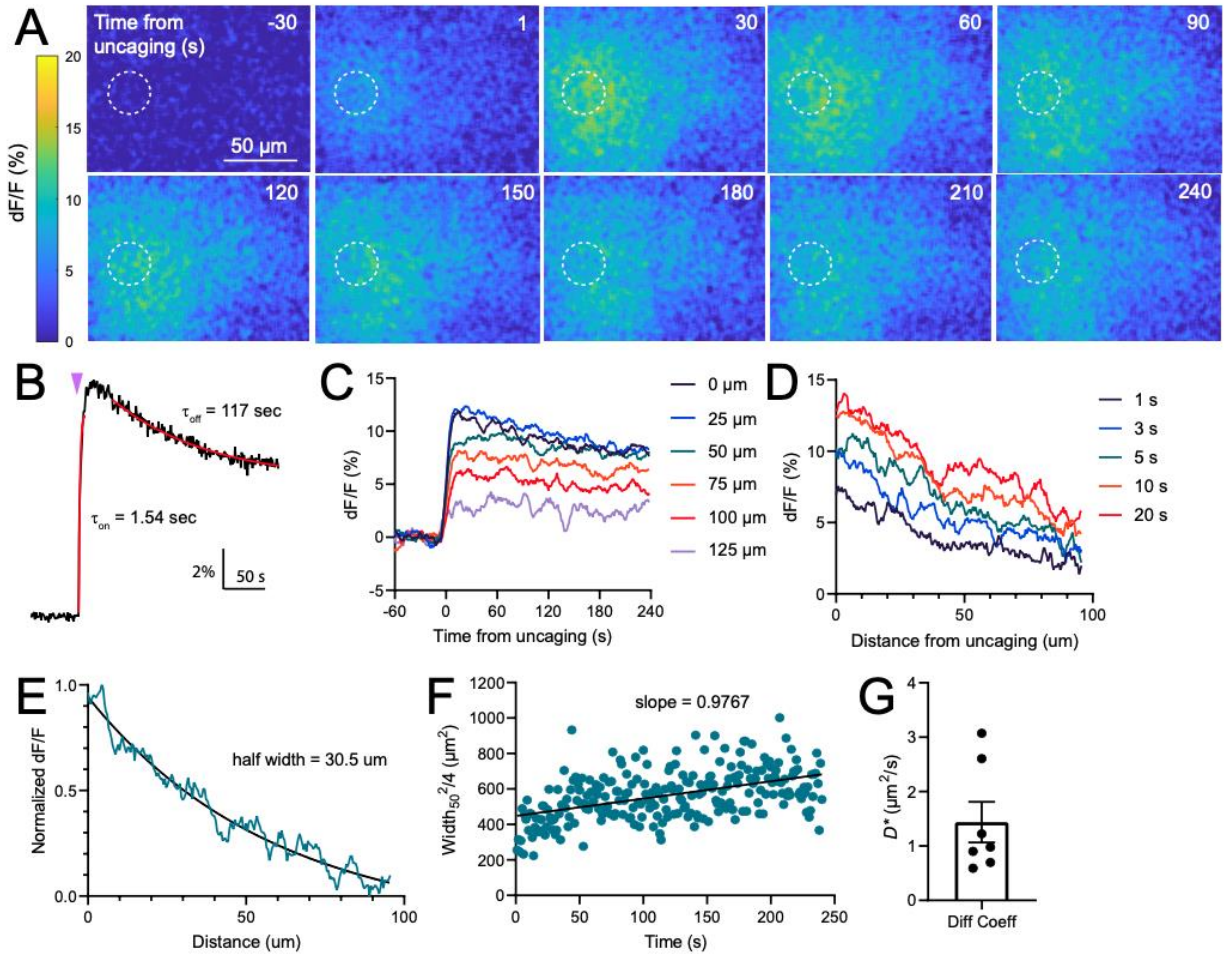

Figure 3.4. Using small spot uncaging of dynorphin to study spatiotemporal dynamics of peptide signaling and spread.

A. Timecourse of kLight1.2a photoactivation after CYD8 (5 µM) uncaging in striatal tissue. Photoactivation was done by a 50 ms, 355 nm focused laser, steered to the side of the acquisition frame as seen by the dotted circle. Heatmaps show dF/F (%) after the video was corrected for bleaching by the laser. **B.** Average dF/F for the entire ROI within the photoactivation field (dotted circle in A). Purple arrow indicates the 50 ms laser flash. Red curves show the exponential fits to 90% of peak to calculate the rising kinetics (tau on = 1.54 sec) and decay kinetics (tau off = 117 sec). **C.** The fluorescence timecourse for a single pixel along the middle of the imaging plane at differing distances from the center of uncaging. **D.** The fluorescence profile as a function of distance from uncaging spot, for differing times after uncaging. **E.** The fluorescence profile at a single time (5 sec, as in D), normalized and fit to an exponential function to extract the half width (30.5 um). **F.** The fits in E were repeated at every time point to extract half width. The half width squared / 4 was plotted against time and the slope of this linear regression is the apparent diffusion coefficient. **G.** Summary of the apparent diffusion coefficient (as calculated in F) measured through multiple uncaging videos.

Appendix. Detailed methods for spot uncaging acquisition and analysis using Matlab.

Videos are acquired as described in the methods section in the main text above (100 ms exposure, 1 hz frame rate, 20% ND2 blue LED, 50 ms laser, 5 $\mu W/\mu m^2$ laser power, 5 μM CYD8). The major difference is instead of using a wide field collimated laser, a focused laser beam is used, steered to the side of the acquisition frame. Examples of the laser illumination fields are shown below for the two laser configurations.

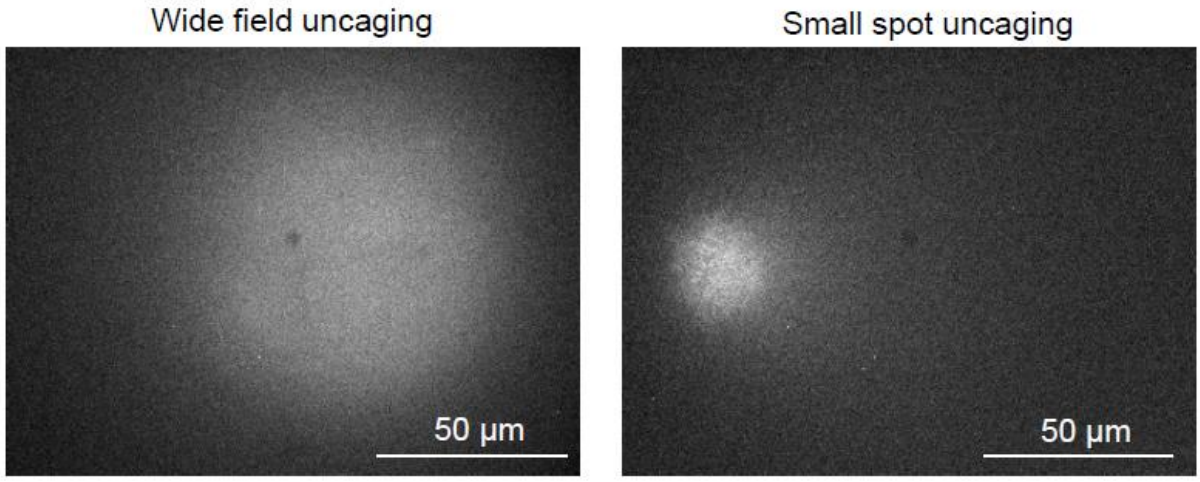

Figure 3.5. Comparison of UV laser illumination area between collimated, wide field laser and focused, small spot laser.

Due to the laser bleaching of kLight tissue, we had to acquire 2 videos per ROI, one before and one after addition of CYD8, in order to subtract the bleaching from the uncaging video. To conserve use of caged compound, we typically imaged 2-3 ROIs before adding caged compound, and the same 2-3 ROIs after, using Lin Lab 2 software to keep track of the stage coordinates. The setup for video acquisition in Matlab and Ocular is shown in **Figure 3.6.** The resulting videos are saved and then processed in Matlab followed by Igor as shown in **Figure 3.7**.

1

Matlab cycle and pulse settings for a 300 s acquisition. DA 0 is set to a blank 301000 ms pulse. As it's setup currently, AUX 2 is the camera, AUX 6 is the LED, AUX 4 is the UV shutter, and AUX 5 is the UV laser.

2

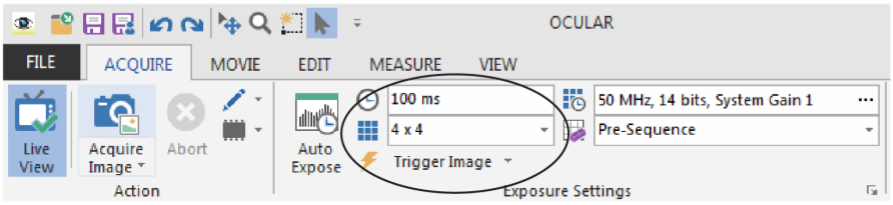

Exposure settings are set in the "Acquire" tab. I typically use 100 ms frames and 4 x 4 binning to maximize light input.

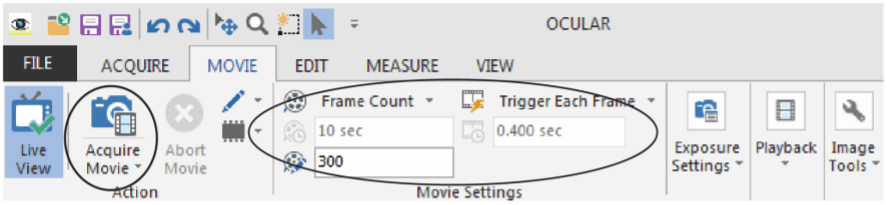

Make sure the frame count is set to desired number of frames, e.g., 300 for a 300 s acquisition at 1 hz. "Trigger each frame" means that the camera will wait for the Matlab command to be triggered. Once everything is ready, hit "Acquire Movie", then "Show Preview" to bring up the active acquisition window.

3

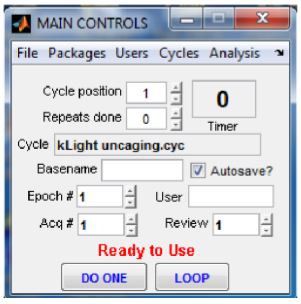

The preview will say "Waiting" as it waits for the Matlab command. Hit "DO ONE" in Matlab and this will start the cycle and trigger the camera and the LED. You should be able to see it switch from "waiting" to "acquiring" in the preview window and see the frames as they come in. Note that the preview window auto-contrasts based on your first image so future videos may look too bright or too dim. That is corrected when the image is analyzed in ImageJ or Matlab.

Figure 3.6. Matlab and Ocular settings to acquire a 5 min video with uncaging at 1 min.

1

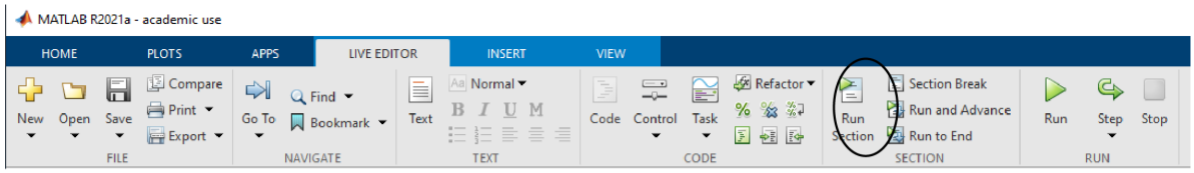

The code is written in chucks so after every section, hit “Run Section” to execute the code.

Navigate to the folder of the ROI of analysis. Rename the before and after videos, “Bleach” and “CYD8”.

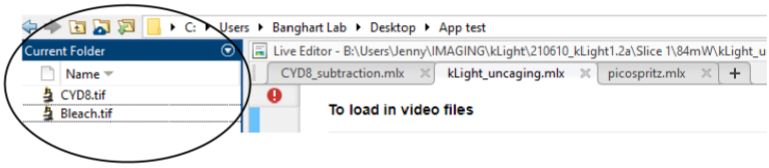

Hit “Run Section” on the first section of code to load in the video files and convert to variables (3D matrices).

2

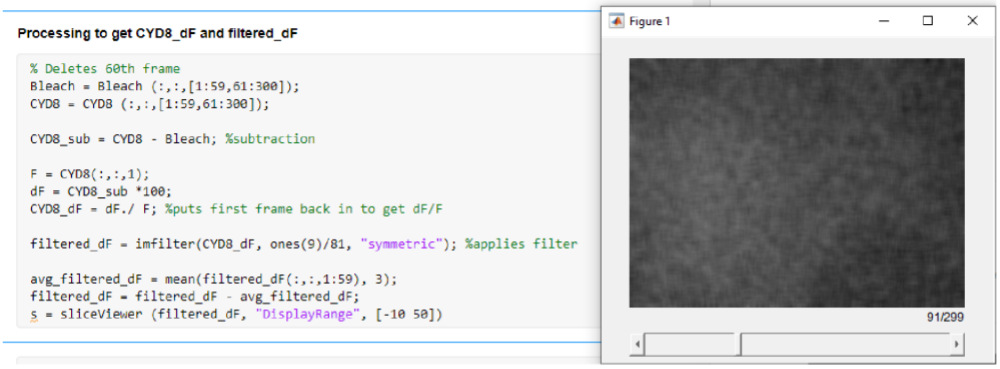

Processing to get the subtracted video. First, deletes the 60th frame of each video (the UV laser frame). Then creates subtracted video, CYD8_sub. Next, processes to get dF/F by taking the change in fluorescence and dividing it by the first frame in the uncaging video. Applies a filter, and then baseline subtracts by the average of the first 59 frames. Pulls up sliceViewer to look at the new, filtered image.

Figure 3.7. Analysis pipeline for processing the video in Matlab (Steps 1-3), and then determining the diffusion coefficient in Igor (Step 4), continued on next page.

3

To plot dF for each frame

```
time_dF = zeros ([299 344], "double");

tic

for time = 1:299

    slice_time = filtered_dF(:,:,time);
    avg_slice = mean(slice_time(100:150, :), 'omitnan'); %change dimensions
    time_dF(time, :) = avg_slice;

end

toc

plot(time_dF)
plot(time_dF')

time_dF_crop = time_dF(60:299, :);
time_dF_crop = time_dF_crop(:, 90:300); % change dimensions based on laser spot
time_dF_crop = time_dF_crop';
plot(time_dF_crop)
writematrix(time_dF_crop); %writes as a .txt to move to igor
```

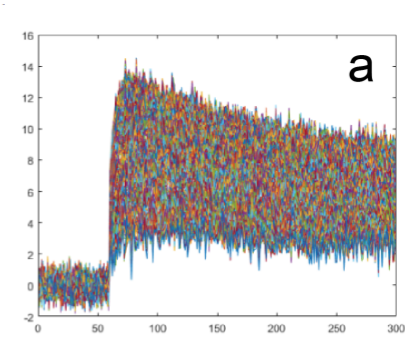

Extracts from the filtered video and makes two plots. 3a is the fluorescence over time for each x-value pixel, averaged between pixels 100-150 in the y-axis (dF as a function of space). 3b is the inverse of 3a, the fluorescence over space for each time point (dF as a function of time). 3c is 3b cropped to just the time points after uncaging, and between x = 90-300, the space where diffusion is analyzed. The data in 3c is saved automoatically as a .txt in the home folder

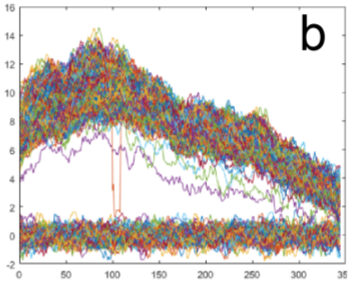

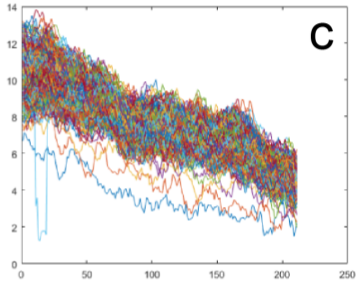

4

KORlight.ipf

```
function halfwidth()

    applytowin ("wavestats /Q %s; %s-=V_min"); //normalizes to min = 0, max = 1
    applytowin ("wavestats/Q %s; %s/=V_max");

    make/o/t/n=0 wavenum; make/o/n=0 half_width, make/o/n=240 half_width_um; make/o/n=240 half_width_um2; make/o/n=240 half_width_um2_4; Duplicate/D/O wave0_n,fit_dest;
        edit wavenum, half_width, half_width_um, half_width_um2;
        applytowin ("addtos(wavenum, nameofwave(%s)); CurveFit/Q/NTHR=0 exp_XOffset  %s /D=fit_dest; FindLevel  /Q/R=(0, 221) fit_dest, 0.5; addto(half_width, V_LevelX)")
        half_width_um = half_width/2.29333;
        half_width_um2 = half_width_um^2;
        half_width_um2_4 = half_width_um2/4;

    display half_width_um2; ModifyGraph mode=3,marker=19,mrkThick=1; ModifyGraph rgb(half_width_um2)=(0,0,0);
    CurveFit/NTHR=0/TBOX=768 line  half_width_um2 /D

end
```

Import the saved .txt file into igor as multiple waves. Dupsuffixplot all waves with _n as a suffix to get 4a. Run halfwidth() on 4a to get 4b (normalized waves) and 4c. To get 4c, each wave in 4b is fit to an exponential function, then the level crossing for y = 0.5 is found to get the half-width. Half-width is converted from pixel to µm, squared, and plotted over time and fit to a linear regression to get 4c. The slope of the line divided by 4 is the apparent diffusion coefficient for that video.

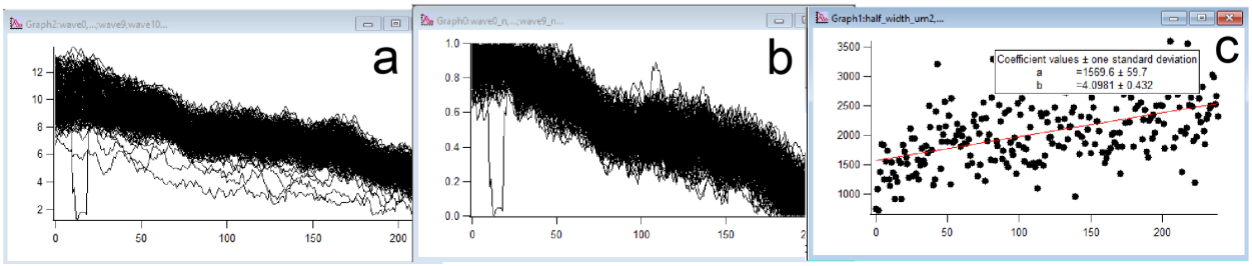

Figure 3.7 continued. Analysis pipeline for processing the video in Matlab (Steps 1-3), and then determining the diffusion coefficient in Igor (Step 4).

References

Banghart, M.R., and Sabatini, B.L. (2012). Photoactivatable neuropeptides for spatiotemporally precise delivery of opioids in neural tissue. Neuron *73*, 249–259.

Coleman, M., Konstant, P., Rothman, B., and Nusbaum, M. (1994). Neuropeptide degradation produces functional inactivation in the crustacean nervous system. J Neurosci *14*, 6205–6216.

Drake, C., Terman, G., Simmons, M., Milner, T., Kunkel, D., Schwartzkroin, P., and Chavkin, C. (1994). Dynorphin opioids present in dentate granule cells may function as retrograde inhibitory neurotransmitters. J Neurosci *14*, 3736–3750.

Gerfen, C.R. (1992). The neostriatal mosaic: multiple levels of compartmental organization. Trends in Neurosciences *15*, 133–139.

Nässel, D.R. (2009). Neuropeptide signaling near and far: how localized and timed is the action of neuropeptides in brain circuits? Invertebr Neurosci *9*, 57.

Nicholson, C., and Tao, L. (1993). Hindered diffusion of high molecular weight compounds in brain extracellular microenvironment measured with integrative optical imaging. Biophys J *65*, 2277–2290.

Qian, T., Wang, H., Wang, P., Geng, L., Mei, L., Osakada, T., Tang, Y., Kania, A., Grinevich, V., Stoop, R., Lin, D., Luo, M., and Li, Y. (2022). Compartmental Neuropeptide Release Measured Using a New Oxytocin Sensor. Biorxiv 2022.02.10.480016.

Soler-Llavina, G.J., and Sabatini, B.L. (2006). Synapse-specific plasticity and compartmentalized signaling in cerebellar stellate cells. Nat Neurosci *9*, 798–806.

Syková, E., and Nicholson, C. (2008). Diffusion in Brain Extracellular Space. Physiol Rev *88*, 1277–1340.

Thorne, R.G., and Nicholson, C. (2006). In vivo diffusion analysis with quantum dots and dextrans predicts the width of brain extracellular space. Proc National Acad Sci *103*, 5567–5572.

Toll, L., Berzetei-Gurske, I.P., Polgar, W.E., Brandt, S.R., Adapa, I.D., Rodriguez, L., Schwartz, R.W., Haggart, D., O'Brien, A., White, A., Kennedy, J. M., Craymer, K., Farrington, L., and Auh, J. S. (1998). Standard binding and functional assays related to medications development division testing for potential cocaine and opiate narcotic treatment medications. NIDA Research Monograph *178*, 440–466.

Trieu, B.H., Remmers, B.C., Toddes, C., Brandner, D.D., Lefevre, E.M., Kocharian, A., Retzlaff, C.L., Dick, R.M., Mashal, M.A., Gauthier, E.A., Xie, W., Zhang, Y., More, S. S. and Rothwell, P. E. (2022). Angiotensin-converting enzyme gates brain circuit–specific plasticity via an endogenous opioid. Sci New York N Y eabl5130.

Xiong, H., Lacin, E., Ouyang, H., Naik, A., Xu, X., Xie, C., Youn, J., Kumar, K., Kern, T., Aisenberg, E., Kircher, D., Li, X., Zasadzinski, J. A., Mateo, C., Kleinfeld, D., Hrabetova, S., Slesinger, P. A., and Qin, Z. (2021). Probing neuropeptide volume transmission in vivo by a novel all-optical approach. Biorxiv 2021.09.10.459853.

CHAPTER 4. Future directions of neuropeptide signaling

Other possible mechanisms for presynaptic MOR and DOR signaling

In Chapter 2, we show that MOR and DOR signal independently, but through convergent signaling pathways. At the presynaptic terminal, both MOR and DOR inhibit calcium influx through VGCCs by about 30% individually, and 40% when activated together. Because the relationship between calcium influx and vesicle release is non-linear (Wu and Saggau, 1997), we believe that this can account for the entirely of the IPSC suppression. However, it does leave open the possibility for other mechanisms of neurotransmitter suppression, the main candidate being through inhibition of SNARE machinery through SNAP-25 (Gerachshenko et al., 2005). To test if MOR and DOR could be acting presynaptically downstream of VGCCs, we recorded asynchronous IPSCs by using a picospritzer to apply hypertonic sucrose over the pyramidal cell while blocking calcium channels with cadmium. Addition of DAMGO or SNC suppressed the current by 27% and 24%, respectively (**Figure 4.1A-B**), indicating that MOR and DOR can act downstream of VGCCs, potentially through SNAP-25.

To ask if MOR or DOR could be acting through Gβγ binding to SNAP-25, we obtained knockout (KO) mice from Dr. Heidi Hamm's lab at Vanderbilt. These mice have the C-terminus of SNAP-25 truncated such that Gβγ can no longer bind, impacting the signaling of certain $G_{i/o}$ coupled receptors (Zurawski et al., 2019). The SNAP25Δct mice demonstrated intact suppression of IPSCs by MOR and DOR (**Figure 4.1C**) and intact suppression of sucrose currents by MOR (**Figure 4.1A-B**). SNC162 failed to suppress the sucrose current in the KO mice, hinting at a role for SNAP-25 in opioid modulation by DORs. However, using uncaging assays for ligand potency and kinetics as described in Chapter 2, we found that DOR was not significantly impacted in the SNAP25Δct mice compared to their null littermates, although there was a trend

for DORs in the KO mice to have a larger time constant of activation (**Figures 4.1C-F**) (at 10 hz, CTOP WT = 255.7 ± 55.9 ms, CTOP KO = 358.3 ± 50.2 ms, p = 0.18, Mann-Whitney test; at 50 hz, CTOP WT = 173.2 ± 41.1 ms, CTOP KO = 298.6 ± 47.5 ms, p = 0.052, Mann-Whitney test). The kinetics of MOR signaling were also unaffected in the KO mice, although we did not compare the ligand potency to the littermate controls. Because these data on the role of SNAP-25 were ambiguous, we excluded it from the final manuscript. Our data leaves open the possibility of MOR and DOR acting through SNAP-25 or another mechanism downstream of VGCCs, but intact SNAP-25 is not necessary for MOR and DOR to fully suppress synaptic output.

As discussed in Chapter 1, opioid receptors have been shown to act through a diversity of other mechanisms to inhibit the cell that they're present on. These include, but are not limited to, inhibition of cAMP and PKA production, closing of HCN channels, opening of K_v channels, and opening of GIRK channels. These mechanisms have been shown for opioid receptors at the somato-dendritic compartment by others, and indeed in Chapter 2 we have shown that somato-dendritic MOR and DOR do activate a GIRK current. To ask if any of these mechanisms could be at play at the presynaptic terminal, we recorded electrically-evoked IPSCs (eIPSCs) as described in Chapter 2, and applied MOR and DOR agonists DAMGO and SNC162 in the presence of various pharmacological agents.

We used H89 to inhibit PKA, forskolin (FSK) to activate adenylyl cyclase (AC) and elevate cAMP, ZD7288 to block HCN channels, and 4-Aminopyridine (4-AP) to close K_v channels. The application of H89, FSK, or ZD7288 alone did not change the amplitude of the eIPSCs, while 4-AP increased the eIPSC amplitude (H89 = 1.04 ± 0.04, FSK = 1.12 ± 0.08, ZD4288 = 0.99 ± 0.07, 4-AP = 2.14 ± 0.38) (**Figure 4.2A**). DAMGO suppression of eIPSCs in the presence of H89, FSK, and ZD7288 were unchanged, implying that presynaptic MOR does

not act through the AC/cAMP pathway or through HCN channels (DAMGO = 0.69 ± 0.02, H89 = 0.70 ± 0.03, FSK = 0.57 ± 0.06, ZD7288 = 0.70 ± 0.05) (**Figure 4.2B**). SNC162 suppression of eIPSCs was unaffected by H89 and ZD7288, but was reduced in the presence of FSK, suggesting that DOR may be modulated by AC activity (SNC = 0.63 ± 0.06, H89 = 0.57 ± 0.06, FSK = 0.27 ± 0.05, ZD7288 = 0.47 ± 0.03, $p = 0.005$, Kruskal-Wallis test with Dunn's multiple comparisons) (**Figure 4.2C**). Both DAMGO and SNC162 were ineffective in the presence of 4-AP (DAMGO+4-AP = -0.005 ± 0.03, $p = 0.003$; SNC+4-AP = -0.002 ± 0.02, $p < 0.0001$, Kruskal-Wallis test with Dunn's multiple comparisons) (**Figure 4B-C**), however this may be expected due to the depolarization from 4-AP leading to Gβγ disengagement from VGCCs (Brody and Yue, 2000; Park and Dunlap, 1998).

These data suggest a segregation in the role of presynaptic MOR and DOR downstream of Gα activity. More experimentation will be needed to tease apart these pathways and determine if ligand potency and kinetics are changed in these pharmacological conditions. This could imply that DOR is more sensitive to modulation by other GPCRs, while MOR remains stable under different neuromodulatory conditions. A recent study shows that presynaptic MORs are highly mobile and rapidly recycle for more effective signaling (Jullié et al., 2019). It remains to be determined if DORs behave similarly at the presynaptic terminal, as that could affect its signaling processes too. These preliminary data show that there could be a divergence in the pathways between MOR and DOR at multiple levels, although more work will need to be done to determine the functional significance of these differences.

Redundant signaling by MOR and DOR

One of the main takeaways from Chapter 2 is that DOR dominates the response to enkephalin uncaging at both the presynaptic terminal and somato-dentritic compartments of PV cells. This was surprising because the role of DOR in the hippocampus has been understudied compared to MOR. In fact, opioid effects on PV cells are often fully attributed to MORs (Freund and Katona, 2007; Glickfeld et al., 2008). Related to that, the understanding in the field is that the majority of DORs are immature and found in intracellular compartments, rather than the plasma membrane (Cahill et al., 2001a). In the periacqueductal gray region of the brain, DORs were found in DCVs, often colocalizing with enkephalin (Commons et al., 2001). These intracellular receptors are thought to be trafficked to the plasma membrane in response to stimulus or change in brain state, such as chronic morphine (Cahill et al., 2001b). The increased surface density of DORs from receptor trafficking to the membrane leads to increased potency of the receptor (Cahill et al., 2007). Although our study did not focus on intracellular localization of DORs, we did show that DORs are highly potent and effective receptors compared to MORs. If there is an intracellular pool of DORs, it serves to heighten the response rather than limit DOR signaling.

We showed that DOR has a higher ligand potency to enkephalin and has faster receptor onset kinetics than MOR. This suggests that in a physiological context of endogenous enkephalin release, DORs may be selectively engaged from lower concentrations of enkephalin. This raises the question of why MOR is present if DOR is sufficient to engage the opioid signaling pathway. One possibility is that the receptors could have divergent signaling downstream of the effectors that we characterized. Presumably, both MOR and DOR suppress cAMP production (Minneman

and Iversen, 1976), but whether or not this ultimately leads to different consequences to cellular physiology is unknown.

Our data suggests that the reason MOR is relatively ineffective in PV cells is lower receptor abundances compared to DOR. This was supported by our data showing overexpression of MOR leading to faster kinetics and increased current amplitudes. It is possible that MOR could be naturally upregulated under certain brain states or behavioral contexts such that MOR signaling would be selectively enhanced. Rats that undergo peripheral inflammatory pain have increased MOR mRNA in the dorsal root ganglion, but not DOR mRNA (Puehler et al., 2004). In humans, cocaine-dependent men show increased MOR binding in a PET assay compared to nonaddicted controls (Zubieta et al., 1996), indicating upregulation of MORs involved in addiction and dependence. If similar contexts lead to MOR upregulation in the hippocampus, that would potentially engage MOR signaling to a greater extent than in the naïve state.

Another argument for the role of MOR would be the presence of a ligand that is selective for MOR over DOR. β-endorphin is an endogenous opioid peptide that is composed of 31 amino acids and generated from pro-opiomelanocortin (Dalayeun et al., 1993). β-endorphin displays greater binding affinity for MORs over DORs (Schoffelmeer et al., 1991; Toll et al., 1998), and so would preferentially bind MOR if released in the hippocampus. The source of β-endorphins is mostly relegated to the hypothalamus, in the arcuate nucleus (Reiner, 1988). Fragments of β-endorphin have been found in the hippocampus (Zakarian and Smyth, 1979), although the forms found were inactive at opioid receptors (Zakarian and Smyth, 1979). Therefore, a likely source of β-endorphin is from release from the arcuate nucleus into the cerebrospinal fluid (CSF) through neighboring ventricles (Veening et al., 2012). Following a passive avoidance learning procedure, β-endorphin was elevated in the CSF of rats within 5 minutes (Wan et al., 1996).

Additionally, β-endorphin levels demonstrate diurnal variation in human CSF (Barreca et al., 1986). This leaves open the possibility that brain-wide volume transmission of β-endorphin through the CSF in various behavioral contexts could selectively engage MORs, while local release of enkephalin would selectively engage DORs.

Sources of enkephalin in the hippocampus

The key to understanding the role of MOR and DOR in this hippocampal circuit would be to know the source of local enkephalin release and what drives release in slice and *in vivo*. Enkephalin-immunoreactive cells have been found in all layers of the CA1 region of the hippocampus (Blasco-Ibáñez et al., 1998). They are defined as interneurons that innervate other interneurons because they are colocalized with GABA, as well as with VIP and calretinin, and have boutons that terminate on other GABA cells. The authors note that enkephalin-reactive cells were sparse compared to other interneuron populations. Another group identified a sub-population of enkephalin cells that project from CA1 to subiculum that preferentially innervates PV cells (Fuentealba et al., 2008). These data show that enkephalin-expressing cells are present in the right place, although direct evidence connecting enkephalin release to PV cell activity is yet to be seen. It's also worth noting that antibodies for enkephalin or its precursor peptide are notoriously poor (personal correspondence and unpublished data from the lab), so further validation of enkephalin expressing cells would be more convincing.

That being said, there is evidence of enkephalin release in the hippocampus particularly in CA2 but also in CA1. After chronic morphine treatment and re-exposure to drug context, DORs were found to be internalized in response to endogenous enkephalin release (Faget et al., 2012). This effect was highest, but still sparse, in CA1 neurons, at 9% of the DOR-eGFP

population. In CA2, high frequency stimulus leads to LTD caused by enkephalin release that is dependent on DORs, but not MORs (Piskorowski and Chevaleyre, 2013). The same stimulus only yielded transient suppression in CA1. A recent paper built on this finding to show that enkephalin is being released by VIP cells in CA2 to generate DOR-dependent LTD, which was required for social memory (Leroy et al., 2021). These data are consistent with our findings that enkephalin release primarily engages DORs and not MORs. They also suggest a role for enkephalin in drug memory and social memory. Future studies will be focused on determining the source of enkephalin in CA1 by driving and detecting release using assays described in Chapter 2. The highlighted literature demonstrates that release can be achieved through electrical stimulus and optogenetic stimulus. We aim to mouse lines specific for the enkephalin precursor, proenkephalin (*Penk*) or VIP to optogenetically drive enkephalin release and detect responses in PV cells in either somato-dendritic or presynaptic compartments. Based on the literature and our findings, we hypothesize that any response to endogenous enkephalin will be selectively driven by DORs. Following that, the next step would be to determine the behavioral contexts for enkephalin release in CA1, starting with drug-context memory or social memory as likely candidates.

Another area of exploration is the differential regulation of neuropeptide expression and release across brain state and behavioral contexts. It is possible that not only the sparse interneurons are capable of producing and releasing enkephalin. Data from cortical neurons show that the majority of neurons, including glutamatergic neurons, express multiple neuropeptides (Smith et al., 2019). In fact, an early study mentions that enkephalin-immunoreactivity was occasionally found in pyramidal cells in CA1 (Gall et al., 1981). In our own hands, we have found that the *Penk-cre* mouse line also labels pyramidal cells (unpublished observations from

the lab). This raises the question of whether or not pyramidal cells can produce and release enkephalin and what triggers this differential neuropeptide expression?

One possibility is that *Penk* expression can be triggered by strong neural activity, like a seizure. Studies show that kainic acid induced seizures causes depletion of met-enkephalin immediately after the seizure, but long term upregulation of enkephalin immunoreactivity in the mossy fibers which can be seen up to 4 days later (Gall, 1988; Kanamatsu et al., 1986). Kainic acid induced seizures also elevate *Penk* mRNA expression 4 hours after seizure, and up to a year later (Bing et al., 1997). While these changes were primarily shown in the mossy fibers, it's unknown if seizures would induce expression in pyramidal cells in CA1. Kainic acid induced seizures may not be behaviorally relevant in a healthy animal, but other stimuli can also cause changes in gene expression, such exposing a lab mouse to an enriched environment (Bloodgood et al., 2013; Brigidi et al., 2019; Hartzell et al., 2018).

The differential expression of neuropeptides in glutamatergic cells would have huge implications on the study of neuromodulation, and the system we have laid out in the hippocampus is a prime area to study it. Future experiments involve inducing seizures in mice with kainic acid and seeing if that leads to *Penk* expression in pyramidal cells using *in-situ* hybridization or the induction of cre-recominbase in a *Penk-cre* mouse line. If it does, we can try to drive release from the pyramidal cell using optogenetics. This would implicate a feedback mechanism by which pyramidal cells can modulate their own excitability through the inhibition of PV interneurons. Beyond the scope of our immediate work, it would be hugely insightful to determine other behavioral contexts that drive *Penk* expression. Whether or not pyramidal cells can release enkephalin in the hippocampus, the idea of differential expression of neuropeptides can be investigated with other neuropeptides and in other brain regions.

Future of neuropeptide sensors

In Chapter 3, I've described the process for simultaneous dynorphin uncaging and imaging with the novel kLight sensor to obtain the apparent diffusion coefficient of dynorphin in brain slices. While not it's not the absolute diffusion coefficient, the apparent value still allows us to make comparisons and ask questions about how diffusion differs. For example, using similar tools, a recent study found that diffusion of SST is faster in neocortex after hyaluronidase treatment to degrade the extracellular matrix, which can have implications in diseased states (Xiong et al., 2021). Relative dynorphin diffusion can be compared by using our approach in different brain areas (such as cortex vs striatum) and microcircuits (patch vs matrix in striatum). It can also be used to compare diffusion in larger and smaller model organisms, such as rat or zebrafish. Does diffusion scale with brain size, such that diffusion happens faster in a rat brain? Similarly, would diffusion be slower in a zebrafish brain? If not, that could imply a different role of neuropeptides in the circuit processing of a smaller brain.

Immediate future experiments involve determining the diffusion coefficient in the presence of peptidase inhibitors and comparing it to absence of peptidase inhibitors. Preliminary data shows that kLight activation after dynorphin uncaging is enhanced by peptidase inhibitors (**Figure 4.3**), consistent with prior work (Banghart and Sabatini, 2012). We hypothesize that peptidase inhibitors will also increase the speed of diffusion by preventing clearance and increasing the effective concentration of the peptide. The difference in diffusion coefficients will highlight the role of peptidases in defining the range of neuropeptide signaling. This can also be compared across brain regions, to compare the relative involvement of peptidases in areas of the brain known to release dynorphin to areas of the brain that do not.

Another goal for kLight in particular is to be able to detect endogenous dynorphin release – either in brain slice or *in vivo*. Thus far, we have been unable to detect endogenous dynorphin release in slice with kLight following high frequency electrical stimulus. The electrical stimulus alone causes fluorescence artifacts – activation and/or bleaching – that can contaminate dynorphin responses. This can be corrected for with robust activation by endogenous dynorphin, but we have yet to see that. The kLight sensor as it is may not be sensitive enough to detect low concentrations of dynorphin. Moving to a laser scanning microscopy setup, like a confocal or two-photon microscope, may also favor detection of dynorphin release because it limits the scattering by out of focus light. We've also experienced issues with buffering, where high expressing tissue has smaller dynamic ranges, presumably due to excess of pre-bound sensor that limits the response. Reducing expression of kLight through smaller injections, dilution of virus, or controlled expression systems to label a small subset of cells could enhance the range of kLight and make it more sensitive to smaller concentration changes.

These modifications to our protocol may help with detecting endogenous release in slice and also *in vivo*. kLight has already been used *in vivo* to detect endogenous dynorphin release in the prefrontal cortex in response to naloxone-precipitated withdrawal (Abraham et al., 2021). However, this kLight response was long lasting and relied on naloxone, which can directly block kLight at high enough concentrations. Improvements in the sensor application can facilitate kLight imaging of transient dynorphin signals in other types of behaviors thought to evoke dynorphin release, such as foot shock and forced swim (Shirayama et al., 2004). A novel oxytocin sensor from Yulong Li's group demonstrate that this approach is feasible to detect endogenous oxytocin in slice and *in vivo* during male courtship behavior (Qian et al., 2022). With some optimization, kLight can be the first opioid sensor to do the same.

Once we are able to detect endogenous release with kLight in brain slices, we can use the assay to ask mechanistic questions about dynorphin release and neuropeptide release more broadly. Questions of interest include: Where in the neuron are DCVs released from? What types of stimuli drive release? What is the calcium dependence of DCV release and what types of calcium channels evoke release? How is neuropeptide release modulated by other GPCRs? We have preliminary evidence that dynorphin release from D1 MSNs in the striatum can be driven by G_s signaling. Expression of a genetically encoded G_s coupled opsin, β_2-optoXR (Airan et al., 2009) in D1 MSNs and activation with blue light (**Figure 4.4A**) leads to an opioid dependent suppression of inhibitory currents that is blocked by naloxone (**Figure 4.4B**). We were only able to partially recapitulate this with endogenous G_s signaling through the D1 dopamine receptor which is Gs coupled (**Figure 4.4C**). Addition of a D1R agonist, SKF 81297 led to suppression of inhibitory currents that was only partially blocked by naloxone (**Figure 4.4D**). It is unclear the exact mechanism by which G_s signaling can drive DCV release, but one possible mechanism is through PKA phosphorylation of the active zone protein RIM1α (Lonart et al., 2003; Persoon et al., 2019). Neuropeptide sensors such as kLight may prove to be a better avenue to tackle these questions than electrophysiology because they are less subject to the noise and variability of electrophysiological recordings and can provide high throughput and less biased screening of postsynaptic targets. In addition, based on unpublished data from our lab, some sensors may even be more sensitive to neuropeptides than electrophysiology assays. Addressing these fundamental questions about neuropeptides using these novel tools will be greatly influential to the field of neuromodulation.

The field of neuropeptide signaling is at an exciting moment in time where we are starting to understand the abundance of neuropeptides and are beginning to have the tools

necessary to study them. Up until recently, neuropeptides were not thought to be expressed as abundantly as classical neurotransmitters. It was thought that only certain cells express neuropeptides, and that a select few specialized cells can express multiple neuropeptides, such as interneurons and hypothalamic neurons (van den Pol, 2012). However, a growing body of transcriptomic evidence shows that almost all cortical neurons express at least one neuropeptide, with the vast majority expressing multiple (even up to ten) neuropeptides (Smith et al., 2019; Yao et al., 2021). The implications of such extensive neuropeptide signaling are difficult to fathom with our current knowledge. However, with these novel tools, we can begin to make some headway. Genetically encoded sensors are being developed not just for opioid peptides, but for all the common neuropeptides. The transcriptomic data can inform the implementation of the sensors in circuits of the brain to determine the role of multiple peptides in the circuit. Development of sensors in different channels will allow simultaneous imaging of multiple peptides to ask if and how they are differentially released. This will ultimately lead to a deeper understanding of how neurons communicate in the brain beyond synaptic transmission.

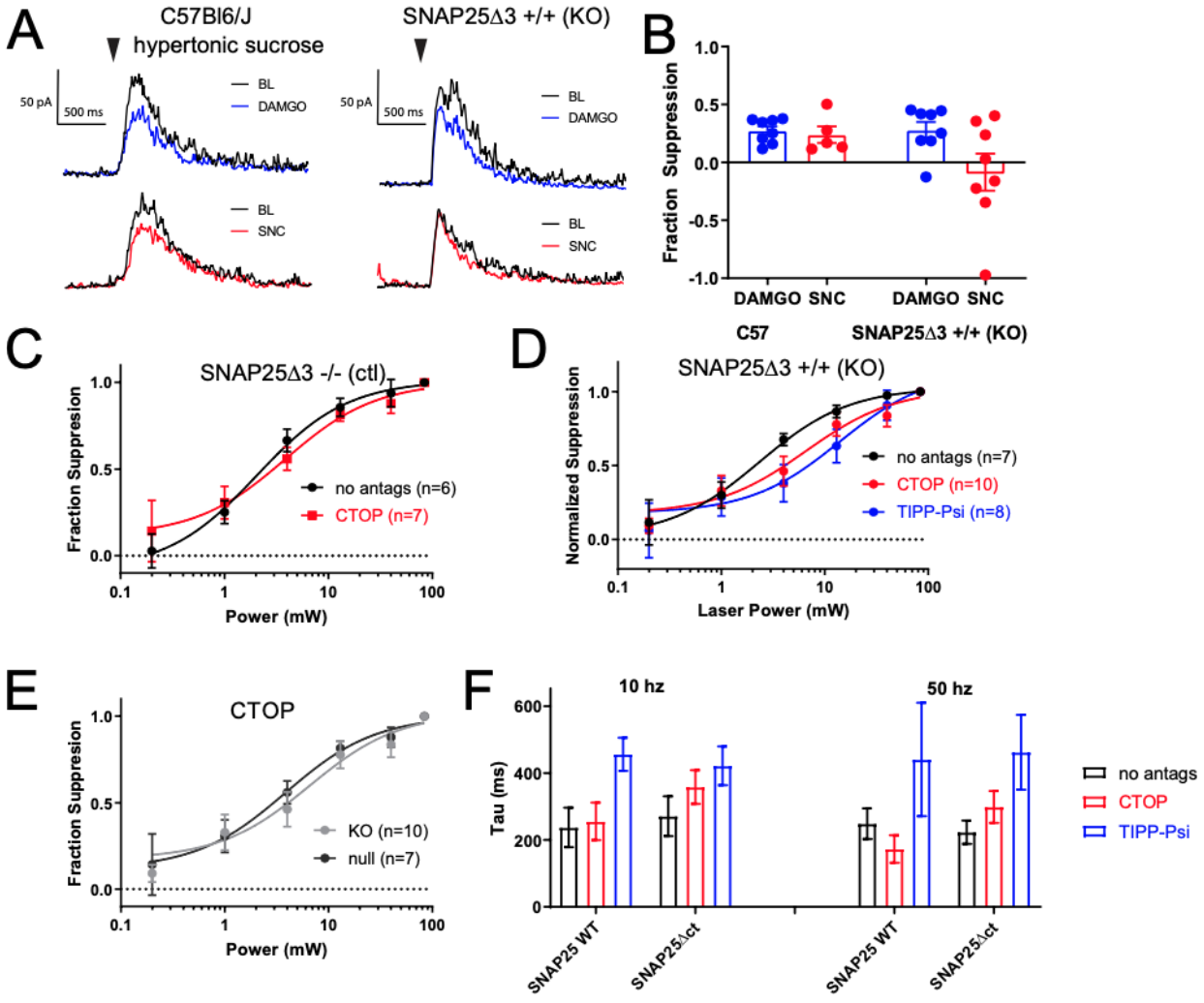

Figure 4.1. MOR and DOR actions downstream of VGCCs

A. Example IPSCs evoked by puffing hypertonic sucrose solution (500 mM) at the cell body of recorded pyramidal neurons before (black) and after application of DAMGO (blue) or SNC162 (red) in wild type (C57) mice or SNAP25Δ3 KO mice. **B.** Summary of the fraction of hypertonic sucrose-evoked IPSC suppression by DAMGO and SNC162 for C57 mice and SNAP25Δ3 KO mice. **C.** Dose response curve of normalized suppression of electrically-evoked IPSCs using MNV-LE uncaging at different laser intensities with no antagonists (black) or with CTOP (red) in SNAP25Δ3 null littermates. **D.** Dose response curve of normalized suppression of electrically-evoked IPSCs with no antagonists (black), CTOP (red), or TIPP-Psi (blue) in the SNAP25Δ3 KO mice. **E.** Direct comparison of the dose response curves in the CTOP conditions from **C** and **D**. **F.** Time constants of suppression of electrically evoked IPSC trains using CYLE uncaging at 10 hz and 50 hz in the presence of no antagonists (black), CTOP (red), or TIPP-Psi (blue) for both SNAP25Δ3 KO mice and their null littermates.

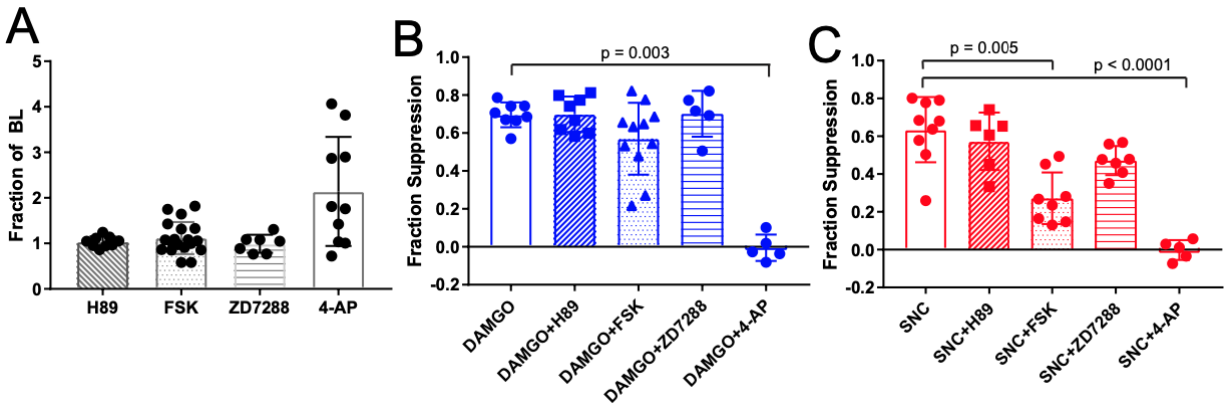

Figure 4.2. Presynaptic DOR is sensitive to modulation by adenylyl cyclase

A. Bath application of H89 (10 μM), ZD7288 (10 μM), and FSK (10 μM) do not affect baseline currents measured through electrical stimulus. 4-AP increases the baseline current by 2-fold. **B.** Fraction suppression of IPSC currents by DAMGO (1 μM) and by DAMGO in the presence of H89, ZD7288, FSK, and 4-AP. **C.** Fraction suppression of IPSC currents by SNC162 (1 μM) and by SNC162 in the presence of H89, ZD7288, FSK, and 4-AP.

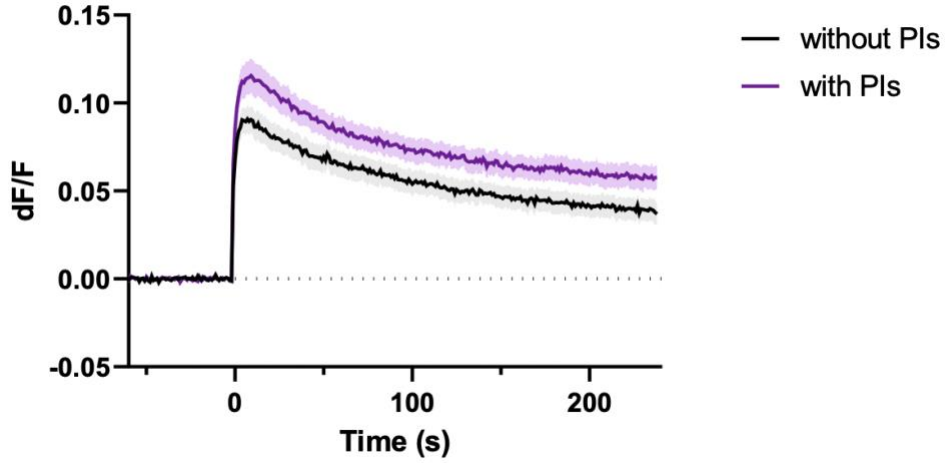

Figure 4.3. Dynorphin uncaging with and without peptidase inhibitors.

Fluorescence change of kLight1.2a in response of 5 μM MNV-D8 uncaging with 40 mW 355 nm laser with and without peptidase inhibitors (PIs). dF/F is measured as the average fluorescence in a small spot ROI of the uncaging area. Peptidase inhibitors used were 10 μM captopril, 20 μM bestatin, and 3 μM thiorphan.

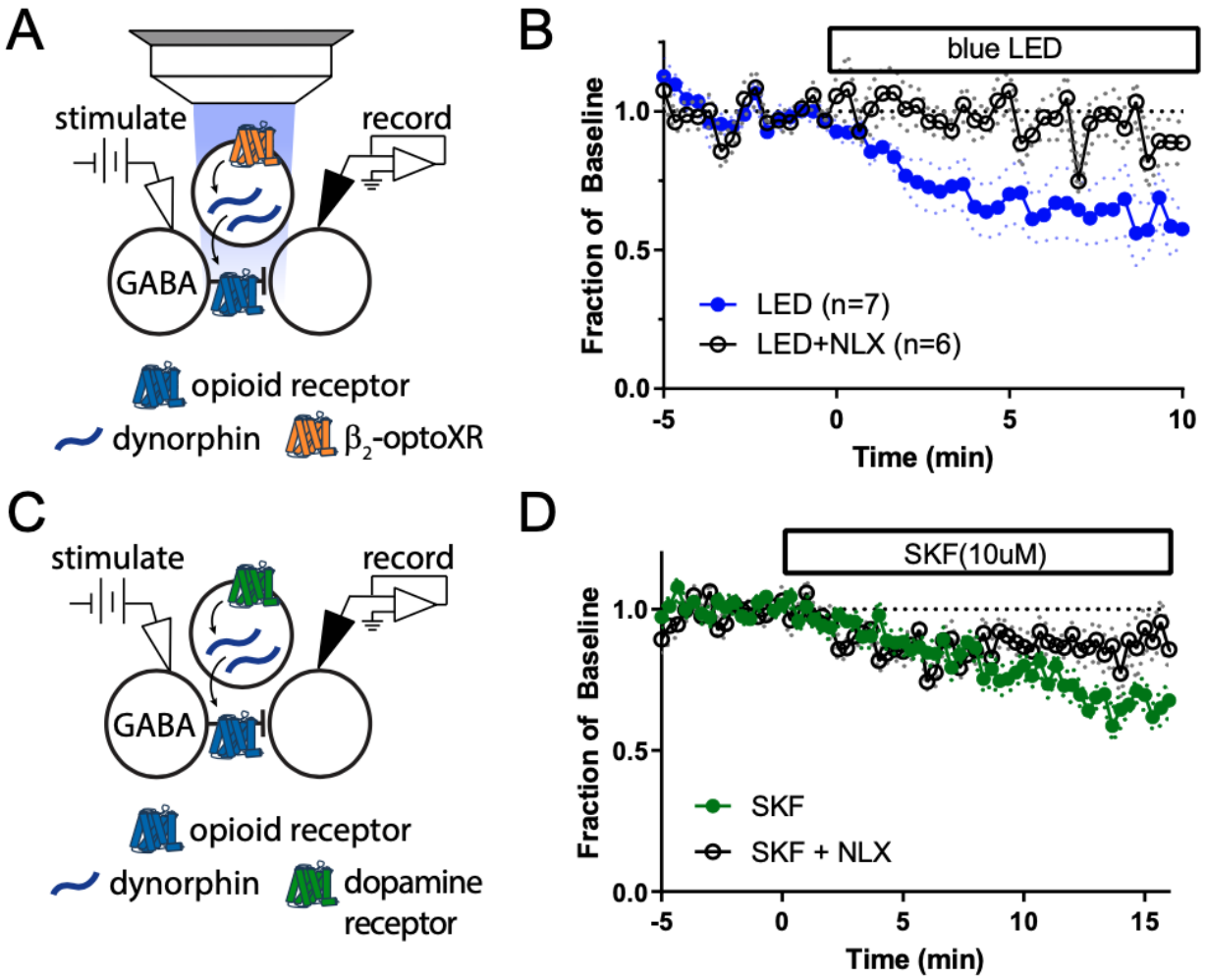

Figure 4.4. G_s activation leads to opioid dependent suppression of striatal IPSCs

A. Schematic of experimental configuration of recording from MSNs in the striatum while electrically stimulating IPSCs in tissue infected with the β_2-optoXR in D1 MSNs using AAV injected into D1-cre mice. **B.** Activation of the β_2-optoXR with a blue LED leads to suppression of IPSCs (blue, filled circles) that is blocked in the presence of NLX (black, open circles). **C.** Schematic of experimental configuration of recording from MSNs in the striatum while electrically stimulating IPSCs. The D1 dopamine receptor is shown in D1 MSNs which also express dynorphin. **D.** Addition of 10 μM SKF 81297 leads to suppression of IPSCs (green, filled circles) that is partially blocked by NLX (black, open circles) in the late phase.

References

Abraham, A.D., Casello, S.M., Schattauer, S.S., Wong, B.A., Mizuno, G.O., Mahe, K., Tian, L., Land, B.B., and Chavkin, C. (2021). Release of endogenous dynorphin opioids in the prefrontal cortex disrupts cognition. Neuropsychopharmacol *46*, 2330–2339.

Airan, R.D., Thompson, K.R., Fenno, L.E., Bernstein, H., and Deisseroth, K. (2009). Temporally precise in vivo control of intracellular signalling. Nature *458*, 1025–1029.

Banghart, M.R., and Sabatini, B.L. (2012). Photoactivatable neuropeptides for spatiotemporally precise delivery of opioids in neural tissue. Neuron *73*, 249–259.

Barreca, T., Siani, C., Franceschini, R., Francaviglia, N., Messina, V., Perria, C., and Rolandi, E. (1986). Diurnal beta-endorphin changes in human cerebrospinal fluid. Life Sci *38*, 2263–2267.

Bing, G., Wilson, B., Hudson, P., Jin, L., Feng, Z., Zhang, W., Bing, R., and Hong, J.-S. (1997). A single dose of kainic acid elevates the levels of enkephalins and activator protein-1 transcription factors in the hippocampus for up to 1 year. Proceedings of the National Academy of Sciences *94*, 9422–9427.

Blasco-Ibáñez, J., Martínez-Guijarro, F., and Freund, T. (1998). Enkephalin-containing interneurons are specialized to innervate other interneurons in the hippocampal CA1 region of the rat and guinea-pig. European Journal of Neuroscience *10*, 1784–1795.

Bloodgood, B.L., Sharma, N., Browne, H.A., Trepman, A.Z., and Greenberg, M.E. (2013). The activity-dependent transcription factor NPAS4 regulates domain-specific inhibition. Nature *503*, 121–125.

Brigidi, G.S., Hayes, M.G.B., Santos, N.P.D., Hartzell, A.L., Texari, L., Lin, P.-A., Bartlett, A., Ecker, J.R., Benner, C., Heinz, S., and Bloodgood, B. L. (2019). Genomic Decoding of Neuronal Depolarization by Stimulus-Specific NPAS4 Heterodimers. Cell *179*, 373-391.e27.

Brody, D., and Yue, D. (2000). Relief of G-protein inhibition of calcium channels and short-term synaptic facilitation in cultured hippocampal neurons. The Journal of Neuroscience : The Official Journal of the Society for Neuroscience *20*, 889–898.

Cahill, C.M., McClellan, K.A., Morinville, A., Hoffert, C., Hubatsch, D., O'Donnell, D., and Beaudet, A. (2001a). Immunohistochemical distribution of delta opioid receptors in the rat central nervous system: Evidence for somatodendritic labeling and antigen-specific cellular compartmentalization. J Comp Neurol *440*, 65–84.

Cahill, C.M., Morinville, A., Lee, M.-C., Vincent, J.-P., Collier, B., and Beaudet, A. (2001b). Prolonged Morphine Treatment Targets δ Opioid Receptors to Neuronal Plasma Membranes and Enhances δ-Mediated Antinociception. J Neurosci *21*, 7598–7607.

Cahill, C.M., Holdridge, S.V., and Morinville, A. (2007). Trafficking of δ-opioid receptors and other G-protein-coupled receptors: implications for pain and analgesia. Trends Pharmacol Sci *28*, 23–31.

Commons, K.G., Beck, S.G., Rudoy, C., and Bockstaele, E.J.V. (2001). Anatomical evidence for presynaptic modulation by the delta opioid receptor in the ventrolateral periaqueductal gray of the rat. J Comp Neurol *430*, 200–208.

Dalayeun, J.F., Norès, J.M., and Bergal, S. (1993). Physiology of β-endorphins. A close-up view and a review of the literature. Biomed Pharmacother *47*, 311–320.

Faget, L., Erbs, E., Merrer, J.L., Scherrer, G., Matifas, A., Benturquia, N., Noble, F., Decossas, M., Koch, M., Kessler, P., Vonesch, J.-L., Schwab, Y., Kieffer, B. L., Massotte, D. (2012). In Vivo Visualization of Delta Opioid Receptors upon Physiological Activation Uncovers a Distinct Internalization Profile. The Journal of Neuroscience *32*, 7301–7310.

Freund, T.F., and Katona, I. (2007). Perisomatic Inhibition. Neuron *56*, 33–42.

Fuentealba, P., Tomioka, R., Dalezios, Y., Márton, L.F., Studer, M., Rockland, K., Klausberger, T., and Somogyi, P. (2008). Rhythmically Active Enkephalin-Expressing GABAergic Cells in the CA1 Area of the Hippocampus Project to the Subiculum and Preferentially Innervate Interneurons. The Journal of Neuroscience *28*, 10017–10022.

Gall, C. (1988). Seizures induce dramatic and distinctly different changes in enkephalin, dynorphin, and CCK immunoreactivities in mouse hippocampal mossy fibers. J Neurosci *8*, 1852–1862.

Gall, C., Brecha, N., Karten, H.J., and Chang, K. (1981). Localization of enkephalin-like immunoreactivity to identified axonal and neuronal populations of the rat hippocampus. J Comp Neurol *198*, 335–350.

Gerachshenko, T., Blackmer, T., Yoon, E.-J., Bartleson, C., Hamm, H.E., and Alford, S. (2005). Gβγ acts at the C terminus of SNAP-25 to mediate presynaptic inhibition. Nature Neuroscience *8*, nn1439.

Glickfeld, L.L., Atallah, B.V., and Scanziani, M. (2008). Complementary Modulation of Somatic Inhibition by Opioids and Cannabinoids. The Journal of Neuroscience *28*, 1824–1832.

Hartzell, A.L., Martyniuk, K.M., Brigidi, G.S., Heinz, D., Djaja, N.A., Payne, A., and Bloodgood, B.L. (2018). Npas4 recruits CCK basket cell synapses and enhances cannabinoid-sensitive inhibition in the mouse hippocampus. ELife *7*.

Jullié, D., Stoeber, M., Sibarita, J.-B., Zieger, H.L., Bartol, T.M., Arttamangkul, S., Sejnowski, T.J., Hosy, E., and Zastrow, M. von (2019). A Discrete Presynaptic Vesicle Cycle for Neuromodulator Receptors. Neuron *105*, 663-677.e8.

Kanamatsu, T., Obie, J., Grimes, L., McGinty, J., Yoshikawa, K., Sabol, S., and Hong, J. (1986). Kainic acid alters the metabolism of Met5-enkephalin and the level of dynorphin A in the rat hippocampus. J Neurosci *6*, 3094–3102.

Leroy, F., Solis, C.A. de, Boyle, L.M., Bock, T., Lofaro, O.M., Buss, E.W., Asok, A., Kandel, E.R., and Siegelbaum, S.A. (2021). Enkephalin release from VIP interneurons in the hippocampal CA2/3a region mediates heterosynaptic plasticity and social memory. Mol Psychiatr 1–22.

Lonart, G., Schoch, S., Kaeser, P.S., Larkin, C.J., Südhof, T.C., and Linden, D.J. (2003). Phosphorylation of RIM1alpha by PKA triggers presynaptic long-term potentiation at cerebellar parallel fiber synapses. Cell *115*, 49–60.

Minneman, K.P., and Iversen, L.L. (1976). Enkephalin and opiate narcotics increase cyclic GMP accumulation in slices of rat neostriatum. Nature *262*, 313–314.

Park, D., and Dunlap, K. (1998). Dynamic Regulation of Calcium Influx by G-Proteins, Action Potential Waveform, and Neuronal Firing Frequency. J Neurosci *18*, 6757–6766.

Persoon, C.M., Hoogstraaten, R.I., Nassal, J.P., Weering, J.R.T. van, Kaeser, P.S., Toonen, R.F., and Verhage, M. (2019). The RAB3-RIM Pathway Is Essential for the Release of Neuromodulators. Neuron.

Piskorowski, R.A., and Chevaleyre, V. (2013). Delta-Opioid Receptors Mediate Unique Plasticity onto Parvalbumin-Expressing Interneurons in Area CA2 of the Hippocampus. The Journal of Neuroscience *33*, 14567–14578.

Puehler, W., Zöllner, C., Brack, A., Shaqura, M.A., Krause, H., Schäfer, M., and Stein, C. (2004). Rapid upregulation of μ opioid receptor mrna in dorsal root ganglia in response to peripheral inflammation depends on neuronal conduction. Neuroscience *129*, 473–479.

Qian, T., Wang, H., Wang, P., Geng, L., Mei, L., Osakada, T., Tang, Y., Kania, A., Grinevich, V., Stoop, R., Lin, D., Luo, M., and Li, Y. (2022). Compartmental Neuropeptide Release Measured Using a New Oxytocin Sensor. Biorxiv 2022.02.10.480016.

Reiner, A. (1988). Handbook of Chemical Neuroanatomy. Volume 4: GABA and Neuropeptides in the CNS, Part I . A. Björklund , T. Hökfelt. Q Rev Biology *63*, 244–245.

Schoffelmeer, A.N., Warden, G., Hogenboom, F., and Mulder, A.H. (1991). Beta-endorphin: a highly selective endogenous opioid agonist for presynaptic mu opioid receptors. J Pharmacol Exp Ther *258*, 237–242.

Shirayama, Y., Ishida, H., Iwata, M., Hazama, G., Kawahara, R., and Duman, R.S. (2004). Stress increases dynorphin immunoreactivity in limbic brain regions and dynorphin antagonism produces antidepressant-like effects. J Neurochem *90*, 1258–1268.

Smith, S.J., Sümbül, U., Graybuck, L.T., Collman, F., Seshamani, S., Gala, R., Gliko, O., Elabbady, L., Miller, J.A., Bakken, T.E., Bakken, T. E., Rossier, J., Yao, Z., Lein, E., Zeng, H., Tasic, B., and Hawrylycz, M. (2019). Single-cell transcriptomic evidence for dense intracortical neuropeptide networks. Elife *8*, e47889.

Toll, L., Berzetei-Gurske, I.P., Polgar, W.E., Brandt, S.R., Adapa, I.D., Rodriguez, L., Schwartz, R.W., Haggart, D., O'Brien, A., White, A., Kennedy, J. M., Craymer, K., Farrington, L., and Auh, J. S. (1998). Standard binding and functional assays related to medications development division testing for potential cocaine and opiate narcotic treatment medications. NIDA Research Monograph *178*, 440–466.

van den Pol, A.N. (2012). Neuropeptide Transmission in Brain Circuits. Neuron *76*, 98–115.

Veening, J.G., Gerrits, P.O., and Barendregt, H.P. (2012). Volume transmission of beta-endorphin via the cerebrospinal fluid; a review. Fluids Barriers Cns *9*, 16.

Wan, R.Q., Wiegant, V.M., Jong, W. de, and Wied, D. de (1996). Alterations of β-endorphin-like immunoreactivity in CSF following behavioral training using a passive avoidance procedure. Psychoneuroendocrino *21*, 503–513.

Wu, L.-G., and Saggau, P. (1997). Presynaptic inhibition of elicited neurotransmitter release. Trends in Neurosciences *20*, 204–212.

Xiong, H., Lacin, E., Ouyang, H., Naik, A., Xu, X., Xie, C., Youn, J., Kumar, K., Kern, T., Aisenberg, E., Kircher, D., Li, X., Zasadzinski, J. A., Mateo, C., Kleinfeld, D., Hrabetova, S., Slesinger, P. A., and Qin, Z. (2021). Probing neuropeptide volume transmission in vivo by a novel all-optical approach. Biorxiv 2021.09.10.459853.

Yao, Z., Velthoven, C.T.J. van, Nguyen, T.N., Goldy, J., Sedeno-Cortes, A.E., Baftizadeh, F., Bertagnolli, D., Casper, T., Chiang, M., Crichton, K., Ding, S.-L., Fong, O., Garren, E., Glandon, A., Gouwens, N. W., Gray, J., Graybuck, L. T., Hawrylycz, M. J., Hirschstein, D., Kroll, M., Lathia, K., Lee, C., Levi, B., McMillen, D., Mok, S., Pham, T., Ren, Q., Rimorin, C., Shapovalova, N., Sulc, J., Sunkin, S. M., Tieu, M., Torkelson, A., Tung, H., Ward, K., Dee, N., Smith, K. A., Tasic, B. T., and Zeng, H. (2021). A taxonomy of transcriptomic cell types across the isocortex and hippocampal formation. Cell *184*, 3222-3241.e26.

Zakarian, S., and Smyth, D. (1979). Distribution of active and inactive forms of endorphins in rat pituitary and brain. Proc National Acad Sci *76*, 5972–5976.

Zubieta, J.-K., Gorelick, D.A., Stauffer, R., Ravert, H.T., Dannals, R.F., and Frost, J.J. (1996). Increased mu opioid receptor binding detected by PET in cocaine–dependent men is associated with cocaine craving. Nat Med *2*, 1225–1229.

Zurawski, Z., Gray, A.D., Brady, L.J., Page, B., Church, E., Harris, N.A., Dohn, M.R., Yim, Y.Y., Hyde, K., Mortlock, D.P., Jones, C. K., Winder, D. G., Alford, S., and Hamm, H. E. (2019). Disabling the Gβγ-SNARE interaction disrupts GPCR-mediated presynaptic inhibition,

leading to physiological and behavioral phenotypes. *Science Signaling*. American Association for the Advancement of Science, 12(569). doi: 10.1126/scisignal.aat8595.